UNIVERSIDADE DE SÃO PAULO
INSTITUTO DE FÍSICA DE SÃO CARLOS

Willian M. Serenone

Landau's Two-Component Superfluid Model and the Quark-Gluon Plasma

São Carlos

2019

Willian M. Serenone

Landau's Two-Component Superfluid Model and the Quark-Gluon Plasma

Thesis presented to the Graduate Program in Physics at the Instituto de Física de São Carlos, Universidade de São Paulo, to obtain the degree of Doctor in Science.

Concentration area: Basic Physics

Advisor: Profa. Dra. Tereza Cristina da Rocha Mendes

Original version

São Carlos

2019

Serenone, Willian Matioli
Landau’s two-component superfluid model and the quark-gluon plasma / Willian Matioli Serenone; advisor Tereza Cristina da Rocha Mendes -- São Carlos 2019.
136 p.

Thesis (Doctorate - Graduate Program in Física Básica) -- Instituto de Física de São Carlos, Universidade de São Paulo - Brasil , 2019.

1. Quark-gluon plasma. 2. Lattice QCD. 3. Quantum chromodynamics. 4. Relativistic heavy-ion collisions. 5. Path integrals. I. Mendes, Tereza Cristina da Rocha, advisor. II. Title.

FOLHA DE APROVAÇÃO

Willian Matioli Serenone

Tese apresentada ao Instituto de Física de São Carlos da Universidade de São Paulo para obtenção do título de Doutor em Ciências. Área de Concentração: Física Básica.

Aprovado(a) em: 25/04/2019

Comissão Julgadora

Dr(a). Tereza Cristina da Rocha Mendes

Instituição: (IFSC/USP)

Dr(a). Bruno Werneck Mintz

Instituição: (UERJ/Rio de Janeiro)

Dr(a). Ricardo D'Elia Matheus

Instituição: (UNESP/São Paulo)

Dr(a). Donato Giorgio Torrieri

Instituição: (UNICAMP/Campinas)

Dr(a). Leonardo Paulo Maia

Instituição: (IFSC/USP)

To my wife, who supported me throughout this journey and helped me to stay focused on my goal.

ACKNOWLEDGEMENTS

First and foremost I thank God, who many times provided me the strength to pursue the conclusion of this work. He is the one who surrounded me with the right persons which supported me during the project development. Among these persons, is my wife. I am an easily distracted person and was only with her help and support that I managed to stay focused on my work. I also thank my parents for even today still teaching me lessons about life.

Surely, I must also thank my supervisor, Prof. Dr. Tereza Mendes, who motivated me and tutored me since my undergraduate days. She provided me invaluable advices and for sure I would not be where I am without her help and counseling.

I must also thank Dr. Benoît Blossier. I am very grateful for the many technical details that he taught me during my stay at Paris-Sud/LPT. Some of these were employed directly in this work and improved the quality of our results. I also acknowledge CAPES (National Council for the Improvement of Higher Education) for funding the sandwich doctorate that enabled the collaboration with him.

This research was funded by CNPq (National Council for Scientific and Technological Development), grant #142468/2014-2, for which I am grateful.

"... the opinion has time and again been expressed since the famous trial against Galileo that scientific truth cannot be brought into harmony with the religious interpretation of the world. Although I am convinced of the unassailability of scientific truth in its own sphere, I have never been able to dismiss the content of religious thinking

—*Werner Heisenberg* "Scientific Truth and Religious Truth." CrossCurrents, vol. 24, no. 4, 1975, pp. 463–473.

ABSTRACT

SERENONE, W. M. **Landau's two-component superfluid model and the quark-gluon plasma**. 2019. 136p. Thesis (Doctor in Science) - Instituto de Física de São Carlos, Universidade de São Paulo, São Carlos, 2019.

In this thesis we aim to test if Landau's two-component superfluid model is compatible with the quark-gluon-plasma description. We follow the test proposed by Chernodub *et. al.* [Two-component liquid model for the quark-gluon plasma. **Theor. Math. Phys.**, v. 170, p. 211–216, 2012]. We start by reviewing the building process of a field theory with gauge symmetries and discussing the conservation laws associated to the theory's symmetries. We explore the thermodynamic approach to quantum theory and the interesting fact that, when combined with a field theory, the path-integral formulation for quantum field theories emerges naturally. We also present the necessity of introducing a momentum cutoff into the theory and show that embedding space-time on a lattice is a way to introduce this cutoff and renormalize the theory. As a bonus, this also allows the numerical and non-perturbative evaluation of observables. We overview the phenomenological aspects of relativistic heavy-ion collisions and Landau's two-component model for superfluids, along with a quantum-field-theory motivation for it, and explain details of the test proposed by Chernodub *et. al.*. Lastly, we show the implementation details of our simulation along with results. We do not see evidence that the proposed superfluid model is able to describe the plasma. We speculate that this might be caused by the absence of fermions in our simulations.

Keywords: Quark-gluon plasma. Lattice QCD. Quantum chromodynamics. Relativistic heavy-ion collisions. Path integrals.

RESUMO

SERENONE, W. M. **Modelo de superfluido de duas componentes de Landau e o plasma de quarks e gluons**. 2019. 136p. Tese (Doutorado em Ciências) - Instituto de Física de São Carlos, Universidade de São Paulo, São Carlos, 2019.

Nesta tese nosso objetivo é testar se o modelo de Landau de duas componentes para superfluidos é compatível com a descrição do plasma de quarks e glúons. Seguimos o teste proposto por Chernodub *et. al.* [Two-component liquid model for the quark-gluon plasma. **Theor. Math. Phys.**, v. 170, p. 211–216, 2012]. Começamos revisando o processo de construção de uma teoria de campo com simetria de gauge e discutindo as leis de conservação associadas às simetrias da teoria. Exploramos a abordagem termodinâmica para teoria quântica e o interessante fato de que, quando combinada com uma teoria de campo, a formulação de integrais de trajetória para teorias quânticas de campo emerge naturalmente. Também apresentamos a necessidade de se introduzir um corte de momento na teoria, e mostramos que embutir o espaço-tempo em uma rede é um meio de introduzir o corte na teoria e renormalizá-la. Como um bônus, isso também permite o cálculo numérico e não-perturbativo de observáveis. Apresentamos um panorama dos aspectos fenomenológicos da colisão de íons pesados relativísticos e o modelo de duas componentes de Landau para superfluidos, bem como uma motivação de teoria quântica de campo para ele, e explicamos detalhes do teste proposto por Chernodub *et. al.*. Por fim, mostramos os detalhes de nossa implementação juntamente com nossos resultados. Não vemos evidência de que o modelo de superfluidod proposto seja capaz de descrever o plasma. Nós especulamos que isto possa ser causado pela ausência de férmions em nossas simulações.

Palavras-chave: Plasma de quarks e glúons. QCD na rede. Cromodinâmica quântica. Colisão de íons pesados relativística. Integrais de trajetórias.

LIST OF FIGURES

LIST OF TABLES

CONTENTS

Chapter 1

Introduction

> "*And the earth was without form, and void; and darkness was upon the face of the deep. And the Spirit of God moved upon the face of the waters.*"
>
> Genesis 1.2 — King James Bible

In the first two decades of the XXI century there were three major breakthroughs in fundamental physics: the confirmation of the existence of the quark-gluon plasma[1–2] (QGP) in 2005 by the experiments at the Relativistic Heavy Ion Collider (RHIC), the Higgs boson detection[3–4] at the Large Hadron Collider (LHC) in 2012 and the gravitational wave detection by the LIGO experiment in 2016.[5] All of these were experimental confirmations of theoretically predicted phenomena. As the title of this thesis indicates, our work explores the description of the first of these breakthroughs.

The theoretical motivation for the QGP came shortly after Quantum Chromodynamics (QCD) was formulated.[6–7] QCD is the theory that describes the force between quarks inside protons and neutrons. It is responsible for the binding of these nucleons (protons and neutrons) inside the atomic nucleus. Once one understands QCD's basic features, the existence of QGP and the conditions necessary for its occurrence become intuitive.

QCD appeared as the answer for the "particle zoo" that physicists were facing in the 1960's. It proposed that all *hadrons*, i.e. protons, neutrons, mesons and so on, were formed by a set of more fundamental particles, which were called quarks. Quarks are spin-1/2 particles that come in six *flavors*. The main differences between the various flavors are their masses, their electric charges and their couplings to the weak force. They also have the peculiarity of being the only known particles to carry fractionally charge. They also carry QCD charge, named *color*. Contrary to electromagnetism, which has only one

charge type[i], QCD color charge comes into three types, namely *red*, *green* and *blue*.

Deep inelastic scattering experiments conducted by MIT-SLAC in the 1960's have confirmed the above picture by the detection of three point-like fermions inside the proton, with the right quantum numbers.[8] Despite this, the theory was widely accepted only in the decades of 1970 and 1980, with the discovery of quarks charm, bottom and top (later, in the 1995). The reason for the disbelief is that a quark was never seen isolated. They are always inside hadrons. This QCD feature is called *confinement*. There is no proof for how it works. However, there is a qualitative explanation for the phenomenon. To explain it, we need to introduce QCD's force carrier particle: the gluons.

There are eight types of gluons. Loosely speaking, each one carries a pair of color and anti-color charge. More precisely, using the quantum mechanics notation for particle states of brackets, and denoting the color states by r, g and b (with a bar on top of them to represent the anti-colors), we may write each one of these states as[ii]

$$\begin{aligned}
g_1 &= \frac{1}{2}\left(|r\bar{g}\rangle + |g\bar{r}\rangle\right) , \quad g_2 = \frac{i}{2}\left(|g\bar{r}\rangle - |r\bar{g}\rangle\right) , \\
g_3 &= \frac{1}{2}\left(|r\bar{r}\rangle - |g\bar{g}\rangle\right) , \quad g_4 = \frac{1}{2}\left(\left|r\bar{b}\right\rangle + |b\bar{r}\rangle\right) , \\
g_5 &= \frac{i}{2}\left(|b\bar{r}\rangle - \left|r\bar{b}\right\rangle\right) , \quad g_6 = \frac{1}{2}\left(|b\bar{g}\rangle + \left|g\bar{b}\right\rangle\right) , \\
g_7 &= \frac{i}{2}\left(|b\bar{g}\rangle - \left|g\bar{b}\right\rangle\right) , \quad g_8 = \frac{1}{2\sqrt{3}}\left(|r\bar{r}\rangle + |g\bar{g}\rangle - 2\left|b\bar{b}\right\rangle\right) .
\end{aligned} \tag{1.1}$$

Since the gluons carry color charges as well, they interact with each other. Thus, instead of the interaction field spreading through space, as happens in electrodynamics, it concentrates into a tube bridging the quarks, as depicted in Fig. 1. If one tries to take the quarks farther apart, the energy deposited in the interaction will increase linearly. If the energy in the interaction is high enough, the system may convert part of it into a quark anti-quark pair, "breaking the string". One then has two hadrons that will fly apart on their own. Therefore, an isolated quark is never seen.

Another key feature of QCD is called *asymptotic freedom*. It deals with the opposite regime of confinement, i.e. when quarks are near each other. In this situation quarks interact very weakly. If we observe the limit in which two quarks are in the same place, the interaction between them approaches zero *asymptotically* and they would behave as free particles, hence the name.

Having illustrated these two basic features of QCD, we look at situations of high density. Notice that when one speaks of a high density situation, we are already making the

i The negative charge is just the anti-charge for the positive one (and vice-versa).

ii If one denotes each color by a unitary vector of dimension three, with the anti-color being its transpose vector, a state $|c\bar{c}'\rangle$ is the tensorial product between the vectors c and $\bar{c}'$, yielding a 3×3 matrix. Then one can verify that each gluon g_i is an element of SU(3)'s Lie Algebra.

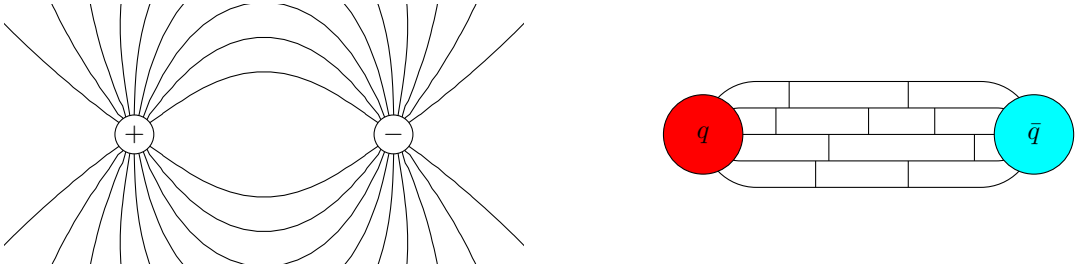

Figure 1 – **Left:** Field lines for electric dipole. **Right:** Analogous dipole for QCD. Notice the vertical lines connecting the parallel ones in QCD dipole. These represent the gluons interacting with each other, confining the field lines in a tube and avoiding its spread through space. This makes the force between the quarks constant, regardless of the distance. Source: Elaborated by the author.

assumption that we will be dealing with a high number of baryons. In these situations, on average, quarks are nearer each other and thus we may say that, on average, the interaction strength between them is weak. If the density gets large enough, the interaction strength gets so weak that one may say that hadrons "melted" and the only thing remaining is quarks and gluons flying freely. The situation is similar to what is commonly known as a plasma, i.e. when electrons are ripped out from their atomic orbits and fly freely.[9] Hence, this new state of matter was called a quark-gluon plasma[iii].

High density situations are not the only possibility for QGP's occurrence. One may use De Broglie's wave matter hypothesis

$$\lambda = \frac{h}{p} \tag{1.2}$$

by associating the typical inter-quark distance to its wave-length λ. With this, one sees that the equivalent situation of quarks being nearer each other (small λ) is for them to carry large momentum. By definition, a system with a large number of particles which, on average, carry large amounts of momentum has a high temperature.

The questions that follow are: how dense or how hot must the system be for it to transition to the QGP phase? The answer lies in what is known as the QCD scale. It tell us what is the energy scale for which the QCD interaction strength gets weak. Its value is[10] $\Lambda_{QCD} \sim 200\,\text{MeV}$. The calculation of the equivalent densities and temperatures, performed in more detail in Chapter 4, results in two situations were there is the possibility for the QGP to exist naturally. The first one is in the core of neutron stars, due to its very high density. The second one is in the early moments of the universe, when the temperature was high enough to prevent the formation of hadrons. Therefore, to know how to describe and to understand the QGP has importance for both cosmology and astrophysics.

[iii] In astrophysical contexts, one often talks about "quark-matter" instead of QGP. This is because it is not certain yet if there is the presence of a usual QGP in dense states or if it transitioned to a color-superconductor phase. However, in both cases we have that quarks and gluons would be in a deconfined phase.

Of course, the core of neutron stars and the first moments of the universe are not easy conditions to be probed. Therefore, if we aim to build a theoretical model for QGP and validate it experimentally, the best thing would be to reproduce it experimentally. This is done by accelerating heavy-ions (gold or lead, usually) to relativistic speeds and colliding them. The temperatures and densities achieved in these collisions are enough to melt the protons and neutrons into the QGP. The study of the debris of these collisions allows us to understand the properties of the plasma.

As already mentioned, the collider that managed to provide the first concrete evidence of QGP's existence was the Relativistic Heavy Ion Collider (RHIC) at Brookhaven National Laboratory in 2005. And with it, came an unexpected result. Instead of a weakly coupled gas, the measurements indicated that the QGP was behaving as a strongly-coupled, low viscosity liquid. In fact, the viscosity is near to the minimum predicted by some AdS/CFT models.[11]

Such low viscosity motivates us to compare QGP with a superfluid. The canonical example of superfluidity is helium, which becomes superfluid at temperatures below 2.17 K. In helium, the superfluidity is caused by the Bose-Einstein condensation of atoms, i.e. a macroscopic number of atoms go to their quantum ground state. This allows one to treat the fluid as possessing two independent and interpenetrating components, associating to the Bose-Einstein condensate a near-zero viscosity, while the other component retains the normal helium viscosity. This model was first proposed by L. Tisza[12] and L. Landau[13] and is very successful to describe liquid helium.

Considering the success of Landau's model and the low viscosity of QGP, Chernodub *et. al.* proposed[14] that one could model the plasma by a two-component superfluid. They also propose that computation of momentum density correlation function in QCD may be used to verify if the model is compatible with the theory.

One might think that such a computation could be performed analytically, by means of perturbation theory, since the reason for QGP formation is precisely the theory's coupling getting weak. However, a phenomenon known as Linde's problem prevents the applicability of perturbation theory.[15] Essentially, since the quarks and gluons inside the plasma are deconfined, the gluons screen the color charges of quarks. The effective result is that gluons acquire a dynamical mass. This dynamical mass enters in the theory in such a way as to cancel the additional powers of the coupling, rendering perturbation theory unreliable, even in this situation. Therefore, a non-perturbative approach must be used.

We will be using the lattice QCD approach to compute these correlation functions. Albeit being a numerical approach, it is an *ab-initio* and *non-perturbative* one. In it, one looks at QCD at finite temperature as a system at thermodynamical equilibrium, but instead of following a Boltzmann distribution $e^{-\beta E}$, it follows a distribution e^{-S}. The degrees of freedom will not be the particle velocity and position, but the field values at

every point. Then, in the same way one would perform a Monte Carlo simulation of a statistical mechanical system by sorting particles' velocities and positions according to the Boltzmann distribution, one samples field values following the exponential of the action. Then, it is just a matter of computing the correlation between momentum densities in these configurations and averaging over them.

We will start by building quantum field theories in Chapter 2, with an emphasis on their symmetries and conserved quantities. In that chapter, we also see that when one applies statistical mechanics to a quantum field theory, Feynman's path integral in Euclidean space emerges naturally. In this framework, we work out the example of a complex scalar field. In chapter 3, we pick up from the example of the previous chapter and show that a renormalization procedure is necessary for an interacting theory. We present the lattice approach as a way to introduce a regulator to the theory and to perform the renormalization non-perturbatively, with the possibility of performing numerical simulations. In chapter 4, we take a detour from the theoretical approach to present the phenomenology of heavy-ion collisions and of superfluidity, as well as present Landau's two component model for superfluids and the test proposed in Ref. 14. In Chapter 5 we give some details of the Monte Carlo algorithms implemented as well as the results obtained. We end this thesis with final considerations and conclusions in Chapter 6.

Chapter 2

Quantum Field Theory and its relation to statistical mechanics

> "*... nature isn't classical, dammit, and if you want to make a simulation of nature, you'd better make it quantum mechanical...*"
>
> Richard P. Feynman
> *Int. J. Theor. Phys.*, Vol 21, Nos. 6/7, 1982

In this chapter, we condense an overview of several key aspects needed to understand a quantum field theory at finite temperature. We adopt a constructive approach. Assuming Lorentz invariance, we build the Dirac equation and its Lagrangian. The gauge field is then introduced by means of imposition of local gauge invariance in the Dirac Lagrangian. Since the gauge field is an additional degree of freedom, we build a gauge invariant Lagrangian for it. We then state Noether's theorem and derive the energy-momentum tensor. We show that a naive derivation of the tensor does not guarantee its gauge invariance, nor that it will respect angular momentum conservation. We show how to correct these flaws and connect their presence due to translations in different Lorentz reference frames and in different gauges not being equivalent. At last, we turn to quantum thermodynamics and show that it is possible to use it to build a quantum field theory at finite temperature from the classical one.

2.1 Dirac equation and its Lagrangian density

Paul Dirac developed his equation in 1928 in an effort to describe the doubling of spectral lines in hydrogen atom without the need to perform "arbitrary assumptions", as he says in the introduction of his paper.[16] He correctly interpreted that the doubling phenomenon was relativistic in nature. Thus, a relativistic equation for the electron was

necessary to describe the experiments. His equation led to the discovery of the positron and other particles. The Dirac equation was shown to be applicable to any half-spin particle.

Our approach will be based in the book by Peskin and Schroeder,[17] which is rather different from the one adopted by Dirac. Our requirement is to find the simplest Lagrangian which satisfies Lorentz Invariance and has at least one derivative. As an initial assumption, we will say that a field $\psi(x)$ transforms under a Lorentz transform as

$$\psi(x) \;\rightarrow\; \psi'(x') \;=\; M(\Lambda)\psi(x). \tag{2.1}$$

Since a composition of two Lorentz transforms is a Lorentz transform itself and since we can always find an inverse for a given Lorentz transform, $M(\Lambda)$ must be a representation of a group, the *Lorentz group*. However there is no single representation for a group. In fact, the spin of the field will be fixed by the choice of the representation of $M(\Lambda)$. Our aim will be to determine which one is suitable for half-spin particles.

We know that rotations form a subgroup of Lorentz transformations. Since rotations form a Lie group, we will require for the Lorentz group to form a Lie group as well. Therefore, we can write an element $M(\Lambda)$ of the group as

$$M(\Lambda) \;=\; \exp\left(i\Lambda_i J_i\right), \tag{2.2}$$

where J_i is an element of the *Lie algebra* associated to the group. The index i on J_i is a placeholder. A Lie Algebra element may carry more than one index to identify it, as we will see momentarily.

Let us continue looking at the rotation group. The elements of the Lie Algebra associated to it are the angular momentum operators $J_i = -i\varepsilon_{ijk}x^j\partial^k$, where ε_{ijk} is the Levi-Civita symbol. The group parameter will be given by the rotation angle θ_i and the argument of the exponential in Eq. (2.2) becomes $\theta^i\varepsilon_{ijk}x^j\partial^k$. This expression for J_i is useful when thinking of rotations as being around an axis k. However, the idea of a rotation axis is a trick that only works in a three-dimensional space. In such a case, there is only one linearly independent vector perpendicular to each plane, allowing a unique determination of the plane. In higher dimensions this does not happen and rotations must be defined on a plane. We then rewrite the angular momentum operator as

$$J^{ij} \;=\; -i(x^i\partial^j - x^j\partial^i), \tag{2.3}$$

where the indices i, j define the plane of rotation. We redefine the group parameter θ_i as a tensor $\omega_{ij}/2$ to accommodate the new index introduced. The tensor ω_{ij} must have the property $\omega_{ij} = -\omega_{ji}$. This guarantees that if someone swaps the definitions of planes, e.g. by performing the exchange $1 \leftrightarrow 2$, terms like $\omega_{12}J^{12}$ will not change sign. We can relate ω_{ij} and θ^i by requiring $\theta^i\varepsilon_{ijk}x^j\partial^k = i\omega_{ij}J^{ij}/2$. The result is that $\omega_{23} = \theta_1$, $\omega_{31} = \theta_2$ and $\omega_{12} = \theta_3$.

To build the Lorentz group we simply replace the indices i, j by μ, ν. Thus the Lie algebra elements, which are also called the group generators, will be written as

$$J^{\mu\nu} \;=\; i(x^\mu \partial^\nu - x^\nu \partial^\mu)\,. \tag{2.4}$$

The minus sign absent in Eq. (2.4) will be explicitly written in the group element expression

$$M(\omega) \;=\; \exp\left[-\frac{i}{2}\omega_{\mu\nu}J^{\mu\nu}\right]\,. \tag{2.5}$$

Although we have already said that $J^{\mu\nu}$ belongs to a Lie Algebra, we did not prove our statement. Fortunately, the proof is a simple matter of computing the commutator between two algebra elements

$$[J^{\mu\nu},\, J^{\rho\sigma}] \;=\; i\left[g^{\mu\sigma}J^{\nu\rho} + g^{\nu\rho}J^{\mu\sigma} - g^{\mu\rho}J^{\nu\sigma} - g^{\nu\sigma}J^{\mu\rho}\right] \;=\; if^{\mu\nu\rho\sigma}{}_{\eta\kappa}J^{\eta\kappa}\,, \tag{2.6}$$

where

$$f^{\mu\nu\rho\sigma}{}_{\eta\kappa} \;\equiv\; g^{\mu\sigma}\delta^\nu_\eta\delta^\rho_\kappa + g^{\nu\rho}\delta^\mu_\eta\delta^\sigma_\kappa - g^{\mu\rho}\delta^\nu_\eta\delta^\sigma_\kappa - g^{\nu\sigma}\delta^\mu_\eta\delta^\rho_\kappa \tag{2.7}$$

is the group structure constant.

Eq. (2.4) is just one possible representation of the group's generator. Any other set of objects that obey Eq. (2.6) can be used as a representation. As we already stated, the representation of the group will determine the field's spin. Consequently, we need to pick another representation that will transform the field $\psi(x)$ as a half-spin field. The definition of a half-spin field is the one that under a rotation of 2π on a plane ij will transform as $M(2\pi)\psi(x) = -\psi(x)$. One can verify that a representation fulfilling Eq. (2.6) and the half-spin requirement have the generators defined by the following 4×4 matrices

$$S^{ij} \;\equiv\; \frac{\varepsilon^{ijk}}{2}\begin{pmatrix}\sigma^k & 0\\ 0 & \sigma^k\end{pmatrix} \qquad \text{and} \qquad S^{0i} \;\equiv\; -\frac{i}{2}\begin{pmatrix}\sigma^i & 0\\ 0 & -\sigma^i\end{pmatrix}\,, \tag{2.8}$$

where σ^i are the Pauli matrices.

A verification that the representation defined by these generators transforms the field $\psi(x)$ as a half-spin field is straightforward. Since the Pauli matrices are inserted in the block diagonal entries of the generators, a rotation by an amount θ on a plane ij will be given by

$$\Lambda_{\frac{1}{2}}(\theta) \;\equiv\; M(\theta) \;=\; \mathbb{1}\cos(\theta/2) - i\varepsilon^{ijk}\begin{pmatrix}\sigma^k & 0\\ 0 & \sigma^k\end{pmatrix}\sin(\theta/2)\,. \tag{2.9}$$

The factor $1/2$ inside the trigonometric functions comes from the factor $1/2$ present in the definition of S^{ij}. Thus, $\Lambda_{\frac{1}{2}}(2\pi) = -\mathbb{1}$, implying the desired transformation property for a half-spin field.

We should also check that the generators $S^{\mu\nu}$ satisfy the Lorentz Lie algebra of Eq. (2.6). To this end, let us use as a starting point that $\varepsilon^{ijk}\sigma^k/2 = -i[\sigma^i, \sigma^j]/4$. This enables us to decompose S_{ij} in a very interesting way

$$S^{ij} = \frac{i}{4}\begin{pmatrix}[\sigma^j, \sigma^i] & 0\\ 0 & [\sigma^j, \sigma^i]\end{pmatrix} = \frac{i}{4}\left[\begin{pmatrix}0 & \sigma^i\\ -\sigma^i & 0\end{pmatrix}, \begin{pmatrix}0 & \sigma^j\\ -\sigma^j & 0\end{pmatrix}\right] = \frac{i}{4}[\gamma^i, \gamma^j]\,. \tag{2.10}$$

Let us now extend this expression to Minkowski space, i.e. we suppose that

$$S^{\mu\nu} = \frac{i}{4}\left[\gamma^\mu\,, \gamma^\nu\right]\,. \tag{2.11}$$

When performing this assumption, we introduce a matrix γ^0 that can be determined by requiring that it generates S^{0i}, as defined in Eq. (2.8)

$$S^{0i} = \frac{i}{4}\left[\gamma^0, \gamma^i\right] = -\frac{i}{2}\begin{pmatrix}\sigma^i & 0\\ 0 & -\sigma^i\end{pmatrix}\,. \tag{2.12}$$

The matrices γ^μ are called *Dirac matrices* and they can be defined as

$$\gamma^0 = \begin{pmatrix}0 & \mathbb{1}_{2\times2}\\ \mathbb{1}_{2\times2} & 0\end{pmatrix} \qquad \text{and} \qquad \gamma^i = \begin{pmatrix}0 & \sigma^i\\ -\sigma^i & 0\end{pmatrix}\,. \tag{2.13}$$

The Dirac matrices are 4×4 matrices. This is consistent with $S^{\mu\nu}$ and $\Lambda_{\frac{1}{2}}(\omega)$ being 4×4 matrices as well. As a result, it makes sense to consider the field $\psi(x)$ a dimension four vector, which is called *spinor*. There will be moments when it will be advantageous to deal with the components of the spinor, and we will refer to these components by the indices α, β, etc. These indices are called *spinor indices*.

We will need only one more property of the Dirac matrices to verify that the group generators $S^{\mu\nu}$ belong to the Lie algebra defined in Eq. (2.6). If we compute the anti-commutator of the Dirac matrices, one can observe by direct calculation that

$$\{\gamma^\mu, \gamma^\nu\} = 2g^{\mu\nu}\,. \tag{2.14}$$

By supposing a diagonal metric, the use of the anti-commutation relations leads to $S^{\mu\nu} = i(\gamma^\mu\gamma^\nu - g^{\mu\nu})/2$. Then the commutator of $S^{\mu\nu}$ results in

$$[S^{\mu\nu}, S^{\rho\sigma}] = -\frac{1}{4}\left[\gamma^\mu\gamma^\nu, \gamma^\rho\gamma^\sigma\right]\,. \tag{2.15}$$

We proceed to expand $[\gamma^\mu\gamma^\nu, \gamma^\rho\gamma^\sigma]$ and using once again the relation in Eq. (2.14), one arrives at Eq. (2.6), as we desired to demonstrate.

With the group generators determined, we write the Lorentz group elements as

$$\Lambda_{\frac{1}{2}}(\omega) = \exp\left(-\frac{i}{2}\omega_{\mu\nu}S^{\mu\nu}\right)\,. \tag{2.16}$$

Since the transform always depends on the parameter $\omega_{\mu\nu}$, we will leave it implicit from now on, unless we desire to stress its dependence.

One thing to notice is that the matrices γ^μ are not unique. In fact, if we transform them as $\gamma'^\mu = \Lambda_{\frac{1}{2}}\gamma^\mu\Lambda_{\frac{1}{2}}^{-1}$, the Lie algebra elements $S^{\mu\nu}$ will transform following the same pattern and as a result Eq. (2.6) will be invariant.

To better understand the implications of such a transformation of γ^μ, we write the infinitesimal version of the transform

$$\begin{aligned}\gamma'^\mu \;=\; \Lambda_{\frac{1}{2}}\gamma^\mu\Lambda_{\frac{1}{2}}^{-1} \;&\cong\; \left(\mathbb{1} - \frac{i}{2}\omega_{\rho\sigma}S^{\rho\sigma}\right)\gamma^\mu\left(\mathbb{1} + \frac{i}{2}\omega_{\rho\sigma}S^{\rho\sigma}\right)\\ &\cong\; \gamma^\mu + \frac{i}{2}\omega_{\rho\sigma}\left[\gamma^\mu, S^{\rho\sigma}\right] \;=\; \gamma^\mu + \frac{i}{2}\omega_{\rho\sigma}(\mathcal{J}^{\rho\sigma})^\mu_{\ \nu}\gamma^\nu\,,\end{aligned} \tag{2.17}$$

where

$$(\mathcal{J}^{\mu\nu})_{\alpha\beta} \;=\; i(\delta^\mu_\alpha\delta^\nu_\beta - \delta^\nu_\alpha\delta^\mu_\beta) \tag{2.18}$$

obeys the Lie algebra of Eq. (2.6) as well. In particular, we have that

$$e^{-\frac{i}{2}\omega_{\mu\nu}(\mathcal{J}^{\mu\nu})^\rho{}_\sigma x^\sigma} \;\cong\; x^\rho - \frac{i}{2}\omega_{\mu\nu}(\mathcal{J}^{\mu\nu})^\rho{}_\sigma x^\sigma \;=\; x^\rho - i\omega^\rho{}_\sigma x^\sigma \;=\; x'^\rho\,. \tag{2.19}$$

Eq. (2.19) is nothing more than the Lorentz transform being written in its infinitesimal form. Thus we see that $\Lambda_{\frac{1}{2}}\gamma^\mu\Lambda_{\frac{1}{2}}^{-1} = (\Lambda^{-1})^\mu{}_\nu\gamma^\nu$. Or in other words, a Lorentz transform applied to the spinor indices of the Dirac matrix γ^μ is equivalent to an inverse Lorentz transform applied at its direction index μ. By taking this index as a true Lorentz index, one then deduces that γ^μ *is invariant under Lorentz transformations.*

With the elements present so far, it is not possible to build a Lorentz scalar. As a consequence, we are unable to build a Lagrangian, which is a Lorentz scalar. For instance, the lowest derivative term we can build is $\gamma^\mu\partial_\mu\psi(x)$, which transform as

$$\gamma^\mu\partial_\mu\psi(x) \;\to\; \gamma^\mu\partial'_\mu\psi'(x') \;=\; \gamma^\mu(\Lambda^{-1})^\nu{}_\mu\partial_\nu\Lambda_{\frac{1}{2}}\psi(x) \;=\; \Lambda_{\frac{1}{2}}\gamma^\mu\partial_\mu\psi(x)\,. \tag{2.20}$$

This clearly is not a Lorentz scalar. And it should not be. If one writes the spinor indices explicitly in the above equation, it will be possible to notice that one of them is loose, i.e. not contracted with another index.

To achieve our goal, we introduce a row-like auxiliary field $\bar\psi(x)$ of dimension four, which we treat as independent of $\psi(x)$. We require that this field transform as $\bar\psi'(x') = \bar\psi(x)\Lambda_{\frac{1}{2}}^{-1}$, so it is able to cancel the $\Lambda_{\frac{1}{2}}$ above. With these elements, we are able to construct a Lorentz invariant Lagrangian

$$\mathcal{L}(x) \;=\; \bar\psi(x)(i\partial\!\!\!/ \pm m)\psi(x)\,, \tag{2.21}$$

where we introduced the Feynman slashed notation for contraction of a four-vector with the Dirac matrices, i.e. $A\!\!\!/ \equiv \gamma^\mu A_\mu$. The sign in front of the mass, as we will see shortly,

is a matter of convention. We will carry it along for the moment to show exactly this. Notice that we could add a term $\bar{\psi}(x)\partial^2\psi(x)$ or even $\bar{\psi}(x)\not{\partial}^2\psi(x)$, since these terms are Lorentz scalars. However, we would not have met the simplest Lagrangian requirement we established in the beginning of the current section.

The next step is to build the equation of motion by the use of the Euler-Lagrange equation. This yields

$$\frac{\delta\mathcal{L}}{\delta\bar{\psi}} - \partial_\mu\left[\frac{\delta\mathcal{L}}{\delta(\partial_\mu\bar{\psi})}\right] = (i\not{\partial} \pm m)\psi(x) = 0\,, \tag{2.22}$$

$$\frac{\delta\mathcal{L}}{\delta\psi} - \partial_\mu\left[\frac{\delta\mathcal{L}}{\delta(\partial_\mu\psi)}\right] = \pm m\bar{\psi}(x) - \left[i\partial_\mu\bar{\psi}(x)\right]\gamma^\mu = 0\,. \tag{2.23}$$

So far we have treated $\bar{\psi}(x)$ as an independent variable. Since $\psi_\alpha(x) \in \mathbb{C}$, we perform a variable change $\psi_\alpha = \phi_\alpha + i\chi_\alpha$, where ϕ_α, $\chi_\alpha \in \mathbb{R}$. The two degrees of freedom of the Dirac Lagrangian are now in the real and imaginary part of the spinor. In this scenario, it would be natural to assume that $\bar{\psi} = \psi^\dagger$. This is not the case, since $\psi^\dagger$ transforms as $\psi^\dagger(x) \to \psi'^\dagger(x') = \psi^\dagger(x)\Lambda^\dagger_{\frac{1}{2}} \neq \psi^\dagger(x)\Lambda^{-1}_{\frac{1}{2}}$, due to $\Lambda^{-1}_{\frac{1}{2}} \neq \Lambda^\dagger_{\frac{1}{2}}$. The solution is to set $\bar{\psi} \equiv \psi^\dagger\gamma^0$. The Lorentz transformation becomes

$$\begin{aligned}\psi^\dagger(x)\gamma^0 \to \psi'^\dagger(x')\gamma^0 &= \psi^\dagger(x)e^{\frac{i}{2}\omega_{\mu\nu}S^{\mu\nu\,\dagger}}\gamma^0 = \psi^\dagger(x)\left\{\sum_{n=0}^{\infty}\frac{\omega^n_{\mu\nu}\left([\gamma^\mu,\gamma^\nu]^\dagger\right)}{n!\,8^n}\right\}\gamma^0 \\ &= \psi^\dagger(x)\gamma^0\sum_{n=0}^{\infty}\frac{(-1)^n\omega^n_{\mu\nu}[\gamma^\mu,\gamma^\nu]^n}{n!\,8^n} = \psi^\dagger(x)\gamma^0\Lambda^{-1}_{\frac{1}{2}}\,,\end{aligned} \tag{2.24}$$

where we used the properties $\gamma^{\mu\dagger} = \gamma^0\gamma^\mu\gamma^0$ and $\gamma^0\gamma^0 = \mathbb{1}$. Notice that $\psi^\dagger(x)\gamma^0$ obeys the desired transform for $\bar{\psi}(x)$ and thus is a suitable definition for it.

We established this relation between the spinors $\bar{\psi}(x)$ and $\psi(x)$ because now is evident that if one takes the transpose conjugate of Eq. (2.22) and right multiply the result by γ^0, one obtains Eq. (2.23). Thus, Eq. (2.23) is redundant.

We still need to show that the mass sign is a matter of convention. The easiest way is to actually solve Eq. (2.22) To do so, one uses the Ansatz $\psi(x) = \begin{pmatrix}\eta & \zeta\end{pmatrix}^T e^{ip^\mu x_\mu}$, where η and ζ are dimension 2 vectors. with the aforementioned Ansatz, one easily arrives at

$$\eta = \frac{\boldsymbol{p}\cdot\boldsymbol{\sigma}}{-E \pm m}\zeta \qquad \text{and} \qquad \zeta = \frac{\boldsymbol{p}\cdot\boldsymbol{\sigma}}{-E \mp m}\eta\,. \tag{2.25}$$

The conclusion is that if we swap the sign of the mass we are simply swapping the role of η with ζ. The convention we will follow is to assume a negative sign accompanying the mass term in the Lagrangian in Eq. (2.21).

If we were to proceed with the solution, we would need to set η or ζ equal to $\begin{pmatrix}1 & 0\end{pmatrix}^T$ or $\begin{pmatrix}0 & 1\end{pmatrix}^T$. One then sees that if we set η as one of these values, then we must have[i] $E < 0$ to avoid singularities in ζ. But if we set ζ as one of these vectors, then we need

[i] Assuming $m > 0$.

that $E > 0$ to avoid singularities in η. By interpreting the solution of negative energy as being the antiparticle of the solution of positive energy, we conclude that the change in the convention sign accompanying m just swaps which part of the spinor can be interpreted as describing a particle or its antiparticle.

The solutions in Eq. (2.25) also allow to verify that if we desire non-zero values for $\psi(x)$, than it is necessary that the relativistic dispersion relation $E^2 - \boldsymbol{p}^2 = m^2$ to be obeyed, thus proving that the Dirac equation indeed describes relativistic particles.

2.1.1 Gauge symmetry of the fermion fields

Lorentz invariance is not the only symmetry in the Dirac Lagrangian. If we transform the spinors as $\psi(x) \to \psi'(x) \equiv e^{i\alpha}\psi(x)$, then the Lagrangian is invariant as well. This is a well-known property of quantum mechanics in general, i.e. a global phase change in the wave-function leaves the theory invariant. Since two successive transformations are equivalent to another single one, the elements $U = e^{i\alpha}$ belong to a group, in this case, the unitary group of rank 1, denoted by $U(1)$.

We point out that what makes the Lagrangian invariant under "rotations" of the $U(1)$ group is the unitarity property, i.e. $U^\dagger = U^{-1}$. Thus, it is enough $U \in U(N)$ to keep the Lagrangian invariant. Of course, this opens up the possibility for the spinors to carry an additional index that can be contracted with the group elements. This index will be called a *color index* and range from 1 to N.

Nevertheless, using such a general case will not be useful. The $U(N)$ group contains continuous and discrete subgroups. Later, we will work with local transforms instead of global ones. If we admit a discrete local transform, we will find undesirable divergent derivatives. To avoid this issue later, we will restrict transformations to be in the *special unitary group* SU(N), i.e. besides unitarity, we require that the group elements have determinant equal to one. This is a Lie group as well and thus the transformations are continuous transformations. An element of $SU(N)$ can be expressed as

$$U \;=\; \exp\left(ig\Lambda^a T^a\right) , \tag{2.26}$$

where g is the theory coupling[ii] and T^a are the group generators, which belong to the Lie algebra, defined by

$$\left[T^a, T^b\right] \;=\; if^{abc}T^c \, . \tag{2.27}$$

The tensor f^{abc} is the group constant structure. Its value changes according to the rank of the group. The number of generators is dependent on the group rank as well, being

[ii] The theory coupling is needed for a correct gauge transform of the field $A_\mu(x)$, which we will define in a moment.

N^2-1). Thus the indices a, b, $\ldots \in [1,\, N^2-1]$. They are also normalized such that

$$\mathrm{Tr}\left(T^a T^b\right) \;=\; \frac{1}{2}\delta^{ab}\,. \tag{2.28}$$

Thus far, the transformations have been global transformations. A global phase change resulting in a symmetry is not surprising. If the change is the same everywhere it is perceived as a shift of the measuring referential only. Thus, to get a more interesting result, we will demand more from the theory. We will require for it to be invariant under a *local* phase change $\psi(x) \to \psi'(x) = e^{ig\Lambda^a(x)T^a}\psi(x) = U(x)\psi(x)$. Such transformation is called a *gauge transformation* and when a Lagrangian is invariant under it, we say that the theory is *gauge invariant*. The Dirac Lagrangian, as it stands in Eq. (2.21), it is not gauge invariant

$$\begin{aligned}\mathcal{L}(x) \;\to\; \mathcal{L}'(x) \;&=\; \bar{\psi}(x)U^\dagger(x)(i\partial\!\!\!/ - m)U(x)\psi(x)\\ &=\; \bar{\psi}(x)[i\partial\!\!\!/ - m]\psi(x) + i\bar{\psi}(x)U^\dagger(x)[\partial\!\!\!/ U(x)]\psi(x)\,.\end{aligned} \tag{2.29}$$

To understand why the Lagrangian is not gauge invariant, we look at the geometrical interpretation of the gauge transform. The fact that the spinor field gains a new index indicates that we are attaching to it an "internal" vectorial space. Also, we are allowed to adopt a different reference frame in this internal space for each point of the physical space-time. A gauge transform can be interpreted as a rotation of the internal space's basis. With this geometrical interpretation, it becomes evident that a term like $\bar{\psi}\partial_\mu\psi$ will not be gauge invariant. By writing the derivative's definition

$$\partial_\mu\psi(x) \;\equiv\; \lim_{a\to 0}\frac{\psi(x+a\hat{\mu}) - \psi(x)}{a}\,, \tag{2.30}$$

we see that the derivative subtracts the fields in different points of space-time and, thus, fields which are written in different bases of the internal space. The solution is to define a *covariant derivative* that rotates the field $\psi(x)$ to the same basis as $\psi(x+a\hat{\mu})$

$$D_\mu\psi(x) \;\equiv\; \lim_{a\to 0}\frac{\psi(x+a\hat{\mu}) - e^{igaA^a_\mu(x)T^a}\psi(x)}{a} \;=\; \left[\partial_\mu - igA_\mu(x)\right]\psi(x)\,, \tag{2.31}$$

where $A_\mu(x) \equiv A^a_\mu(x)T^a$ is a new field introduced in the Lagrangian. The gauge invariant Dirac Lagrangian will be given by

$$\mathcal{L}(x) \;=\; \bar{\psi}(x)\left[i\partial\!\!\!/ + gA\!\!\!/ - m\right]\psi(x) \;=\; \bar{\psi}(x)\left[iD\!\!\!/ - m\right]\psi(x)\,. \tag{2.32}$$

The question that immediately follows is how the gauge field A_μ transforms. We answer this question by using that, if Eq. (2.32) is gauge invariant, then we know that $D_\mu\psi(x) \to D'_\mu\psi'(x) = U(x)D_\mu\psi(x)$. We have then

$$\begin{aligned}\left[\partial_\mu - igA'_\mu(x)\right]\left[U(x)\psi(x)\right] \;&=\; U(x)\left[\partial_\mu - igA_\mu(x)\right] \qquad \text{only if}\\ A'_\mu(x) \;&=\; U(x)A_\mu(x)U^\dagger(x) - \frac{i}{g}\left[\partial_\mu U(x)\right]U^\dagger(x)\,.\end{aligned} \tag{2.33}$$

The introduction of the gauge field $A_\mu(x)$ is presented in more detail in Ref. 18.

2.2 Gauge Lagrangian

In the section above we introduced a gauge field $A^a_\mu(x)$, initially as a way to connect fermion fields located at different points. Contrarily to the variable $\Lambda^a(x)$ in the gauge transform, the field $A^a_\mu(x)$ appears in the Lagrangian in Eq. (2.32), thus adding a new degree of freedom to the theory. But it is strange that there is no kinetic term for it, i.e. a term involving its derivative. As a consequence of the lack of such a term, the Euler-Lagrange equation for $A^a_\mu(x)$ is

$$ig\bar{\psi}(x)\gamma^\mu T^a\psi(x) \;=\; 0\,. \tag{2.34}$$

One can recognize the left-hand side of the above equation as the current for the charge g. Note that there is nothing constraining possible values for A^a_μ yet. Motivated by this, we will add a term involving a derivative. The tempting choices would be $\partial_\mu A^\mu$ or $D_\mu A^\mu$. But these are not gauge invariant quantities. We do not want to overuse our trick of introducing a new field to get a gauge invariant Lagrangian, especially when there is a much simpler solution that does not require it.

Let us consider the commutator

$$[D_\mu,\, D_\nu] \;=\; -ig\left(\partial_\mu A_\nu - \partial_\nu A_\mu - ig\,[A_\mu,\, A_\nu]\right). \tag{2.35}$$

Under gauge transformation, the covariant derivative transforms as $D_\mu \to D'_\mu = UD_\mu U^\dagger$, since

$$\begin{aligned} D'_\mu \;&=\; \partial_\mu - igUA_\mu U^\dagger - (\partial_\mu U)U^\dagger \;=\; U\left[U^\dagger\partial_\mu - igA_\mu U^\dagger - U^\dagger(\partial_\mu U)U^\dagger\right] \\ &=\; U\left[\partial_\mu - igA_\mu - U^\dagger(\partial_\mu U) - (\partial_\mu U^\dagger)U\right]U^\dagger \;=\; U[\partial_\mu - igA_\mu]U^\dagger \;=\; UD_\mu U^\dagger\,, \end{aligned} \tag{2.36}$$

where we used $U^\dagger\partial_\mu f = \partial_\mu(U^\dagger f) - (\partial_\mu U^\dagger)UU^\dagger f$ and $U^\dagger\partial_\mu U = -(\partial_\mu U^\dagger)U$. The function f is a placeholder test function. With this, the commutator transforms as

$$[D_\mu,\, D_\nu] \;\to\; \left[D'_\mu,\, D'_\nu\right] \;=\; \left[UD_\mu U^\dagger,\, UD_\nu U^\dagger\right] \;=\; U\,[D_\mu,\, D_\nu]\,U^\dagger\,, \tag{2.37}$$

i.e. it follows the same transformation pattern as D_μ itself. We use this commutator to define the *field strength tensor* as

$$F_{\mu\nu} \;=\; \frac{i}{g}\,[D_\mu,\, D_\nu] \;=\; \partial_\mu A_\nu - \partial_\nu A_\mu - ig\,[A_\mu,\, A_\nu]\,. \tag{2.38}$$

This tensor allows us to construct a Lorentz scalar $F_{\mu\nu}(x)F^{\mu\nu}(x)$. However, this is not gauge invariant yet. Under gauge transformation, it transforms as $F_{\mu\nu}(x)F^{\mu\nu}(x) \to F'_{\mu\nu}(x)F'^{\mu\nu}(x) = U(x)F_{\mu\nu}(x)F^{\mu\nu}(x)U^\dagger(x)$. It is tempting to simply "sandwich" it between $\bar{\psi}(x)$ and $\psi(x)$ to get a gauge invariant quantity. However, we can take a trace over the color indices that are implicit in $F_{\mu\nu}(x)$. The cyclic property allows us to cancel $U(x)$ with $U^\dagger(x)$, yielding a gauge invariant term.

Before writing the Lagrangian for the gauge fields, let us expand $F_{\mu\nu}(x)F^{\mu\nu}(x)$ using Eq. (2.38)

$$\begin{aligned} F_{\mu\nu}F^{\mu\nu} \;=\; 2\Big[&(\partial_\mu A_\nu)(\partial^\mu A^\nu) - (\partial_\mu A_\nu)(\partial^\nu A^\mu) - ig\,\{\partial_\mu A_\nu,\,[A^\mu,\,A^\nu]\} \\ &- g^2 A_\mu A_\nu [A^\mu,\,A^\nu]\Big]\,. \end{aligned} \tag{2.39}$$

The curly braces represent an anti-commutator, as Eq. (2.14). We see in the above expression a global factor two. This motivates us to multiply everything by a normalization factor half. Thus, we define the gauge Lagrangian density as

$$\mathcal{L}(x) \;=\; \frac{1}{2}\,\mathrm{Tr}\left[F_{\mu\nu}(x)F^{\mu\nu}(x)\right]\,. \tag{2.40}$$

The full gauge Lagrangian is then finally written as

$$\mathcal{L}(x) \;=\; \bar{\psi}(x)(i\not{D} - m)\psi(x) + \frac{1}{2}\,\mathrm{Tr}\left[F_{\mu\nu}(x)F^{\mu\nu}(x)\right]\,. \tag{2.41}$$

The corner stone of our work will be the computation of the energy-momentum tensor for a quantum gauge field theory with SU(3) symmetry group. Thus, we will skip the derivation of the equations of motion for this Lagrangian and proceed to a brief review of Noether's theorem. A different approach, which partially overlaps with some calculations performed so far, but includes the derivation of the classical equations of motions, can be found in the author's dissertation[iii] in [Ref. 19, Sec. 2]. A much more in-depth study of gauge theories can be found in.[18]

2.3 Noether's current and the energy-momentum tensor

As we will see in Chapter 4, the energy-momentum tensor will play an important role on our work. Thus, we need to know its expression for the Lagrangian density in Eq. (2.41). To this end, we will briefly review Noether's theorem. We will not derive it here, but will state it, as found in [Ref. 20, Chap. 8, p. 206].

> **Theorem:** For every continuous transformation of the field functions and coordinates which leaves the action unchanged, there is a definite combination of the field functions and their derivatives which is conserved (i.e., a constant in time).

Mathematically, if the Lagrangian is invariant under an infinitesimal transformation

$$\begin{aligned} x^\mu \;\to\; x^\mu \;&=\; x^\mu + \lambda_i^\mu \varepsilon^i\,, \\ \phi_\alpha(x) \;\to\; \phi'_\alpha(x') \;&=\; \phi_\alpha(x) + \Omega_{\alpha i}(x)\varepsilon^i\,, \end{aligned} \tag{2.42}$$

[iii] In the referred dissertation we used the metric $g^{\mu\nu} = \mathrm{diag}(-1,1,1,1)$ while in the present work we use $g^{\mu\nu} = \mathrm{diag}(1,-1,-1,-1)$. Consequently, some results may show a sign difference.

then there will exist a (conserved) current $\mathcal{O}_i^\mu$, given by

$$\mathcal{O}_i^\mu \;=\; \frac{\delta\mathcal{L}}{\delta\left(\partial_\mu\phi_\alpha\right)}\left[\partial_\nu\phi_\alpha\lambda_i^\nu - \Omega_{\alpha i}\right] - \mathcal{L}\lambda_i^\mu\,, \tag{2.43}$$

which obeys the continuity equation

$$\partial_\mu\mathcal{O}_i^\mu \;=\; 0\,. \tag{2.44}$$

The field $\phi_\alpha(x)$ is a placeholder for any field present in the Lagrangian and its index α represents all possible indices that the field ϕ carries. Similarly, the index i in $\Omega_{\alpha i}$ and λ_i^μ represents all indices used in the transformation. The parameter ε^i is the infinitesimal parameter of the transformation upon which we Taylor expand it.

Since $\mathcal{O}_i^\mu$ obeys the continuity equation, we can associate to it a conserved charge, which is defined as

$$Q_i \;\equiv\; \int d^3x\;\; \mathcal{O}_i^0\,. \tag{2.45}$$

As an example, let us consider the gauge symmetry

$$\begin{aligned}
x^\mu \;&\to\; x'^\mu \;=\; x^\mu\,,\\
\psi_A(x) \;&\to\; \psi'_A(x') \;=\; U_{AB}(x)\psi_B(x) \;\cong\; \psi_A(x) + ig\Lambda^a(x)T^a_{AB}\psi_B(x)\,,\\
\bar\psi_A(x) \;&\to\; \bar\psi'_A(x') \;=\; \bar\psi_B(x)U^\dagger_{BA}(x) \;\cong\; \bar\psi_A(x) + ig\Lambda^a(x)\bar\psi_B T^a_{BA}\,,\\
A^a_\mu(x) \;&\to\; A'^a_\mu(x') \;\cong\; A^a_\mu(x) + \left[-gf^{abc}A^c_\mu(x) + \delta^{ab}\partial_\mu\right]\Lambda^b(x)\,.
\end{aligned} \tag{2.46}$$

We see that, depending of which field the transformation is being applied on, a different Ω is needed

$$\begin{aligned}
(\Omega_A)^{ab}_\mu \;&=\; \delta^{ab}\partial_\mu - gf^{abc}A^c_\mu(x)\,,\\
(\Omega_\psi)^b_A \;&=\; igT^b_{AB}\psi_B(x)\,,\\
(\Omega_{\bar\psi})^b_A \;&=\; -ig\bar\psi_B(x)T^b_{BA}\,,
\end{aligned} \tag{2.47}$$

where the index b is equivalent to the index i in Eq. (2.42) and all other indices are equivalent to α in that equation. Notice as well that $\lambda_i^\mu = 0$, since we do not transform the space-time coordinates in any way.

Using $F_{\mu\nu} = F^a_{\mu\nu}T^a$, one obtains the following set of equations

$$\frac{\delta\mathcal{L}}{\delta(\partial_\mu A^a_\nu)} \;=\; F^{\mu\nu,\,a} \qquad\qquad \frac{\delta\mathcal{L}}{\delta A^a_\mu} \;=\; g\bar\psi T^a\gamma^\mu\psi + gf^{abc}A^b_\nu F^{\mu\nu,\,c}\,, \tag{2.48}$$

$$\frac{\delta\mathcal{L}}{\delta(\partial_\mu\psi)} \;=\; i\bar\psi\gamma^\mu \qquad\qquad \frac{\delta\mathcal{L}}{\delta\psi} \;=\; \bar\psi(g\not{A} - m)\,, \tag{2.49}$$

$$\frac{\delta\mathcal{L}}{\delta(\partial_\mu\bar\psi)} \;=\; 0 \qquad\qquad \frac{\delta\mathcal{L}}{\delta\bar\psi} \;=\; (i\not{\partial} + g\not{A} - m)\psi\,. \tag{2.50}$$

One can then use these functional derivatives to write the conserved current $j^{\mu,a}$ as prescribed in Eq. (2.43)

$$j^{\mu,a} = -\partial_\nu F^{\mu\nu,a} + g f^{abc} A^b_\nu F^{\mu\nu,c} + g\bar{\psi} T^a \gamma^\mu \psi \,. \tag{2.51}$$

This concludes our example. The curious thing in this example is that, if we compute the equation of motion for A^a_μ, we reduce the current to $j^a_\mu = 2g[f^{abc} A^b_\nu F^{\mu\nu,c} + \bar{\psi} T^a \gamma^\mu \psi]$. The factor two is irrelevant for the continuity equation, therefore we drop it. This matches the definition of the full color current in the author's dissertation.[19] The difference is that, in Ref. 19, the current was defined by interpreting the equation of motion, while here it comes from Noether's theorem.

Notice that the full color current can be defined only in the classical case, i.e. when the fields follow their equations of motion. In the quantum case we are not allowed to use the equations of motion and we should use Eq. (2.51).

2.3.1 Energy-momentum tensor for a gauge field theory

Blindly applying Noether's theorem will yield an energy-momentum tensor that has some issues. In this section we will show what are these issues and how to patch them. The results obtained match the ones in Ref. 21, which are computed using a different route, via general relativity. The main advantage of this procedure is that it is simpler to follow for those not used to some aspects of general relativity, especially in the fermion sector.

To our study, it will be easier to break the Lagrangian density into a fermionic part and a bosonic part

$$\mathcal{L}_F(x) = \bar{\psi}(x) \left[i\not{D} - m \right] \psi(x) \,, \tag{2.52}$$

$$\mathcal{L}_B(x) = \frac{1}{2} \mathrm{Tr} \left[F_{\mu\nu}(x) F^{\mu\nu}(x) \right] \,. \tag{2.53}$$

Or yet, with all indices shown

$$\mathcal{L}_F(x) = \bar{\psi}^\alpha_A(x) \left[i\delta_{AB} (\gamma^\mu)^{\alpha\beta} \partial_\mu + g A^a_\mu(x) (\gamma^\mu)^{\alpha\beta} (T^a)_{AB} - \delta_{AB} \delta^{\alpha\beta} m \right] \psi^\beta_B(x) \,, \tag{2.54}$$

$$\mathcal{L}_B(x) = \frac{1}{4} F^a_{\mu\nu}(x) F^{\mu\nu,a(x)} \,. \tag{2.55}$$

We then will compute the energy-momentum tensor for each of these parts in separate. The full tensor will be the sum of the two results.

The symmetry that generates the invariance is translations, i.e. $x^\mu \to x'^\mu = x^\mu + \delta^\mu_\nu a^\nu$. The fields are not affected by such a transformation i.e. $\phi'(x') = \phi(x)$ for $\phi = A$, ψ, $\bar{\psi}$. One then identifies a^ν with the infinitesimal transformation parameter and then $\lambda^\mu_\nu = \delta^\mu_\nu$. Since the fields are not affected by the transformation, then $\Omega_{\alpha i} = 0$ for all fields.

2.3.1.1 Bosonic energy-momentum tensor

Using Eq. (2.48), one can easily build the bosonic part of the tensor[iv]

$$T^{\mu\nu} \;=\; \frac{\delta\mathcal{L}}{\delta(\partial_\mu A^a_\rho)} g^{\nu\sigma}\partial_\sigma A^a_\rho - g^{\mu\nu}\mathcal{L}_B \;=\; F^{\mu\rho,\,a}\partial^\nu A^a_\rho - \frac{g^{\mu\nu}}{4}F^{\rho\sigma,\,a}F^a_{\rho\sigma}\,. \tag{2.56}$$

This is called the canonical energy-momentum tensor.[22] However, it has at least two issues. Firstly, note that, since one can interpret its components in terms of energy or momentum density, it must be an observable and thus, gauge invariant. The presence of a term $\partial^\nu A^a_\rho$ already suggests that this is not the case for the canonical tensor in Eq. (2.56). And indeed, writing it in matrix notation and performing a gauge change, we can see the presence of an extra term in the transformed tensor

$$\begin{aligned} T'^{\mu\nu} \;&=\; 2\,\mathrm{Tr}\left[UF^{\mu\rho}U^\dagger\partial^\nu\left(UA_\rho U^\dagger - \frac{i}{g}(\partial_\rho U)U^\dagger\right)\right] - \frac{g^{\mu\nu}}{2}\,\mathrm{Tr}\left[UF^{\rho\sigma}U^\dagger UF_{\rho\sigma}U^\dagger\right] \\ &=\; T^{\mu\nu}_B + 2\,\mathrm{Tr}\left\{\left[A_\rho,\,F^{\mu\rho}\right]U^\dagger\partial^\nu U - \frac{i}{g}F^{\mu\rho}U^\dagger\left[\partial^\nu\partial_\rho U + (\partial_\rho U)(\partial_\nu U^\dagger)U\right]\right\}. \end{aligned} \tag{2.57}$$

Another issue comes from the fact that the canonical energy-momentum tensor is not symmetric. A non-symmetric tensor implies that angular-momentum, defined as

$$M^{\mu\rho\sigma} \;=\; x^\rho T^{\mu\sigma} - x^\sigma T^{\mu\rho}\,, \tag{2.58}$$

will not be conserved[v]. This is because $\partial_\mu M^{\mu\rho\sigma} = T^{\rho\sigma} - T^{\sigma\rho}$, which will be zero only if $T^{\mu\nu}$ is symmetric.

A solution to this issue is the one presented in Ref. 22. If one considers a "super-potential" $\chi^{\rho\mu\nu}$ which is anti-symmetric in its first two indices, then we can add $\partial_\rho\chi^{\rho\mu\nu}$ to the canonical tensor without violating the continuity equation. This happens because $\partial_\mu\partial_\nu\chi^{\rho\mu\nu}$ will be the contraction of a symmetric tensor $(\partial_\mu\partial_\nu)$ with the anti-symmetric part of the superpotential.

As an *Ansatz* to the superpotential, we will choose $\chi^{\rho\mu\nu} = F^{\rho\mu}A^\nu$. Therefore, the term we will add to the tensor will be $\partial_\rho F^{\rho\mu}A^\nu - F^{\mu\rho}\partial_\rho A^\nu$ (beware of the reversed indices in the second term, which is compensated by the negative sign in front of it). The expression for the energy-momentum tensor then becomes

$$T^\mu{}_\nu \;=\; 2\,\mathrm{Tr}\left[F^{\mu\rho}\left(\partial_\nu A_\rho - \partial_\rho A_\nu\right) + \left(\partial_\rho F^{\rho\mu}\right)A_\nu\right] - \frac{\delta^\mu_\nu}{2}\,\mathrm{Tr}\left[F_{\rho\sigma}F^{\rho\sigma}\right]\,. \tag{2.59}$$

[iv] To avoid cluttering the equations, from now on we may omit the dependence of position, unless in situations where it is needed to be stressed out.

[v] One can convince himself that $M^{\mu\rho\sigma}$ is the relativistic angular momentum by identifying $p^i = T^{0i}$ and then noticing that $L_k = \varepsilon_{ijk}M^{0ij}/2$.

We then use the definition of $F_{\nu\rho}$ in Eq. (2.38), the equation of motion $D_\rho F^{\rho\mu\,,a} = j_F^{\mu,\,a}$ and the fact that[vi] $D_\rho F^{\rho\nu} = \partial_\rho F^{\rho\nu} - ig\,[A_\rho,\, F^{\rho\mu}]$ to obtain

$$\begin{aligned} T^\mu{}_\nu \;=\; \frac{\delta^\mu_\nu}{2}\,\mathrm{Tr}\left[F_{\alpha\beta}F^{\alpha\beta}\right] - 2\,\mathrm{Tr}\,\{F^{\mu\rho}F_{\nu\rho} \\ + ig\,(F^{\mu\rho}\,[A_\rho,\,A_\nu] + A_\nu\,[A_\rho\,,F^{\mu\rho}]) + A_\nu j_F^\mu\}\;. \end{aligned} \tag{2.60}$$

Lastly, we use the property $\mathrm{Tr}(A[B,\,C]) = \mathrm{Tr}(C[A,\,B])$ to cancel the two commutators. The fermionic current j_F^μ will contribute to the fermionic part of the tensor, thus we drop it for now. The result is a symmetric energy-momentum tensor

$$T^\mu{}_\nu \;=\; 2\,\mathrm{Tr}\left[F^{\mu\rho}F_{\nu\rho} - \frac{\delta^\mu_\nu}{4}F^{\rho\sigma}F_{\rho\sigma}\right]\,. \tag{2.61}$$

2.3.1.2 Fermionic energy-momentum tensor

We will initially perform a blind derivation of the fermionic energy-momentum tensor, using Eqs. (2.49) and (2.50), as we did in the bosonic case

$$\begin{aligned} T^\mu{}_\nu \;&=\; \frac{\delta\mathcal{L}_F}{\delta(\partial_\mu\psi)}\delta^\rho_\nu\partial_\rho\psi + (\partial_\rho\bar\psi)\frac{\delta\mathcal{L}_F}{\delta(\partial_\mu\bar\psi)}\delta^\rho_\nu + \frac{\delta\mathcal{L}_F}{\delta(\partial_\mu A^a_\sigma)}\delta^\rho_\sigma\partial_\rho A^a_\sigma - \delta^\rho_\nu\mathcal{L}_F \\ &=\; i\bar\psi\gamma^\mu\partial_\nu\psi - \delta^\rho_\nu\mathcal{L}_F\,. \end{aligned} \tag{2.62}$$

The absence of the field A_μ already tells us that this expression is not gauge invariant. One way out of this is to remember that, when we were symmetrizing the bosonic tensor, we dropped the term proportional to the fermionic current $A^a_\nu j_F^{\mu,\,a} = gA^a_\nu\bar\psi\gamma^\mu T^a\psi$. We must then add it here and arrive at

$$T^\mu{}_\nu \;=\; \bar\psi\,(i\gamma^\mu\partial_\nu + g\gamma^\mu A_\nu)\,\psi - \delta^\mu_\nu\mathcal{L}_F\,, \tag{2.63}$$

which is clearly gauge invariant. However, we still do not have a symmetric tensor.

Before symmetrizing the fermionic energy-momentum tensor, let us introduce the operator $\overleftarrow{D}_\mu$, which acts on $\bar\psi$ as

$$\bar\psi\overleftarrow{D}_\mu \;=\; -\partial_\mu\bar\psi - ig\bar\psi A_\mu\,. \tag{2.64}$$

We then rewrite the equation of motion for $\bar\psi$ in Eq. (2.23) as $\bar\psi(\overleftarrow{\not{D}} - m) = 0$. However, the operator $\overleftarrow{D}_\mu$ is absent in the fermionic Lagrangian density. As it stands, the Lagrangian does not deal with $\bar\psi$ and ψ in a symmetric way. But we can build a symmetric Lagrangian by replacing the operator D_μ by $\overleftrightarrow{D}_\mu = (D_\mu + \overleftarrow{D}_\mu)/2$. Eqs. (2.49) and (2.50) become

$$\frac{\delta\mathcal{L}_F}{\delta(\partial_\mu\psi)} \;=\; \frac{i}{2}\bar\psi\gamma_\mu \qquad \frac{\delta\mathcal{L}_F}{\delta\psi} \;=\; \bar\psi\left(-\frac{i}{2}\overleftarrow{\not\partial} + g\not{A} - m\right)\,, \tag{2.65}$$

$$\frac{\delta\mathcal{L}_F}{\delta(\partial_\mu\bar\psi)} \;=\; -\frac{i}{2}\gamma_\mu\psi \qquad \frac{\delta\mathcal{L}_F}{\delta\bar\psi} \;=\; \left(\frac{i}{2}\not\partial + g\not{A} - m\right)\psi\,, \tag{2.66}$$

[vi] See Refs. 18–19

where we used the notation $\overleftarrow{\partial}_\mu$ to indicate that the derivative will be acting on a function from its left. If one proceeds to compute the equations of motion for this Lagrangian, the same expressions as in Eq. (2.22) and Eq. (2.23) will be obtained. Thus, using

$$\mathcal{L}_F \;=\; \bar{\psi}\left(\overleftrightarrow{\not{D}} - m\right)\psi \tag{2.67}$$

as the fermionic Lagrangian will not change the physics.

We calculate the energy-momentum tensor for this Lagrangian using Eqs. (2.43), (2.65) and (2.66), obtaining

$$\begin{aligned} T^{\mu}{}_{\nu} \;&=\; \frac{\delta\mathcal{L}_F}{\delta(\partial_\mu\psi)}\partial_\nu\psi + (\partial_\nu\bar{\psi})\frac{\delta\mathcal{L}_F}{\delta(\partial_\mu\bar{\psi})} + \frac{\delta\mathcal{L}_F}{\delta(\partial_\mu A_\sigma)}\partial_\nu A_\sigma - \delta^\mu_\nu\mathcal{L}_F + \bar{\psi}\gamma^\mu A_\nu\psi \\ &=\; i\bar{\psi}\gamma^\mu\overleftrightarrow{D}_\nu\psi - \delta^\mu_\nu\mathcal{L}_F\,. \end{aligned} \tag{2.68}$$

This tensor is not symmetric yet. In this case, it is easy to notice that if we permute the indices of the first term and add the result to it, we would arrive at a symmetric tensor. Before doing so, we will verify if the extra term added, i.e. $i\bar{\psi}\gamma^\nu\overleftrightarrow{D}_\mu\psi$, satisfies the continuity equation.

The contraction of ∂_μ with $i\bar{\psi}\gamma^\nu\overleftrightarrow{D}_\mu\psi$ yields

$$\partial_\mu\left[i\bar{\psi}\gamma^\nu\overleftrightarrow{D}^{\mu}\psi\right] \;=\; \frac{i}{2}\left[\bar{\psi}\gamma^\nu\Box\psi - (\Box\bar{\psi})\gamma^\nu\psi\right] + g\partial_\mu\left(\bar{\psi}\gamma^\nu A^\mu\psi\right)\,, \tag{2.69}$$

where $\Box = \partial_\mu\partial^\mu$.

We then exploit the fact that ψ and $\bar{\psi}$ must satisfy the Klein-Gordon equation, i.e. $\left(D^\mu D_\mu - m^2\right)\psi = 0$ and $\bar{\psi}\left(\overleftarrow{D}^{\mu}\overleftarrow{D}_\mu - m^2\right) = 0$. By expanding the definitions of D_μ and $\overleftarrow{D}_\mu$, we write the Klein-Gordon equation for them as

$$\Box\psi - ig\left[\partial_\mu A^\mu + 2A^\mu\partial_\mu\right]\psi \;=\; m^2\psi + gA_\mu A^\mu\psi\,, \tag{2.70}$$

$$\Box\bar{\psi} + ig\bar{\psi}\left[\partial_\mu A^\mu + 2\overleftarrow{\partial}_\mu A^\mu\right] \;=\; m^2\bar{\psi} + g\bar{\psi}A_\mu A^\mu\,. \tag{2.71}$$

Next, we left-multiply Eq. (2.70) by $i\bar{\psi}\gamma^\nu/2$ and right multiply Eq. (2.71) by $i\gamma^\nu\psi/2$. Subtracting the resulting equations, we obtain

$$\frac{i}{2}\left[\bar{\psi}\gamma^\nu\Box\psi - (\Box\bar{\psi})\gamma^\nu\psi\right] + g\partial_\mu\left(\bar{\psi}\gamma^\nu A^\mu\psi\right) \;=\; 0\,. \tag{2.72}$$

This is telling us that the right-hand side of Eq. (2.69) is zero. Thus, we are allowed to add $i\bar{\psi}\gamma^\nu\overleftrightarrow{D}^{\mu}\psi$ to the energy-momentum tensor. Thus, it is written as

$$T^{\mu\nu} \;=\; \bar{\psi}\left[\gamma^\mu\overleftrightarrow{D}^{\nu} + \gamma^\nu\overleftrightarrow{D}^{\mu}\right]\psi - g^{\mu\nu}\bar{\psi}\left(\overleftrightarrow{\not{D}} - m\right)\psi\,, \tag{2.73}$$

which is a symmetrical and gauge invariant tensor.

The method we presented above is a variation of what is commonly known as *Belinfante method*, named after J. Belinfante who first proposed it.[23] The main difference is that, instead of performing an Ansatz, Belinfante prescribed a way of computing the missing terms. However, it is still bothersome that we needed to patch Noether's theorem's result to get an energy-momentum tensor which is gauge invariant. E. Eriksen and J. M. Leinaas pointed out in Ref. 24 that, in a pure gauge theory with U(1) symmetry group, i.e. electromagnetism without fermions, if one performs a translation taking into account that the field A_μ is gauge dependent, then the resulting tensor is the same as the one we found. It is easy to understand why this happens. A naive translation as we performed does not take into account that the internal space base changes as we move through space. Consequently, the end result will be gauge dependent, unless we "inform" Noether's theorem of the gauge symmetry.

Although taking into account gauge symmetry at translations fixes the issue of a gauge dependent tensor, it will not always fix the symmetry of it. For instance, Y. Takahashi computed in [Ref. 25, Sec. 6] the energy-momentum tensor for electromagnetism with fermions, taking into account gauge symmetry. His results were gauge independent, but the fermionic term was not symmetric. However, in [Ref. 25, Sec. 4] he clearly associates the symmetry of the EMT with the need to take into account the Lorentz invariance alongside the translation. We also point out that he modified the fermionic term of the Lagrangian to include a backward derivative, just as we did.

Another way of performing the same calculation is presented in Ref. 21, which makes use of general relativity in building the Lagrangian and the energy-momentum tensor, only taking the limit of flat space as a last step. However, the core idea of needing to take into account the Lorentz transform alongside the translation is the same and indeed, Ref. 21 arrives at the same expression for the tensor as the one showed here.

2.4 Quantum field theory at finite temperature

So far, we have treated field theory from a classical point of view. But we are interested in field theories at a quantum level. In this section we will show that a natural approach to quantization is using statistical mechanics. The drawback of this approach is that we will be limited to studying systems at thermodynamic equilibrium. We will start by briefly presenting the application of the statistical mechanics approach to quantum theories using the grand canonical partition function. This will enable us to build the foundations to write the path integral formalism of quantum field theories, which is a key ingredient in the formulation of lattice QCD.

This section is based on Ref. 26. Furthermore, Ref. 27 provides a more traditional approach to the subject at hand.

2.4.1 Statistical mechanics approach to quantum theory

Let us suppose that we desire to compute the expected value of an operator $\hat{A}$ for a quantum system in thermodynamic equilibrium. In a given instant of time the system is in a state denoted by $|\psi_n\rangle$. Then, the expected value of $\hat{A}$ will be given by $\langle\psi_n|\,\hat{A}\,|\psi_n\rangle$. However, when an experimentalist performs a measurement, it typically happens in a time interval much larger than the one during which the system stays in the state $|\psi_n\rangle$. Thus, what is measured is an average over many states. Denoting by p_n the probability that we will find the system in the state $|\psi_n\rangle$, the expected value will be given by

$$\langle A\rangle \;=\; \sum_n \langle\psi_n|\,\hat{A}\,|\psi_n\rangle\, p_n\,, \tag{2.74}$$

By considering that $|\psi_n\rangle$ is a set of vectors that form an orthonormal basis, we can insert the relation $\mathbb{1} = \sum_m |\psi_m\rangle\langle\psi_m|$. twice in Eq. (2.74) and obtain

$$\langle A\rangle \;=\; \sum_{n,i,j} \langle\psi_n|\psi_i\rangle\langle\psi_i|\,\hat{A}\,|\psi_j\rangle\langle\psi_j|\psi_n\rangle\, p_n \;=\; \sum_{i,j} \langle\psi_j|\psi_i\rangle\langle\psi_i|\,\hat{A}\,|\psi_j\rangle\, p_i \;=\; \mathrm{Tr}\left(\hat{\rho}\hat{A}\right), \tag{2.75}$$

where $\hat{\rho}$ is called the statistical operator, defined as

$$\hat{\rho} \;=\; \sum_n |\psi_n\rangle\langle\psi_n|\, p_n\,. \tag{2.76}$$

The sum over n runs over all possible states of the system. Although in an experiment this does not happen, we will suppose that the measure is taken over a long enough time so that the system visits the majority of the most probable states. The contribution of non-visited states is negligible due to its very small probability value.

Eqs. (2.75) and (2.76) tell us that all information we need to know is encoded into the statistical operator $\hat{\rho}$. But since it is not always possible to know p_n and $|\psi_n\rangle$, we need an alternative procedure to computing $\hat{\rho}$.

To this end, let us suppose that the only relevant characteristics to label the different states are their energies E_m and a set of conserved charges[vii] n. In this section, we will consider a single conserved charge to simplify notation, since the calculation for an arbitrary number of conserved charges is the same. although we use these quantities to label them, two different states may have the same energy and charges.

Let us suppose as well that our system is in contact with a much larger heath-bath system, with which it exchanges energy and charge, i.e. we are using the *grand canonical ensemble* approach. We will call the number of states in the system with energy E_m and

[vii] We mean by charge any conserved number that comes from the spatial integration of the zero-th component of a conserved current, as defined in Section 2.3. A system may have more than one conserved charge.

charge n by $\Gamma(E_m, n)$. We use a similar notation for the number of states in the heath-bath system, i.e. $\Gamma^H(E', n')$. We notice yet that if the total energy and charge available are respectively E and N, the heath-bath quantities will be $E' = E - E_m$ and $n' = N - n$. Since it is the heath-bath the one to fix the energy and charge in the system, we say that the probability of finding a state with energy E_m and charge n will be proportional to $\Gamma^H(E - E_m,\, N - n)$. Therefore,

$$p_{m,n} \;=\; \frac{\Gamma^H(E - E_m,\, N - n)}{\sum_m \left[\Gamma^H(E - E_m,\, N - n) + \Gamma(E_m,\, n)\right]}\,. \tag{2.77}$$

By hypothesis, $E \gg E_m$, $N \gg n$ and, remembering that[viii] entropy is defined as $S \equiv \ln \Gamma$, we have that

$$\ln \Gamma^H(E - E_m, N - n) \;\approx\; S(E, N) - E_m \left.\frac{\partial S^H}{\partial E}\right|_{E_m=0,n=0} - n \left.\frac{\partial S^H}{\partial n}\right|_{E_m=0,n=0}\,. \tag{2.78}$$

The derivatives of the entropy can be written in terms of the temperature T and chemical potential μ via $\partial S/\partial E = 1/T = \beta$ and $\partial S/\partial N = -\beta\mu$. Thus, we obtain the relation

$$\ln \Gamma^H(E - E_m, N - n) \;\approx\; S(E, N) - \beta E_m + \beta\mu n\,. \tag{2.79}$$

Inverting the above relation to isolate $\Gamma^H(E - E_m, N - n)$, we write the probability $p_{m,n}$ as

$$p_{m,n} \;=\; \frac{\Gamma^H(E, N)}{\Gamma^H(E - E_m, N - n) + \Gamma(E_m, n)} \times \exp\left[-\beta\left(E_m - \mu n\right)\right]\,. \tag{2.80}$$

Notice that, since energy and charge are conserved, the factor in front of the exponential is a constant, which we will call Z^{-1}.

We are ready to return to Eq. (2.76). The states in it, $|\psi_n\rangle$, are replaced by $|E_m,\, n\rangle$. These are eigenstates of the Hamiltonian operator $\hat{H}$ and conserved charge operator $\hat{N}$. Thus, we may write the statistical operator as

$$\hat{\rho} \;=\; \frac{\sum_m e^{-\beta(E_m - \mu n)}\, |E_m,\, n\rangle\, \langle E_m,\, n|}{Z} \;=\; \frac{e^{-\beta(\hat{H} - \mu\hat{N})}}{Z}\,. \tag{2.81}$$

At last, we can use Eq. (2.81) in Eq. (2.75) to write the expected value of an operator $\hat{A}$ in terms of the Hamiltonian and conserved charge operator as

$$\langle A \rangle \;=\; \frac{\mathrm{Tr}\left[e^{-\beta(\hat{H} - \mu\hat{N})}\,\hat{A}\right]}{Z}\,. \tag{2.82}$$

Notice that we have Z only in terms of the number of states in the system and in the heath-bath. Of course, these are very difficult to calculate. However, a trivial case is to set operator $\hat{A}$ to $\mathbb{1}$. Then the expected value will be one and we get

$$Z \;=\; \mathrm{Tr}\left[e^{-\beta(\hat{H} - \mu\hat{N})}\right]\,, \tag{2.83}$$

[viii] We use temperature units such that $k_B = 1$.

which is called the *grand partition function* of the system.

Eq. (2.82) is useful when one knows how $\hat{H}$, $\hat{N}$ and $\hat{A}$ act in the orthonormal states of the chosen basis. This may not always be the case. The partition function formalism, which we will study in the next section, does not use operators and provides a way to deal with those cases.

2.4.2 The path-integral formulation of the partition function

As said in the previous section, the computation of the partition function and expected values of observables is not always possible using Eqs. (2.82) and (2.83). The easiest procedure to evaluate these quantities would be to find the eigenstates of the Hamiltonian and charge operators to use them in the trace calculation. However, except for a few simple cases, obtaining these eigenstates is not possible. Thus, the alternative which we will follow is to get rid of the operators by using the path-integral formalism.

The path-integral formalism can be derived, perhaps in a simpler way, by considering a system of a point-like particle, perhaps under the influence of a potential $V(x)$. The drawback is that we would need to make the additional hypothesis that the same procedure generalizes to field theory. Using the approach presented above, the connection with statistical mechanics would come later instead of being our starting point. And even then, the connection would come through a Wick rotation, which introduces the concept of imaginary time, motivated only by the desire to make an analogy with statistical mechanics.

Due to the drawbacks outlined above, we choose to start by considering that there exists a Hilbert space whose base $|\phi\rangle$ consists of eigenstates of a field operator $\hat{\phi}(\boldsymbol{x})$. The field $\phi(\boldsymbol{x})$, as in Noether's theorem, is a placeholder to represent the set of all fields present in the theory, e.g. for QCD with a single quark flavor that would be $\phi(\boldsymbol{x}) = \{A^a_\mu(\boldsymbol{x}), \psi^a_\alpha(\boldsymbol{x})\}$. Notice also that we are making fields explicitly space dependent, while the states $|\phi\rangle$ are not. Otherwise, one could always adopt $\hat{\phi}(\boldsymbol{x}) \equiv e^{i\boldsymbol{P}\cdot\boldsymbol{x}}\hat{\phi}e^{-i\boldsymbol{P}\cdot\boldsymbol{x}}$ and $|\phi\rangle \equiv |\phi(0)\rangle = e^{i\boldsymbol{P}\cdot\boldsymbol{x}}\,|\phi(\boldsymbol{x})\rangle$. Notice furthermore that there is no time dependence in the operators. This is because we desire to describe a system in equilibrium. Therefore, everything in the system must be time independent. All this said, to avoid cluttering our equations, we once again will omit the space dependence of the operators from now on, writing it just in the cases where it needs to be stressed.

Since $|\phi\rangle$ forms a continuous set, the trace will be written in terms of an integral instead of a sum. The partition function in Eq. (2.83) will be given by

$$Z \;=\; \int d\phi\; \langle\phi|\, e^{-\beta(\hat{H}-\mu\hat{N})}\,|\phi\rangle\;, \tag{2.84}$$

where the Hamiltonian is

$$\hat{H} \;=\; \int d^3x\, \mathcal{H}[\hat{\pi}(\boldsymbol{x}), \hat{\phi}(\boldsymbol{x})]\,. \tag{2.85}$$

The operator $\hat{\pi}$ is the conjugate momentum to $\hat{\phi}$. Similarly, we assume that it is possible to write the number operator as

$$\hat{N} \;=\; \int d^3x\, \mathcal{N}[\hat{\pi}(\boldsymbol{x}), \hat{\phi}(\boldsymbol{x})]\,. \tag{2.86}$$

The next step is to decompose the exponential in N pieces. For convenience, we will define $a \equiv \beta/N$. We then insert the completeness relation $\int d\phi_i \; |\phi_i\rangle \langle\phi_i| = \mathbb{1}$ between each exponential. The index i refers to an auxiliary "time" direction, which we introduce to distinguish the different completeness relations. We then obtain, after some algebra in which we use $\langle\phi_i|\phi_j\rangle = \delta(\phi_j - \phi_i)$

$$Z \;=\; \prod_{i=1}^{N} \int d\phi_i \; \langle\phi_{i+1}|\, e^{-a(\hat{H}-\mu\hat{N})}\, |\phi_i\rangle\, \delta_{N+1,\,1}\,. \tag{2.87}$$

The problem at hand is then to compute $\langle\phi_{i+1}|\, e^{-a(\hat{H}-\mu\hat{N})}\, |\phi_i\rangle$. To this end, we insert the completeness relation $\int d\pi_i/(2\pi)\, |\pi_i\rangle \langle\pi_i| = \mathbb{1}$. We then apply the property $\langle\phi|\pi\rangle = \exp[i \int d^3x\, \pi(\boldsymbol{x})\phi(\boldsymbol{x})]$, where $\phi(\boldsymbol{x})$ and $\pi(\boldsymbol{x})$ are the eigenstates of the operators $\hat{\phi}(\boldsymbol{x})$ and $\hat{\pi}(\boldsymbol{x})$ respectively. Next, we assume that the following relation is true:

$$\langle\pi_i|\, e^{-a\int d^3x \left[\hat{\mathcal{H}}(\hat{\pi},\hat{\phi}) - \mu\hat{\mathcal{N}}(\hat{\pi},\hat{\phi})\right]}\, |\phi_i\rangle \;=\; e^{-a\int d^3x [\mathcal{H}(\pi_i,\phi_i) - \mu\mathcal{N}(\pi_i,\phi_i)]}\, \langle\pi_i|\phi_i\rangle\,. \tag{2.88}$$

Of course, Eq. (2.88) does not hold true in a general case and its validity should be checked for each Hamiltonian. Usually the check involves the use of the Baker-Campbell-Hausdorff [Ref. 28, Eq. (1.2)] formula to write $e^{a\mathcal{H}} = e^{a\mathcal{T}+a\mathcal{V}} \approx e^{a\mathcal{T}} e^{a\mathcal{V}} e^{a^2[\mathcal{T},\mathcal{V}]} \ldots$ Then, terms proportional to a^2 are dropped under the argument that they will vanish when the continuum limit is taken[ix], as will be done below. The result will be

$$\langle\phi_{i+1}|\, e^{-a(\hat{H}-\mu\hat{N})}\, |\phi_i\rangle \;=\; \int \frac{d\pi_i}{(2\pi)} e^{i\int d^3x\, \pi_i(\phi_{i+1}-\phi_i) - a\int d^3x\, [\mathcal{H}(\pi_i,\phi_i) - \mu\mathcal{N}(\pi_i,\phi_i)]}\,. \tag{2.89}$$

At this point, depending on the Hamiltonian's form, it may be possible to integrate out the momentum. The most common case is for the Hamiltonian to depend on momentum only by a quadratic term. Then, after square completing the argument of the exponential, we have at hand a Gaussian integral which allows the integration to be performed. Although this is a common case, it is an additional hypothesis which will not be adopted for the time being. In the next section, we will exemplify such a procedure with the complex scalar field.

[ix] By continuum limit, we mean we take $N \to \infty$ and $a \to 0$ in such a way that $\beta = aN$ always.

With the result from Eq. (2.89) we may write the partition function as

$$Z = \prod_{i=1}^{N} \int \frac{d\pi_i}{(2\pi)} \int d\phi_i \, \delta_{N+1,1} \times \exp\left[a \sum_{i=1}^{N} \int d^3x \, i\pi_i \frac{\phi_{i+1} - \phi_i}{a} - \mathcal{H}(\pi_i, \phi_i) + \mu \mathcal{N}(\pi_i, \phi_i) \right] . \tag{2.90}$$

Notice that the field ϕ, which originally depended only on the position, now depends of the index i as well. If we take the limit $a \to 0$ and $N \to \infty$ simultaneously, as to keep $\beta = aN$, the index i will become a continuous variable τ. The sum in $a \sum_{i=1}^{N}$ becomes an integral and the fraction is just the discretized version of a derivative in τ. Summarizing, we have the following transformations as we take the continuum limit

$$\begin{aligned} \phi_i(\boldsymbol{x}) &\to \phi(\boldsymbol{x}, \tau) \\ a \sum_{i=1}^{N} &\to \int_0^\beta d\tau \\ \frac{\phi_{i+1}(\boldsymbol{x}) - \phi_i(\boldsymbol{x})}{a} &\to \partial_\tau \phi(\boldsymbol{x}, \tau) . \end{aligned} \tag{2.91}$$

We also adopt the following definitions

$$\lim_{\substack{a \to 0 \\ N \to \infty}} \prod_{i=1}^{N} \int \frac{d\pi_i}{(2\pi)} \int d\phi_i \delta_{N+1,1} \equiv \int \mathcal{D}\pi \int_P \mathcal{D}\phi . \tag{2.92}$$

The P in $\int_P \mathcal{D}\phi$ is an indicative that the integration in the variable ϕ should be done respecting the constraint $\phi(\boldsymbol{x}, 0) = \phi(\boldsymbol{x}, \beta)$.

With Eqs. (2.90, 2.91) and (2.92), we write the partition function as

$$Z = \int \mathcal{D}\pi \int_P \mathcal{D}\phi \, e^{\int_0^\beta d\tau \int d^3x \, i\pi(\boldsymbol{x},\tau)\partial_\tau \phi(\boldsymbol{x},\tau) - \mathcal{H}[\pi(\boldsymbol{x},\tau),\phi(\boldsymbol{x},\tau)] + \mu\mathcal{N}[\pi(\boldsymbol{x},\tau),\phi(\boldsymbol{x},\tau)]} . \tag{2.93}$$

Notice that τ is acting quite-like a time variable. Also, the term $i\pi\partial_\tau\phi - \mathcal{H}$ is very similar to the Legendre transform that would yield the system's Lagrangian. In fact, by saying that τ is a *complex time* related to the real time by $\tau = it$, we arrive precisely at our usual Legendre transform. Eq. (2.93) is then written as

$$Z = \int \mathcal{D}\pi \int_P \mathcal{D}\phi \, e^{i \int_0^{-i\beta} dt \int d^3x \, \pi(\boldsymbol{x},t)\partial_0 \phi(\boldsymbol{x},t) - \mathcal{H}[\pi(\boldsymbol{x},t),\phi(\boldsymbol{x},t)] + \mu\mathcal{N}[\pi(\boldsymbol{x},t),\phi(\boldsymbol{x},t)]} . \tag{2.94}$$

The argument of the exponential could then be identified with iS. The only things stopping this identification are the integration limits and the path integral in the conjugate momentum π. The conclusion drawn is that a quantum field theory at finite temperature and in equilibrium can be evaluated by an analytic continuation of the time variable to the complex plane and by changing the integration path of the action to be along the imaginary axis.

This conclusion is powerful and is responsible for allowing us to perform Monte Carlo simulations. Of course, this also tells us that systems which are not in thermal equilibrium are not available to study by means of Monte Carlo simulations. Similarly, results from a Monte Carlo simulation cannot be extrapolated to real time, unless the desired observables are known, allowing us to perform the analytic continuation safely. This procedure is generally known as Wick rotation.

2.5 Quantum field theory example: the complex scalar field

We will take as an example a complex scalar field theory, with the fields interacting by means of a potential $V(|\phi|^2)$

$$\mathcal{L} \;=\; \partial_\mu\phi(x)\partial^\mu\phi^*(x) - m^2|\phi(x)|^2 - V(|\phi|^2)\,. \tag{2.95}$$

For the same reasons discussed in Section 2.1.1, this theory is symmetric under global phase transformations

$$\begin{aligned} \phi'(x) \;&=\; e^{i\alpha}\phi(x) \;\cong\; \phi(x) + i\alpha\phi(x) \\ \phi^{*\prime}(x) \;&=\; e^{-i\alpha}\phi^*(x) \;\cong\; \phi(x) - i\alpha\phi^*(x)\,. \end{aligned} \tag{2.96}$$

By means of the Noether theorem (see Section 2.3), we have that $\Omega_\phi = i\alpha$ and $\Omega_{\phi^*} = -i\alpha$. We then have that the conserved current is given by

$$j^\mu \;=\; i\left[\phi^*(x)\partial^\mu\phi(x) - \phi(x)\partial^\mu\phi^*(x)\right]\,. \tag{2.97}$$

The fields $\phi(x)$ and $\phi^*(x)$ are good degrees of freedom to notice the symmetry and derive its associated current. However, for the computation of the path integral, they are not the easiest degrees of freedom to work with. It will greatly simplify our lives to perform the following change of variables

$$\phi(x) \;=\; \frac{\phi_1(x) + i\phi_2(x)}{\sqrt{2}} \qquad \text{and} \qquad \phi^*(x) \;=\; \frac{\phi_1(x) - i\phi_2(x)}{\sqrt{2}}\,, \tag{2.98}$$

where $\phi_i(x) \in \mathbb{R}$, $i = 1, 2$. The Lagrangian is then written as

$$\mathcal{L} \;=\; \frac{1}{2}\left[\partial_\mu\phi_1\partial^\mu\phi_1 + \partial_\mu\phi_2\partial^\mu\phi_2 - m^2\left(\phi_1^2 + \phi_2^2\right)\right] - V\left(\frac{\phi_1^2 + \phi_2^2}{2}\right) \tag{2.99}$$

and the conserved current

$$j^\mu \;=\; \phi_2\partial^\mu\phi_1 - \phi_1\partial^\mu\phi_2\,. \tag{2.100}$$

We need to find the Hamiltonian for the theory. The first step is to consider the conjugate momentum of ϕ_i

$$\phi_i \;=\; \frac{\delta\mathcal{L}}{\delta\dot{\phi}_i} \;=\; \dot{\phi}_i\,, \tag{2.101}$$

where $\dot{\phi}_i = \partial_0 \phi_i$.

Now, we perform the usual Legendre transformation $\mathcal{H} = \pi_1 \dot{\phi}_1 + \pi_2 \dot{\phi}_2 - \mathcal{L}$ and obtain

$$\mathcal{H} = \frac{\pi_1^2}{2} + \frac{\pi_2^2}{2} + \frac{\left(\boldsymbol{\nabla}\phi_1\right)^2}{2} + \frac{\left(\boldsymbol{\nabla}\phi_2\right)^2}{2} + \frac{m^2}{2}\left(\phi_1^2 + \phi_2^2\right) + V\left(\frac{\phi_1^2 + \phi_2^2}{2}\right). \tag{2.102}$$

The next step is to input the above Hamiltonian in Eq. (2.94). Identifying as the conserved charge density the zero-th component of j^μ, i.e. $\mathcal{N} = \phi_2 \dot{\phi}_1 - \phi_1 \dot{\phi}_2 = \phi_2 \pi_1 - \phi_1 \pi_2$, we have that the expression inside the space-time integrals in Eq. (2.94) is

$$\begin{aligned} \pi_1 \dot{\phi}_1 + \pi_2 \dot{\phi}_2 - \frac{\pi_1^2}{2} - \frac{\pi_2^2}{2} - \frac{\left(\boldsymbol{\nabla}\phi_1\right)^2}{2} - \frac{\left(\boldsymbol{\nabla}\phi_2\right)^2}{2} - \frac{m^2}{2}\left(\phi_1^2 + \phi_2^2\right) - V\left(\frac{\phi_1^2 + \phi_2^2}{2}\right) \\ + \mu\left(\phi_2 \pi_1 - \phi_1 \pi_2\right). \end{aligned} \tag{2.103}$$

Notice that, since the path integral runs over ϕ_i *and* π_i, we cannot simply replace π_i by $\dot{\phi}_i$. In other words, they must be treated as independent of each other. The strategy adopted is to complete the squares for π_i. In this way, after a variable change, we will arrive at a Gaussian integral that can be trivially evaluated.

Let us forget for a moment the terms that depend only on ϕ_i and focus only on the ones depending on π_i. One can also notice that the dependence on the momentum π_2 is the same as the one for π_1, except for a sign in the term proportional to the chemical potential μ. Thus, we may write

$$\begin{aligned} \pi_i \dot{\phi}_i - \frac{\pi_i^2}{2} - (-1)^i \mu \phi_j \pi_i &= -\frac{1}{2}\left\{\pi_i^2 - 2\pi_i\left[\dot{\phi}_i - (-1)^i \mu \phi_j\right]\right\} \\ &= -\frac{1}{2}\left[\pi_i - \dot{\phi}_i + (-1)^i \mu \phi_j\right]^2 + \frac{1}{2}\left[\dot{\phi}_i - (-1)^i \mu \phi_j\right]^2, \end{aligned} \tag{2.104}$$

where $j = 1$ if $i = 2$ and vice-versa.

Upon expanding the term independent of π_i in Eq. (2.104), we obtain that Eq. (2.103) becomes

$$\begin{aligned} &\frac{1}{2}\left[\partial_\mu \phi_1 \partial^\mu \phi_1 + \partial_\mu \phi_2 \partial^\mu \phi_2 + \left(\mu^2 - m^2\right)\left(\frac{\phi_1^2 + \phi_2^2}{2}\right)\right] - V\left(\frac{\phi_1^2 + \phi_2^2}{2}\right) \\ &+ \mu\left(\dot{\phi}_1 \phi_2 - \dot{\phi}_2 \phi_1\right) - \frac{1}{2}\left[\left(\pi_1 - \dot{\phi}_1 - \mu \phi_2\right)^2 + \left(\pi_2 - \dot{\phi}_2 + \mu \phi_1\right)^2\right]. \end{aligned} \tag{2.105}$$

One then performs a variable transformation to "shifted" momentum coordinates $\tilde{\pi}_1 = \pi_1 - \dot{\phi}_1 - \mu \phi_2$ and $\tilde{\pi}_1 = \pi_2 - \dot{\phi}_2 + \mu \phi_1$. The integral to be evaluated is therefore

$$Z = \left(\int_P \mathcal{D}\phi_1 \mathcal{D}\phi_2 e^{i \int_0^{-i\beta} \int d^3x \, \mathcal{L}\left[\partial_\mu \phi_1, \partial_\mu \phi_2, \frac{\phi_1^2 + \phi_2^2}{2}\right]}\right) \times \tag{2.106}$$

$$\left(\int \mathcal{D}\tilde{\pi}_1 \mathcal{D}\tilde{\pi}_2 e^{-i \int_0^{-i\beta} \int d^3x \, \frac{\tilde{\pi}_1^2 + \tilde{\pi}_2^2}{2}}\right), \tag{2.107}$$

where

$$\mathcal{L}\left[\partial_\mu\phi_1,\, \partial_\mu\phi_2,\, \frac{\phi_1^2+\phi_2^2}{2}\right] = \frac{1}{2}\left[\partial_\mu\phi_1\partial^\mu\phi_1 + \partial_\mu\phi_2\partial^\mu\phi_2 + \left(\mu^2 - m^2\right)\left(\frac{\phi_1^2+\phi_2^2}{2}\right)\right] - V\left(\frac{\phi_1^2+\phi_2^2}{2}\right) + \mu\left(\dot{\phi}_1\phi_2 - \dot{\phi}_2\phi_1\right) \tag{2.108}$$

is an effective Lagrangian which incorporates the effects of the chemical potential.

To perform the integral in the shifted momentum, one discretizes the space-time into a hiper-cubic lattice of spacing a. The path integral is then written as a product of integrals, with an integral for each site. All integrals will be Gaussian and each one will bring a factor $\sqrt{2\pi}$. If we do not limit the space to be a box, there will be infinite factors. Even if limiting the space to be a box of side L, the number of factors will be $N_s^3 \times N_t$, where $N_s = L/a$ and $N_t = \beta/a$ are the number of lattice sites in the spatial and temporal directions, respectively. Then, as the limit $a \to 0$ is taken, the number of factors goes to infinity anyway.

The picture just described seems to be problematic. However, one must remember that we are never interested in the partition function by itself, but rather in some expectation value, as in Eq. (2.82). Now, suppose that an operator $\hat{A} = f[\hat{\phi}, \hat{\phi}^*]$ does not depend on the momenta conjugate to the fields. We can perform the same procedure as in Section 2.4.2 and in the current section and we would have arrived at Eq. (2.107) with $f[\hat{\phi}, \hat{\phi}^*]$ inside the integrand of the path integral. Therefore, the evaluation of the path integral in the shifted momentum results in the same constant as before. Since this will need to be divided by the partition function, the constant will be canceled and no divergence problem will be present in the computation of the expectation value of $\hat{A}$.

Eq. (2.108) has an interesting property, which is better seen when we rewrite the Lagrangian in terms of the complex fields ϕ and ϕ^*. After some algebra, one arrives at

$$\mathcal{L}\left[\partial_\mu\phi,\, \partial_\mu\phi^*,\, |\phi|^2\right] = |(\partial_0 - i\mu)\,\phi|^2 - |\boldsymbol{\nabla}\phi|^2 - m^2|\phi|^2 - V(|\phi|^2)\,. \tag{2.109}$$

Now, if one takes the Lagrangian in Eq. (2.95) and repeats the procedure of Section 2.1.1, generalizing the local symmetry to a global one, a gauge field will be introduced. This field is introduced by means of a covariant derivative $D_\mu = \partial_\mu - igA_\mu$. The Lagrangian in this case is

$$\mathcal{L}\left[\partial_\mu\phi,\, \partial_\mu\phi^*,\, |\phi|^2\right] = |(\partial_\mu - igA_\mu)\,\phi|^2 - m^2|\phi|^2 - V(|\phi|^2)\,. \tag{2.110}$$

Thus, the chemical potential enters in the Lagrangian in the same way as the temporal component of a gauge field.

With this, one writes the partition function as

$$Z = \int_P \mathcal{D}[\phi^*, \phi] \exp\left[i\int_0^{-i\beta}\int dt\, d^3x |(\partial_0 - i\mu)\,\phi|^2 - |\boldsymbol{\nabla}\phi|^2 - m^2|\phi|^2 - V(|\phi|^2)\right], \tag{2.111}$$

where $\mathcal{D}[\phi^*,\phi] = \mathcal{D}\phi^*\mathcal{D}\phi$. The expected value of an observable becomes

$$\langle \hat{A}[\hat{\phi}^*,\hat{\phi}]\rangle \;=\; \frac{1}{Z}\int_P \mathcal{D}\phi^*\mathcal{D}\phi\, A[\phi,\phi] e^{i\int_0^{-i\beta} dt \int d^3x |(\partial_0 - i\mu)\phi|^2 - |\boldsymbol{\nabla}\phi|^2 - m^2|\phi|^2 - V(|\phi|^2)}\,. \tag{2.112}$$

There is one further thing that must be said about the chemical potential. It breaks explicitly Lorentz symmetry. This is no surprise. It is associated to the charge density, which is reference-frame dependent, since it is a component of a four-vector. Thus, every time we use it, we will need to explicitly say which reference frame we are adopting.

We stress that, although we picked a rather simple theory, the general procedure stays the same for a more complex theory, e.g. QCD. The main feature needed for a similar procedure to be applicable is that the Hamiltonian needs to be quadratic in the conjugate momentum of the fields, without any other field accompanying these terms. This allows one to complete squares, and to perform the change of variables to the shifted momentum. This transforms the integral into a Gaussian one, enabling its easy evaluation.

There is one more similarity between this simple theory and QCD. When one introduces the chemical potential associated to the conservation of baryon number, it enters inside the fermionic Lagrangian in a similar way as in Eq. (2.109). In this case, it contributes to the Lagrangian as a temporal component of a complex gauge field, i.e. the fermionic Lagrangian becomes[29]

$$\mathcal{L}_F \;=\; \bar{\psi}\left(i\not{D} + i\gamma^0\mu - m\right)\psi\,. \tag{2.113}$$

The next step is then to define a suitable operator $\hat{A}$ and evaluate the path-integral. We refer to Eq. (2.92), which prescribes how to compute the path-integral. The introduction of a lattice to discretize space, with its removal through the limit $a \to 0$ is unavoidable. This should be made with care, or else infinities may appear. We leave the details of such computations for the next chapter.

Chapter 3

Lattice QCD

> "*Monte Carlo is an extremely bad method; it should be used only when all alternatives are worse.*"
>
> Alan D. Sokal
> Monte Carlo Methods in Statistical Mechanics: Foundations and New Algorithms (1996)

In Chapter 2 we overviewed field theories and derived the path integral formalism as a quantization method for them. However, we left pending the computation of observables. The reason for this is that a non-perturbative approach is mandatory when evaluating QCD path integrals. This is accomplished by numerical simulations. In this chapter, we will pick as a suitable observable an n-point correlation function and look in detail at its evaluation for the complex scalar field. Using perturbation theory, we will show that, for an interacting theory, the 2-point correlation function diverges if one naively takes the limit $a \to 0$. This indicates the need for a renormalization procedure. We will proceed to outline the Monte Carlo procedure for simulations of non-perturbative theories, such as QCD, and present a renormalization method for them.

3.1 Evaluation of n-point correlation functions

In Section 2.5, we concluded that the expectation value for an observable $\hat{A}$ is given by

$$\langle \hat{A} \rangle \;=\; \frac{1}{Z} \int \mathcal{D}\{\phi\}\, e^{iS[\{\phi\}]} A[\{\phi\}]\,, \tag{3.1}$$

where $\{\phi\}$ represents the set of fields in the theory. To evaluate the path-integral, we will Wick rotate to Euclidean space, which is more natural for a thermal theory. Thus, we will have that $x^0 = t = -i\tau = x_4$. As a consequence, the notation throughout this chapter will

be slightly different. An index μ runs from 1 through 4 and since the metric is $g_{\mu\nu} = \mathbb{1}$, there is no need to make a distinction between covariant and contravariant components.

We will continue the example of the complex scalar field from Chapter 2. The Lagrangian in Eq. (2.110) is in Minkowski space-time. Rotating to Euclidean time, one has

$$\begin{aligned} \mathcal{L} \;\to\; -\mathcal{L}_E \;&=\; -\left[(\partial_4+\mu)\,\phi^*\right]\left[(\partial_4-\mu)\,\phi\right] - |\boldsymbol{\nabla}\phi|^2 - m^2|\phi|^2 - V\left(|\phi|^2\right) \\ &=\; -|\partial_\mu\phi|^2 - \left(\mu^2+m^2\right)|\phi|^2 + \mu\left[\phi^*\left(\partial_4\phi\right) - \left(\partial_4\phi^*\right)\phi\right]\,. \end{aligned} \tag{3.2}$$

Thus, we rewrite Eq. (3.1) as

$$\langle\hat{A}\rangle_E \;=\; \frac{1}{Z_E}\int \mathcal{D}\left\{\phi\right\} e^{-S_E[\{\phi\}]} A[\{\phi\}]\,. \tag{3.3}$$

Since we will be working only in Euclidean time, we drop the index E from now on to avoid to clutter the notation.

As an operator $\hat{A}$, we will choose the n-point correlation function

$$\hat{A}[\hat{\phi}^*(x_1),\ldots,\hat{\phi}(x_n)] \;=\; \hat{\phi}^*(x_1)\hat{\phi}^*(x_2)\ldots\hat{\phi}^*(x_{n-m})\hat{\phi}^*(x_{n-m+1})\ldots\hat{\phi}(x_n)\,. \tag{3.4}$$

The motivation for such a choice comes from the usual operator approach to quantum field theories, where $\hat{\phi}^*$ and $\hat{\phi}$ are proportional to the creation/annihilation operators. Thus, when computing such correlation functions, we are creating and/or annihilating particles at positions $x_1,\ldots,x_n$.

The expectation value of the n-point function will be given by

$$\langle\hat{\phi}^*(x_1)\ldots\hat{\phi}(x_n)\rangle \;=\; \frac{1}{Z}\int_P \mathcal{D}[\phi^*(x)]\mathcal{D}[\phi^*(x)]\left[\phi^*(x_1)\ldots\phi(x_n)\right] e^{-S}\,. \tag{3.5}$$

The calculation is simplified by the introduction of the auxiliary currents $J^*(x)$ and $J(x)$ to the Lagrangian[i]

$$\mathcal{L}[J^*(x),J(x)] \;=\; \mathcal{L}_E + J^*(x)\phi(x)/\sqrt{2} + \phi^*(x)J(x)/\sqrt{2}\,. \tag{3.6}$$

The correlator then is written as

$$\langle\hat{\phi}^*(x_1)\ldots\hat{\phi}(x_{n+m})\rangle \;=\; \frac{1}{Z[J^*,J]}\left[\prod_{i=1}^{n}\frac{\delta}{\delta J(x_i)}\right]\left[\prod_{j=n+1}^{n+m}\frac{\delta}{\delta J^*(x_j)}\right] Z[J^*,J]\Big|_{J^*,\,J=0}\,, \tag{3.7}$$

$$Z[J^*,J] \;=\; \int_P \mathcal{D}[\phi^*(x)]\mathcal{D}[\phi^*(x)] e^{-\int_0^\beta\int d^3x\mathcal{L}[J^*,J]}\,. \tag{3.8}$$

The greatest advantage of this approach is that, if one is able to compute $Z[J^*,J]$ (up to a constant factor), one will be able to calculate any desired correlation function. In

[i] Since there is no time ordering of the operators, the computation that will be performed considers the exchanges $x_n \leftrightarrow x_m$. The factors $1/\sqrt{2}$ are to compensate extra numerical factors due to this exchange.

what follows, we derive a general formula for $Z[J^*, J]$ in the complex scalar field theory example.

As said before, it will be inevitable to evaluate the path integral with the introduction of a lattice discretizing space. This lattice will have N_τ sites in the temporal direction and N_s sites in the spatial directions. The spacing between nearest neighboring sites is denoted by a. The parameter a is such that $\beta = aN_\tau$. This fixes the size of the box in which we are containing our system to be $L = aN_\tau$. As we are taking a finite size lattice, boundary conditions must be imposed. We already have that the fields must be periodic in the time direction. A usual choice is to set periodic boundary conditions in the spatial directions as well. Although this choice is not mandatory, it is the one we will adopt here.

The introduction of the lattice also imposes the need to apply a suitable discretization for the action. For the time being, we will not dwell on a particular one. We will only make the hypothesis that

1. In the naive limit of $a \to 0$, the discretized action has as the limit the continuum one.

2. The discrete action may be written as

$$S \;=\; \sum_{n,m} \phi^*(m) K(m,n) \phi(n)\,, \tag{3.9}$$

where m, n are indexing lattice sites. We are also adopting the notation $\phi(n) = \phi(an)$.

As the above notation suggests, $K(m,n)$ is a matrix $N_s^3 N_\tau \times N_s^3 N_\tau$ and the fields are vectors of dimension $N_s^3 N_\tau$. This enables us to use a matrix multiplication notation, further simplifying the notation. The action is then written as $S = \phi^\dagger K \phi$.

Let us suppose that there exists a matrix M such as that $M^\dagger K M = \mathbb{1}$. We use it to perform the change of variables $\phi^\dagger = \varphi^\dagger M^\dagger$ and $\phi = M\varphi$. The Jacobian determinant for this change of variables is $\det(M^\dagger M)$. We write $Z[J, J^*]$ as

$$Z[J^\dagger, J] \;=\; \det(M^\dagger M) \int_P \mathcal{D}\varphi^\dagger \mathcal{D}\varphi \exp\left[-\varphi^\dagger \varphi + \frac{J^\dagger M \varphi}{\sqrt{2}} + \frac{\varphi^\dagger M^\dagger J}{\sqrt{2}} \right]. \tag{3.10}$$

Once again, we found a form very similar to a Gaussian integral. We can make it explicit by a new change of variables $\varphi = A + iB$ and $\varphi^\dagger = A^T - iB^T$, with A, B being matrices of real numbers. The Jacobian determinant in that case is[ii] $(-2i)^{N_s^3 N_\tau}$. We get

$$\begin{aligned} Z[J^\dagger, J] \;=\; & (-2i)^{N_s^3 N_\tau} \det(M^\dagger M) \times \\ & \int_P \mathcal{D}A \mathcal{D}B \;\; e^{-A^2 - B^2 + \frac{J^\dagger M A}{\sqrt{2}} + \frac{A^T M^\dagger J}{\sqrt{2}} + \frac{i J^\dagger M B}{\sqrt{2}} - \frac{i B^T M^\dagger J}{\sqrt{2}}}\,. \end{aligned} \tag{3.11}$$

[ii] To compute this determinant, one notices that the Jacobian matrix is a 2×2 block matrix $\begin{pmatrix} A & B \\ C & D \end{pmatrix}$, with each block proportional to $\mathbb{1}$. Then, the determinant is just $\det(AD - CB)$.

We may then complete squares

$$-A^2+\frac{J^\dagger MA}{\sqrt{2}}+\frac{A^T M^\dagger J}{\sqrt{2}} \;=\; -\left(A-\frac{M^\dagger J}{\sqrt{2}}\right)^\dagger\left(A-\frac{M^\dagger J}{\sqrt{2}}\right)+\frac{1}{2}J^\dagger MM^\dagger J\,, \tag{3.12}$$

$$-B^2+\frac{iJ^\dagger MB}{\sqrt{2}}+\frac{iB^T M^\dagger J}{\sqrt{2}} \;=\; -\left(B+i\frac{M^\dagger J}{\sqrt{2}}\right)^\dagger\left(M+i\frac{M^\dagger J}{\sqrt{2}}\right)+\frac{1}{2}J^\dagger MM^\dagger J\,. \tag{3.13}$$

At last, one may shift once again the variables to $\tilde{A}=A-M^\dagger J$ and $\tilde{B}=B+iM^\dagger J$, resulting in two Gaussian integrals. Each one will bring a factor $\pi^{N_s^3N_\tau/2}$. The result is finally

$$Z[J^\dagger,J] \;=\; (-2i\pi)^{N_s^3N_\tau}\det(M^\dagger M)e^{J^\dagger MM^\dagger J}\,. \tag{3.14}$$

It remains to determine M. To this end, we use its defining property $M^\dagger KM=\mathbb{1}$. If the matrix M has an inverse, we can right multiply $M^\dagger KM=\mathbb{1}$ by M^{-1} and left multiply it by $(M^\dagger)^{-1}$, resulting in $K=(M^\dagger)^{-1}M^{-1}$. Thus we conclude that $MM^\dagger=K^{-1}$ and we may write

$$Z[J^\dagger,J] \;=\; \frac{(-2i\pi)^{a^4L^3\beta}}{\det K}e^{J^\dagger K^{-1}J}\,. \tag{3.15}$$

Notice that the factor in front of the exponential is a constant, and will cancel out when computing correlation functions. Thus, in what follows, we will neglect it.

As an example, let us consider the two-point function $\langle\phi(n)\phi^*(m)\rangle$. The first functional derivative is with respect to J

$$\frac{\delta}{\delta J}Z[J^\dagger,J] \;=\; e^{J^\dagger K^{-1}J}J^\dagger K^{-1}\,. \tag{3.16}$$

Next, we take the derivative in $J^\dagger$

$$\frac{\delta^2}{\delta J^\dagger\delta J}Z[J^\dagger,J] \;=\; e^{J^\dagger K^{-1}J}\left[K^{-1}JJ^\dagger K^{-1}+K^{-1}\right]\,. \tag{3.17}$$

Thus, the *two-point correlation function* will be given by

$$\langle\phi(n)\phi^*(m)\rangle \;=\; \frac{1}{Z[J^\dagger,J]}\frac{\delta^2}{\delta J^\dagger\delta J}Z[J^\dagger,J]\bigg|_{J^\dagger,\,J=0} \;=\; K^{-1}(n,m)\,. \tag{3.18}$$

The problem now is to compute K^{-1}. To do so, we need to discuss a proper discretization of the action. For now, we will consider the Lagrangian in Eq. (3.2) with $V(|\phi|^2)=0$, i.e. a non-interacting theory. The dictionary to discretize the action will be similar to the one in Eq. (2.91). We get

$$\begin{aligned} S \;=\; & a^2\sum_n\sum_{\mu=1}^4\left[|\phi(n+\hat{\mu})|^2+|\phi(n)|^2-\phi^*(n+\hat{\mu})\phi(n)-\phi^*(n)\phi(n+\hat{\mu})\right] \\ & +a^4\left(\mu^2+m^2\right)\sum_n|\phi(n)|^2+a^3\mu\sum_n\left[\phi^*(n+\hat{4})\phi(n)-\phi^*(n)\phi(n+\hat{4})\right]\,, \end{aligned} \tag{3.19}$$

where the notation $n + m\hat{\mu}$ means that, starting from site n, one hops m sites in the direction $\hat{\mu}$. The symbol $\hat{\mu}$ stands for a unit vector to indicate one of the four directions in (Euclidean) space. It should not be confused with the chemical potential. It is usual to write the action in terms of dimensionless quantities[iii], denoted by a tilde on top of them. In our case this is implemented by means of by making the transformations $\tilde{\phi} = a\phi$, $\tilde{\phi^*} = a\phi^*$, $\tilde{m} = am$ and $\tilde{\mu} = a\mu$. We also point out that

$$\sum_n \sum_{\mu=1}^{4} \tilde{\phi}^*(n+\hat{\mu})\tilde{\phi}(n+\hat{\mu}) \;=\; \sum_n \sum_{\mu=1}^{4} \tilde{\phi}^*(n)\tilde{\phi}(n)\,, \tag{3.20}$$

$$\sum_n \sum_{\mu=1}^{4} \tilde{\phi}^*(n+\hat{\mu})\tilde{\phi}(n) \;=\; \sum_n \sum_{\mu=1}^{4} \tilde{\phi}(n)\tilde{\phi}^*(n-\hat{\mu})\,. \tag{3.21}$$

After some algebra using the above relations, we are able to write the action in the form of Eq. (3.9), with $K(n,m)$ given by

$$\begin{aligned} K(n,m) \;=\; & \sum_{\mu=1}^{4} \left[2\delta(n,m) - \delta(n,m+\hat{\mu}) - \delta(n,m-\hat{\mu})\right] \\ & + \tilde{\mu}\left[\delta(n,m+\hat{4}) - \delta(n,m-\hat{4})\right] + \left(\tilde{\mu}^2 + \tilde{m}^2\right)\delta(n,m)\,. \end{aligned} \tag{3.22}$$

Due to the translation symmetry, one may shift the entire lattice by a given amount and the action does not change. Thus, we say that $K(n,m) = K(n-m)$. With this in mind, we decompose $K(n-m)$ in its Fourier components

$$\begin{aligned} G(k) \;&=\; \left(\sum_{n_i=0}^{N_s-1}\right)^3 \sum_{n_4=0}^{N_\tau-1} K(n) \prod_{\mu=1}^{4} e^{i\frac{2\pi}{N_\mu}k_\mu n_\mu} \;\equiv\; \sum_{n_\mu}^{N_\mu} K(n) e^{i\frac{2\pi}{N_\mu}k_\mu n_\mu} \\ &=\; 4\sum_{\mu=1}^{4} \sin^2\left(\frac{\pi}{N_\mu}k_\mu\right) + 2i\tilde{\mu}\sin\left(\frac{2\pi}{N_\tau}k_4\right) + \tilde{\mu}^2 + \tilde{m}^2\,, \end{aligned} \tag{3.23}$$

where $k_\mu = -N_\mu/2, \ldots, N_\mu/2 - 1$. One writes $K(n-m)$ in terms of its components as

$$K(n-m) \;=\; \frac{1}{N_s^3 N_\tau} \sum_{k_\mu}^{N_\mu} G(k) e^{-i\frac{2\pi}{N_\mu}k_\mu(n_\mu - m_\mu)}\,. \tag{3.24}$$

On the other hand, one has that $K(n,m)K^{-1}(m,l) = \delta(n,l)$ and using Eq. (3.24) we may write

$$\frac{1}{N_s^3 N_\tau} \sum_{k_\mu}^{N_\mu} \sum_{m_\mu}^{N_\mu} G(k) e^{-i\frac{2\pi}{N_\mu}k_\mu(n_\mu - m_\mu)} K^{-1}(m,l) \;=\; \frac{1}{N_s^3 N_\tau} \sum_{k_\mu}^{N_\mu} e^{i\frac{2\pi}{N_\mu}k_\mu(l_\mu - n_\mu)}\,. \tag{3.25}$$

We may expand K^{-1} in its Fourier components as well

$$K^{-1}(m,l) \;=\; \frac{1}{N_s^3 N_\tau} \sum_{q_\mu}^{N_\mu} \Delta(q) e^{-i\frac{2\pi}{N_\mu}q_\mu(m_\mu - l_\mu)}\,, \tag{3.26}$$

[iii] In numerical simulations, this will be important to avoid sums of numbers differing by several orders of magnitude, which in turn would lead to larger numerical errors.

and insert it in Eq. (3.25). The sums in m_μ will result in a factor $N_s^3 N_\tau \delta(q,k)$. The delta may be eliminated by the sum in q_μ. Since the sums in k_μ are on both sides of the equation, one may drop them. The exponentials in both sides will be equal now, and thus cancel each other. The same happens for the remaining normalization factors $1/N_s^3 N_\tau$. As a result, one gets that $\Delta(k)G(k) = 1$. Thus, using this statement and Eqs. (3.18), (3.23) and Eq. (3.26), one arrives at

$$\langle \tilde{\phi}(n)\tilde{\phi}^*(m)\rangle \;=\; \frac{1}{N_s^3 N_\tau}\sum_{k_\mu}^{N_\mu} \frac{e^{-i\frac{2\pi}{N_\mu}k_\mu(n_\mu - m_\nu)}}{4\sum_{\mu=1}^{4}\sin^2\left(\frac{\pi}{N_\mu}k_\mu\right) + 2i\tilde{\mu}\sin\left(\frac{2\pi}{N_\tau}k_4\right) + \tilde{\mu}^2 + \tilde{m}^2}\,. \tag{3.27}$$

We must take the continuum limit and the limit of an infinite box $L \to \infty$. To this end, we bring out the lattice parameter a and write

$$a^2\langle \phi(x)\phi^*(y)\rangle \;=\; \frac{a^4}{L^3\beta}\sum_{k_\mu}^{N_\mu} \frac{e^{i\frac{2\pi}{L_\mu}k_\mu(x_\mu - y_\nu)}}{4\sum_{\mu=1}^{4}\sin^2\left(\frac{a}{2}\frac{2\pi}{L_\mu}k_\mu\right) + 2ia\mu\sin\left(a\frac{2\pi}{\beta}k_4\right) + a^2\left(\mu^2 + m^2\right)}\,, \tag{3.28}$$

where $L_4 = \beta = aN_\tau$ and $L_i = N_s$, for $i = 1,2,3$. To leave the expression in a more familiar form, we perform the variable change $\boldsymbol{p} = 2\pi\boldsymbol{k}/L$. The sum is now in steps of $\Delta p = 2\pi/L$

$$\begin{aligned}\langle \phi(x)\phi^*(y)\rangle \;=\; \frac{1}{(2\pi)^3\beta}\sum_{n_4=-\mathcal{N}_\tau/2}^{N_\tau/2-1}\sum_{p_i=-\pi/a}^{\pi/a-\Delta p}\Bigg[e^{i\boldsymbol{p}\cdot(\boldsymbol{x}-\boldsymbol{y})}e^{i\frac{2\pi}{\beta}aK_4(x_4-y_4)}\left(\Delta p\right)^3\Bigg/ \\ \frac{4}{a^2}\sum_{i=1}^{3}\sin^2\left(\frac{p_i}{2}\right) + \frac{4}{a^2}\sin^2\left(\frac{a}{2}\frac{2\pi}{\beta}K_4\right) + \frac{2i\mu}{a}\sin\left(\frac{a}{2}\frac{2\pi}{\beta}K_4\right) \\ + \mu^2 + m^2\Bigg]\,.\end{aligned} \tag{3.29}$$

Notice that we do not touch the temporal components. Now, we take the limit $L \to \infty$. This implies the limit $\Delta p \to 0$ in the expression above. This is the definition of a Riemann integral and we write

$$\begin{aligned}\langle \phi(x)\phi^*(y)\rangle \;=\; \frac{1}{\beta}\sum_{k=-N_\tau/2}^{N_\tau/2-1}\int_{-\frac{\pi}{a}}^{\frac{\pi}{a}}\frac{d^3p}{(2\pi)^3}\,e^{i\boldsymbol{p}\cdot(\boldsymbol{x}-\boldsymbol{y})}e^{i\omega_k(x_4-y_4)}\Bigg[\frac{4}{a^2}\sum_{i=1}^{3}\sin^2\left(\frac{ap_i}{2}\right) \\ + \frac{4}{a^2}\sin^2\left(\frac{a}{2}\omega_k\right) + 2i\frac{\mu}{a}\sin\left(a\omega_k\right) + \mu^2 + m^2\Bigg]^{-1}\,,\end{aligned} \tag{3.30}$$

where $\omega_k = 2\pi k_4/\beta$ is called the *Matsubara frequency*.[27] In the limit of zero temperature, we may apply the same procedure as for the spatial components and replace the sum by an integral over the spatial component of the four-momentum.

The example above is one particular case where we are able to take the naive continuum limit $a \to 0$ without any issues. For a small, we can approximate $\sin(ap_i/2) \approx ap_i/2$ and $\sin(a\omega_k/2) \approx a\omega_k^2/2$. Notice that, as we decrease a, we must increase N_τ to keep

$\beta = aN_\tau$ and thus $N_\tau \to \infty$. In this way, in the continuum limit, the two-point function becomes

$$\langle \phi(x)\phi^*(y)\rangle \;=\; \frac{1}{\beta}\sum_{k=-\infty}^{\infty}\int_{-\infty}^{\infty}\frac{d^3p}{(2\pi)^3}\,\frac{e^{i\boldsymbol{p}\cdot(\boldsymbol{x}-\boldsymbol{y})}e^{i\omega_k(x_4-y_4)}}{\boldsymbol{p}^2+\omega_k^2+2i\mu\omega_k+\mu^2+m^2}\,. \tag{3.31}$$

We stress that the components x_4 and y_4 are in the auxiliary imaginary-time and should not be interpreted as an actual time variable. This is the reason one does not worry about the time ordering of operators. However, it is possible to relate the thermal propagator to the vacuum one by means of a Wick rotation back to real time. The time ordering then will emerge automatically by means of an appropriate integration path choice.

3.1.1 Perturbation theory and Feynman graphs

A non-interacting theory has an academic importance due to its simplicity. However, typical physical systems do interact. We will devote this section to the treatment of interactions in the case of weakly interacting theories. This means that the potential can be written as

$$V(|\phi|^2) \;=\; \lambda f(|\phi|^2)\,, \qquad\qquad \lambda \;\ll\; 1\,. \tag{3.32}$$

We make such a choice because this is a case where an analytical calculation can be done. This allows us to expose what happens when the limit $a \to 0$ is taken in an interacting theory.

We start by breaking the action into the non-interacting part and the interacting part. Thus the exponential inside the path-integral becomes

$$\exp\left\{-S_E[J,J^\dagger]\right\} \;=\; \exp\left\{-S_0[J,J^\dagger]\right\}\left\{\sum_{n=0}^{\infty}\frac{(-1)^n}{n!}\left[\sum_{n_\mu}^{N_\mu}V\left(\left|\phi(n)^2\right|\right)\right]^n\right\}\,. \tag{3.33}$$

If V is polynomial, then one can generate it by means of functional derivatives of the auxiliary currents, i.e.

$$\exp\left\{-S_E[J,J^\dagger]\right\} \;=\; \sum_{n=0}^{\infty}\frac{(-1)^n}{n!}\left[\sum_{n_\mu}^{N_\mu}V\left(\frac{\delta^2}{\delta J(n)\delta J^*(n)}\right)\right]^n\exp\left\{-S_0[J,J^\dagger]\right\}\,. \tag{3.34}$$

In particular, if $\lambda \ll 1$ and one desires to compute the observable with a fixed precision, one may not need to evaluate all the terms of Eq. (3.34) and truncate the series at a given order.

As an example, we will take the potential $\lambda|\phi|^4$ and compute the two-point correlation function, truncating it after the first order. At order 0, we simply recover the free theory function. The interesting result happens at the first order. This will require

the computation of a fourth-order functional derivatives, which can get quite lengthy and tedious, although the procedure itself is simple. For this reason we will omit this calculation here, only stating the result after setting the auxiliary currents to zero

$$Z_1[0,0] \;=\; 2\lambda \sum_{m_\mu}^{N_\mu} K^{-1}(m,m)K^{-1}(m,m)\,, \tag{3.35}$$

$$\begin{aligned}\frac{\delta^2}{\delta J^\dagger(m)\delta J(n)} Z_1[J^\dagger,J]\bigg|_{J,\,J^\dagger=0} \;&=\; 2\lambda K^{-1}(m,n)\sum_{l_\mu}^{N_\mu} K^{-1}(l,l)K^{-1}(l,l) \\ &\quad + 4\lambda \sum_{l_\mu}^{N_\mu} K^{-1}(m,l)K^{-1}(l,l)K^{-1}(l,l)K^{-1}(l,n)\,.\end{aligned} \tag{3.36}$$

The above equations can be represented graphically if the following rules are applied:

- Each propagator $\Delta(q)$ is represented by a line.
- Every end point n of a propagator brings a factor $e^{(2\pi i/N_\mu)q_\mu n_\mu}$, where q is associated to the momentum of the propagator leaving point q. If the momentum is incoming, its sign is reversed.
- Each point which is summed over is called a vertex and brings a factor λ. It is represented by a dot.
- Each vertex is allowed to have only 4 lines attached to it.
- There is a sum over all momentum variables in each graph.

These rules are called Feynman rules, since Feynman was the one to propose this drawing method of notation. The graphs that originate from them are usually referred to as Feynman graphs or Feynman diagrams. Using this notation, one gets

$Z_1[0,0] \;=\; 2$ 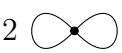 (3.37)

$\dfrac{\delta^2 Z_1[J^\dagger,J]}{\delta J^\dagger(m)\delta J(n)}\bigg|_{J,\,J^\dagger=0} \;=\; 2$ 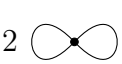 $\times\Big($  $\Big) + 4\Big($ 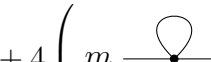 $\Big)\,.$ (3.38)

The two-point correlation function, computed up to first order, will then be

$\langle\hat\phi(m)\hat\phi^*(n)\rangle \;=\;$ 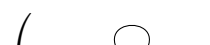 $- 4\Big($  $\Big) \Big/ \Big(1 - 2$ $\Big)\,.$ (3.39)

Notice that the infinity shaped graph amounts to a numerical constant. We leave to deal with it later and focus on the one with the loop attached to it. We will consider the

case of an infinite box, thus avoiding to deal with finite-size effects. To make notation more compact, we will take the case of zero temperature. Lastly, to simplify the calculations, we take the case of zero chemical potential as well. We have

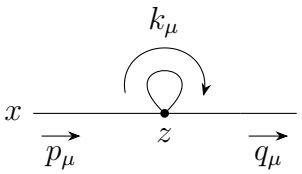

$$
\begin{aligned}
&= \int_{-\pi/a}^{\pi/a} \frac{d^4p}{(2\pi)^4}\frac{d^4q}{(2\pi)^4}\frac{d^4k}{(2\pi)^4}\times \\
&\quad \int d^4z\, \frac{e^{ip_\mu(x-z)_\mu}}{\frac{4}{a^2}\sum_\mu \sin^2\left(\frac{ap_\mu}{2}\right)+m^2}\times \\
&\quad \frac{e^{-iq_\mu(y-z)_\mu}}{\frac{4}{a^2}\sum_\mu \sin^2\left(\frac{aq_\mu}{2}\right)+m^2}\frac{\lambda}{\frac{4}{a^2}\sum_\mu \sin^2\left(\frac{ak_\mu}{2}\right)+m^2} \\
&= \int_{-\pi/a}^{\pi/a} \frac{d^4p}{(2\pi)^4}\frac{d^4k}{(2\pi)^4}\frac{e^{ip_\mu(x-y)_\mu}}{\left[\frac{4}{a^2}\sum_\mu \sin^2\left(\frac{ap_\mu}{2}\right)+m^2\right]^2}\times \\
&\quad \frac{\lambda}{\frac{4}{a^2}\sum_\mu \sin^2\left(\frac{ak_\mu}{2}\right)+m^2}\,.
\end{aligned}
\tag{3.40}
$$

Notice that the integration region is finite and all poles are outside it. Thus, the above integral is finite. However, if we take the continuum limit of $a \to 0$ naively, we have

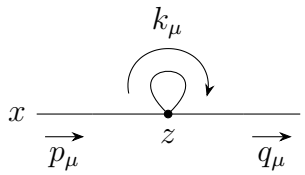

$$
\underset{a\to 0}{=} \int_{-\infty}^{\infty} \frac{d^4p}{(2\pi)^4}\frac{d^4k}{(2\pi)^4}\frac{e^{ip_\mu(x-y)_\mu}}{\left(p^2+m^2\right)^2}\frac{\lambda}{k^2+m^2}\,. \tag{3.41}
$$

Let us evaluate the integral in k. We notice that the integrand is even and thus we can replace the integration limits to be from 0 to ∞ in each one of the 4 integrals. Next, we perform a variable change to (hyper-)spherical coordinates. We get

$$
\int_{-\infty}^{\infty} \frac{d^4k}{(2\pi)^4}\frac{\lambda}{k^2+m^2} = \frac{\lambda}{\pi^4}\int_0^\infty \frac{k^3\,dk}{k^2+m^2}\int d\Omega = \frac{\lambda\Omega}{\pi^4}\int_0^\infty \frac{k^3\,dk}{k^2+m^2}\,. \tag{3.42}
$$

Next, one makes the change of variables $k = \sqrt{p^2-m^2}$. The integral becomes

$$
\frac{\lambda\Omega}{\pi^4}\int_m^\infty \frac{p^2-m^2}{p}dp \to \infty\,. \tag{3.43}
$$

Thus, the integral in k, which was amounting to just a finite numerical factor inside the propagator, diverges when we take the continuum limit naively. This is nothing different from the usual divergences one finds in quantum field theory textbooks. A renormalization procedure must be taken. Therefore, we are able to interpret the lattice not just as a mathematical trick used to compute the path-integral, but as a regularization of the theory, with the regulator being the lattice spacing. And as in any renormalizable theory, its bare

parameters (masses and couplings) depend on the regulator. Consequently, the continuum limit process consists in varying the bare parameters of the theory in such a way as to keep an observable evaluated at a given energy scale constant. The value that one fixes for the observable is usually taken (but not necessarily) to be its value as experimentally measured.

We used the complex scalar theory due to its simplicity. However, such issues appear in gauge theories as well. We will not dwell further on how to renormalize a perturbative theory. This is because we are interested in QCD, which has a running coupling that prevents us from performing this perturbative approach when studying low-energy phenomena. The reason is because the interaction coupling gets of order one or more at low energies. Instead, we will proceed to the description of QCD's discretization on the lattice and the calculation of observables using Monte Carlo simulations. We will return to the topic of renormalization as one of the steps of performing the simulation.

3.2 Discretization of the Yang-Mills action

Quantum Chromodynamics is built as a gauge theory with SU(3) symmetry group. The fermions carrying color charge come in six "flavors", each one with its own mass. We write the QCD Lagrangian (in Minkowski space-time) as

$$\mathcal{L}_{\text{QCD}} \;=\; \sum_{f=1}^{6} \bar{\psi}^f \left(i\gamma^\mu \partial_\mu + g_0 \gamma^\mu A_\mu - m_0^f \right) \psi^f \;-\; \frac{1}{2} \operatorname{Tr} \left[F_{\mu\nu} F^{\mu\nu} \right] . \tag{3.44}$$

Notice that we attached a 0 subscript to the coupling and to the mass. This is to indicate that these are the bare parameters of the theory, which are different from the "dressed" parameters that appears after a renormalization procedure takes place.

An operator $\hat{A}$ will depend on the fields $\bar{\psi}^f$, ψ^f and A_μ. In this way, we write the expectation value of $\hat{A}$ as

$$\langle \hat{A}[\bar{\psi}^f, \psi^f, A_\mu] \rangle \;=\; \frac{1}{Z} \left(\prod_{f=1}^{6} \int \mathcal{D}[\bar{\psi}^f] \mathcal{D}[\psi^f] \right) \mathcal{D}[A_\mu] A[\bar{\psi}^f, \psi^f, A_\mu] \times \\ e^{i \int_0^{-i\beta} dt \int d^3x \mathcal{L}_{\text{QCD}}[\bar{\psi}^f, \psi^f, A_\mu]} . \tag{3.45}$$

As was done for the complex scalar field, we will perform a Wick rotation to Euclidean time. However, here we have to Wick rotate the Dirac matrices as well, since their defining property is metric dependent, i.e. they must obey $\{\gamma_\mu, \gamma_\nu\} = 2\delta_{\mu\nu}$. Furthermore, we have a vector field (A_μ), which must be Wick rotated as well. We summarize the transformations that one must perform below [see Ref. 30 for the Wick rotations of the Dirac matrices]

$$\gamma^{0,\,M} \;=\; \gamma^4 , \qquad \gamma^{i,\,M} \;=\; i\gamma_i , \qquad \partial_0 \;=\; i\partial_4 \qquad \text{and} \qquad A^0 \;=\; -iA_4 . \tag{3.46}$$

For the moment, let us look only at the fermionic term of the Lagrangian. Also, since for all flavors the Lagrangian has the same form, we will consider just one of them. This cleans up the notation and we just need to remember that later we will need to sum over all flavors. With this in mind, we have that the fermionic term in the Lagrangian transforms as

$$\begin{aligned}\mathcal{L}_F &= \bar{\psi}\left(i\gamma^{0,M}\partial_0 + i\gamma^{i,M}\partial_i + g_0\gamma^{0,M}A^0 - g_0\gamma^{i\,M}A^i - m_0\right)\psi \\ &= \bar{\psi}\left(-\gamma_4\partial_4 - \gamma_i\partial_i - ig_0\gamma_0 A_0 - ig_0\gamma_i A_i - m_0\right)\psi \\ &= -\bar{\psi}\left(\gamma_\mu\partial_\mu + ig_0\gamma_\mu A_\mu + m_0\right) = -\mathcal{L}_{F,E}\,.\end{aligned} \tag{3.47}$$

We then turn to the gauge term of the Lagrangian. The sum $F_{\mu\nu}F^{\mu\nu}$ can be rewritten as $-2F^{0i}F^{0i} + 2F_{ij}F^{ij}$. Thus we need only to learn how F^{0i} transforms. We see that

$$F^{0i} = \partial^0 A^i - \partial^i A^0 - ig_0\left[A^0,\, A^i\right] = -i\partial_4 A_i + i\partial_i A_4 - ig_0\left[-iA_4\, A_i\right] = -iF_{4i}\,. \tag{3.48}$$

Therefore the gauge Lagrangian transforms as

$$\begin{aligned}\mathcal{L}_G &= \mathrm{Tr}\left[F^{0i}F^{0i} - F^{ij}F^{ij}\right] = -\,\mathrm{Tr}\left[F_{4i}F_{4i} + F_{ij}F_{ij}\right] \\ &= -\frac{1}{2}\,\mathrm{Tr}\left[F_{\mu\nu}F_{\mu\nu}\right] = -\mathcal{L}_{G,E}\,.\end{aligned} \tag{3.49}$$

From these results, we write the Euclidean Lagrangian as

$$\mathcal{L}_E = \sum_f \bar{\psi}^f\left(\gamma_\mu\partial_\mu + ig_0\gamma_\mu A_\mu + m_0\right)\psi^f + \frac{1}{2}\,\mathrm{Tr}\left[F_{\mu\nu}F_{\mu\nu}\right]\,. \tag{3.50}$$

The expectation value of an observable will be similar to the one in Eq. (3.45), but with the Minkowski Lagrangian replaced by the Euclidean one, the imaginary number in front of the action replaced by a negative sign and the temporal integration limit now running from 0 to β.

With this, we are ready to discretize the theory's action. The strategy, once again, is to consider gauge and fermionic actions separately. Since the fermionic Lagrangian contains the gauge field, it will be simpler to discretize first the gauge action and only then proceed to the fermionic action.

3.2.1 Discretization of the gauge action

The discretization of the gauge action was performed in the author's dissertation in [Ref. 19, Chap. 3]. For completeness, it is reproduced here, with some minor adaptations.

In Eq. (2.31) we see that, in order to compare two fields infinitesimally near each other, one must transport one of them using the factor $e^{iagA_\mu(x)^a T^a}$. Now we wish to describe this transport on a lattice of spacing a between neighboring sites. The transport

through lattice sites can be described as a hopping between neighboring sites. As the particle hops between these sites, it gains the corresponding phase factor. In this way, we can associate an $SU(N)$ group element $U_\mu(x)$ to each link between two adjacent sites (see Fig. 2). The notation used means that this group element corresponds to the lattice link between the points x and $x + a\hat{\mu}$.

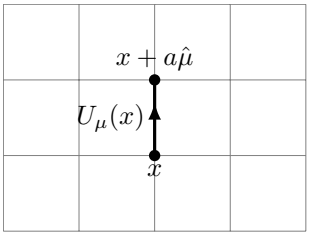

Figure 2 – Visual representation of the association of a group element $U_\mu(x)$ to a link of the lattice. Notice that this defines a "forward direction as well". Source: SERENONE.[19]

Since after the parallel transport $U_\mu(x)\psi(x + a\hat{\mu})$ must behave under gauge transformations as the field at point x, the group element $U_\mu(x)$ behaves under gauge transformations as[iv]

$$U_\mu(x) \;\rightarrow\; V(x)U_\mu(x)\,V^\dagger(x + a\hat{\mu})\,, \tag{3.51}$$

where $V(x)$ is an $SU(N)$ group element as well, associated to the lattice site at position x.

Having discretized the space on a lattice, we can shift the dependence of $U_\mu(x)$ on $A_\mu(x)$ to the position $x + a\hat{\mu}/2$, since we later take the continuum limit $a \to 0$, returning to the original definition. Thus, on the lattice, we relate $U_\mu(x)$ to A_μ by

$$U_\mu(x) \;=\; \exp\left[ig_0 a A_\mu(x + a\hat{\mu}/2)\right]. \tag{3.52}$$

Once we attribute a group element to every link of the lattice, we have fixed a field configuration. If a different configuration is desired, it will be enough to just change the group elements associated with each link. Also, Eq. (3.52) defines a forward direction. With this, we can define oriented closed loops on the lattice. This is achieved by multiplying the group elements of links in the closed loop and taking the trace

$$W(C) \;=\; \mathrm{Tr}\left[\prod_x U_\mu(x)\right], \tag{3.53}$$

where the variable x in the product runs over all the lattice points in the loop. Note that this will require some links to be oriented in the backward direction. When this

[iv] This explanation seems in conflict with the derivation of the covariant derivative in Section 2.1.1. However, one must remember that the derivation there was done in Minkowski space. In Euclidean space the parallel transport must act on $\psi(x + a\hat{\mu})$ instead, to correctly reproduce the sign of $A_\mu(x)$ in Eq. (3.47). Then, $U_\mu(x)$ must gauge transform as stated here.

happens, we must use the inverse element $U_\mu^{-1}(x)$, or equivalently $U_\mu^\dagger(x) \equiv U_{-\mu}(x + a\hat{\mu})$. It is important to notice that these closed loops are gauge-invariant [see Eq. (3.51)]. They are called Wilson loops and play a central role in lattice studies, both for analytical calculations and for computational simulations.

Finally, we need to build an action to use in the statistical weight. This action must correspond, in the limit $a \to 0$, to the integral of Eq. (3.49). We note that $F_{\mu\nu}^a$ is a generalized form of curl. This information can be used to motivate the action in the following way. Firstly we define as a *plaquette* the elementary square on a lattice, i.e. a square of side a (see Fig. 3). Each one of these plaquettes corresponds to the smallest

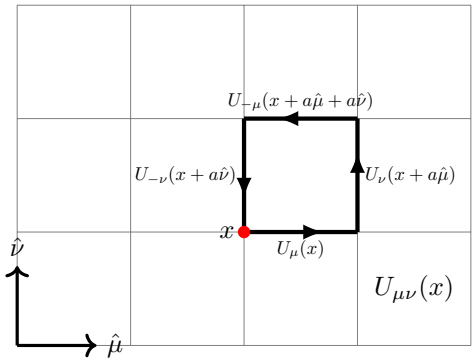

Figure 3 – A graphical representation of a plaquette. Source: SERENONE.[19]

possible closed loop on the lattice, i.e. in some sense, it is a discretized version of a curl on the lattice. The resulting action, introduced by Wilson in 1974,[31] is given by

$$S \;=\; \sum_x \sum_{C(\mu,\nu)} S_{\mu\nu}(x)\,, \tag{3.54}$$

where $C(\mu, \nu)$ stands for the six possible combinations of μ and ν, i.e. we have to consider the plaquettes at point x on all the six planes $[(1,2), (1,3), (1,4), (2,3), (2,4), (3,4)]$. We also sum over all lattice points x. Essentially, $S_{\mu\nu}(x)$ is a quantity that depends on a given plaquette and we are summing over all *oriented* plaquettes on the lattice. We have

$$\begin{aligned} S_{\mu\nu}(x) \;&\equiv\; \beta_0 \left\{ 1 - \frac{1}{N} \Re \operatorname{Tr} \left[U_\mu(x)\, U_\nu(x + a\hat{\mu})\, U_{-\mu}(x + a\hat{\mu} + a\hat{\nu})\, U_{-\nu}(x + a\hat{\nu}) \right] \right\} \\ &\equiv\; \beta_0 \left\{ 1 - \frac{1}{N} \Re \operatorname{Tr} U_{\mu\nu}(x) \right\}\,, \end{aligned} \tag{3.55}$$

where $\Re$ indicates the real part of the trace and N is the dimension of the group matrices, e.g. $N = 2$ for the $SU(2)$ group. Notice that $S_{\mu\nu}$ is clearly gauge-invariant and therefore the Wilson action preserves gauge symmetry exactly, for any value of a. The factor β is related to the bare coupling g_0 by

$$\beta_0 \;=\; \frac{2N}{g_0^2}\,, \tag{3.56}$$

in order to reproduce the gauge action in Eq. (3.49) as we take the limit of zero lattice spacing. To verify this, let us consider a particular plane (μ, ν). We use the Baker–Campbell–Hausdorff formula to reduce $U_{\mu\nu}$ [defined in Eq. (3.55)] to a single exponential. We will keep in our expansion terms up to order a^2 and therefore we can ignore terms containing commutators of commutators. We Taylor expand $A_\mu(x)$ assuming small values of a. The first step consists in calculating $U_\mu(x)U_\nu(x+a\hat{\mu})$

$$\begin{aligned} U_\mu\left(x\right) U_\nu\left(x+a\hat{\mu}\right) &= e^{ig_0 a A_\mu\left(x+\frac{a}{2}\hat{\mu}\right)} e^{ig_0 a A_\nu\left(x+a\hat{\mu}+\frac{a}{2}\hat{\nu}\right)} \\ &\approx e^{ig_0 a\left[A_\mu\left(x+\frac{a}{2}\hat{\mu}\right)+A_\nu\left(x+a\hat{\mu}+\frac{a}{2}\hat{\nu}\right)\right]} e^{\frac{g_0^2 a^2}{2}\left[A_\mu\left(x+\frac{a}{2}\hat{\mu}\right),\, A_\nu\left(x+a\hat{\mu}+\frac{a}{2}\hat{\nu}\right)\right]} . \end{aligned} \tag{3.57}$$

For the calculation of $U_{\mu\nu}(x)$ we need also the expression for $U_{-\nu}(x+a\hat{\nu})U_{-\mu}(x+a\hat{\nu}+a\hat{\mu}) = [U_\nu(x)U_\mu(x+a\hat{\nu})]^\dagger$. Notice that if we make the transformation in the indices $\mu \to \nu$ and $\nu \to \mu$, we obtain that $U_\mu(x)U_\nu(x+a\hat{\mu}) \to U_\nu(x)U_\mu(x+a\hat{\nu})$. Therefore these transformations allow us to get an expression for $U_\nu(x)U_\mu(x+a\hat{\nu})$ from Eq. (3.57). We are now able to calculate $U_{\mu\nu}(x)$

$$\begin{aligned} U_{\mu\nu}(x) &= \left[U_\mu\left(x\right) U_\nu\left(x+a\hat{\mu}\right)\right]\left[U_\nu\left(x\right) U_\mu\left(x+a\hat{\nu}\right)\right]^\dagger \\ &\approx \exp\Big\{ ig_0 a A_\mu\left(x+a\hat{\mu}/2\right) + ig_0 a A_\nu\left(x+a\hat{\mu}+a\hat{\nu}/2\right) \\ &\quad - \frac{g_0^2 a^2}{2}\left[A_\mu\left(x+a\hat{\mu}/2\right),\, A_\nu\left(x+a\hat{\mu}+a\hat{\nu}/2\right)\right] \\ &\quad - ig_0 a A_\nu\left(x+a\hat{\nu}/2\right) - ig_0 a A_\mu\left(x+a\hat{\nu}+a\hat{\mu}/2\right) \\ &\quad - \frac{g_0^2 a^2}{2}\left[A_\nu\left(x+a\hat{\nu}/2\right),\, A_\mu\left(x+a\hat{\nu}+a\hat{\mu}/2\right)\right]^\dagger \Big\} \times \\ &\quad \exp\Big\{ g_0^2 a^2 [A_\mu\left(x+a\hat{\mu}/2\right),\, A_\nu\left(x+a\hat{\nu}/2\right)] \\ &\quad + g_0^2 a^2 [A_\mu\left(x+a\hat{\mu}/2\right),\, A_\mu\left(x+a\hat{\nu}+a\hat{\mu}/2\right)] \\ &\quad + g_0^2 a^2 [A_\nu\left(x+a\hat{\mu}+a\hat{\nu}/2\right),\, A_\nu\left(x+a\hat{\nu}/2\right)] \\ &\quad + g_0^2 a^2 [A_\nu\left(x+a\hat{\mu}+a\hat{\nu}/2\right),\, A_\mu\left(x+a\hat{\nu}+a\hat{\mu}/2\right)] \Big\} . \end{aligned} \tag{3.58}$$

We proceed to perform the Taylor expansion around small a. In the first exponential in Eq. (3.58) we expand up to first order in a, since each A_μ is accompanied by an a and therefore this will result in terms of order up to a^2. For the second exponential, each term in it is already of order a^2, so the expansion must be carried until zeroth order. It is easy to see that with this expansion the argument of the second exponential will be zero and therefore we focus on the expansion in the first exponential. We obtain

$$\begin{aligned} U_{\mu\nu}(x) &= \exp\Big\{ -ig_0 a^2 \left[\partial_\mu A_\nu(x) - \partial_\nu A_\mu(x)\right] - g_0^2 a^2 \left[A_\mu(x),\, A_\nu(x)\right] + \mathcal{O}(a^4)\Big\} \\ &= \exp\left[-ig_0 a^2 F_{\mu\nu} + \mathcal{O}(a^3)\right] . \end{aligned} \tag{3.59}$$

We proceed to Taylor expand the exponential

$$U_{\mu\nu}(x) \;=\; \mathbb{1} \;-\; ig_0a^2F_{\mu\nu} \;-\; \frac{g_0^2a^4}{2}F_{\mu\nu}^2 \;+\; \mathcal{O}(a^6)\,. \tag{3.60}$$

We use Eq. (3.60) in Eq. (3.55) to obtain the contribution of a single plaquette to the action in the limit of small a

$$\begin{aligned} S_{\mu\nu}(x) \;&=\; \beta\left[1-\frac{1}{N}\Re\left(\operatorname{Tr}\mathbb{1}\right)+\frac{g_0a^2}{N}\Re(i\operatorname{Tr}F_{\mu\nu})+\frac{g_0^2a^4}{2N}\Re\left(\operatorname{Tr}F_{\mu\nu}^2\right)\right] \\ &=\; \beta\,\frac{g_0^2a^4}{2N}\Re\left(\operatorname{Tr}F_{\mu\nu}^2\right) \;=\; \operatorname{Tr}\left[\frac{\beta g_0^2a^4}{4N}\left(F_{\mu\nu}F_{\mu\nu}+F_{\mu\nu}^*F_{\mu\nu}^*\right)\right] \\ &=\; \frac{\beta g_0^2a^4}{2N}\operatorname{Tr}\left(F_{\mu\nu}F_{\mu\nu}\right)\,. \end{aligned} \tag{3.61}$$

Notice that $S_{\mu\nu}$ is the contribution of a single plaquette to the action and therefore Einstein's sum rule does not apply for $F_{\mu\nu}F_{\mu\nu}$. The following step is to sum over the plaquettes $S_{\mu\nu}(x)$ of the entire lattice and take the limit $a\to 0$

$$\sum_x \frac{\beta g_0^2a^4}{2N}\operatorname{Tr}\left[F_{\mu\nu}(x)F_{\mu\nu}(x)\right] \quad\to\quad \frac{\beta g_0^2}{2N}\int d^4x\;\; \operatorname{Tr}\left[F_{\mu\nu}(x)F_{\mu\nu}(x)\right]\,. \tag{3.62}$$

When we sum this result over all the six possible planes, we obtain

$$\begin{aligned} S \;=\; \frac{\beta g_0^2}{2N}\int d^4x\operatorname{Tr}\left[F_{41}(x)F_{41}(x)+F_{42}(x)F_{42}(x)+F_{43}(x)F_{43}(x)\right. \\ \left.+\,F_{12}(x)F_{12}(x)+\,F_{13}(x)F_{13}(x)+F_{23}(x)F_{23}(x)\right]\,, \end{aligned} \tag{3.63}$$

which can now be written using Einstein's sum rule as

$$S \;=\; \frac{\beta g_0^2}{2N}\int d^4x\frac{1}{2}\operatorname{Tr}\left[F_{\mu\nu}F_{\mu\nu}\right]\,. \tag{3.64}$$

The factor $1/2$ comes from the fact that, when we sum over the indices, there will be terms $F_{\mu\nu}F_{\mu\nu}$ as well as $F_{\nu\mu}F_{\mu\nu}=F_{\mu\nu}F_{\mu\nu}$.

We compare the result in Eq. (3.64) with Eq. (3.50) integrated (with the fermion fields ψ set to zero). We see that the choice made in Eq. (3.56) makes the lattice action equivalent to the Euclidean action, as we desired to show.

3.2.2 Discretization of the fermionic action

The discretization of the fermionic field is somewhat simpler. For the covariant derivative, one uses the symmetric discretization of variables, as it has a smaller numerical error. However, as was done in the definition of the covariant derivative in Eq. (2.31), one must parallel transport the fields to the central point x. Thus, the discretization of the covariant derivative is written as

$$D_\mu\psi(x) \;\to\; \frac{U_\mu(m)\psi(m+\hat{\mu})-U_{-\mu}(m)\psi(m-\hat{\mu})}{2a}\,. \tag{3.65}$$

Given the above discretization, a candidate to the discrete fermionic action for the flavor f is

$$S_f = a^4 \sum_{m,n} \bar{\psi}^f(m) \left[\sum_{\mu=1}^{4} \gamma_\mu \frac{U_\mu(m)\delta(m+\hat{\mu},n) - U_{-\mu}(m)\delta(m-\hat{\mu},n)}{2a} + m_0^f \delta(m,n) \right] \psi^f(n) \,. \tag{3.66}$$

There is one particularity that must be said about fermions: due to Fermi-Dirac statistics, the order they appear in an observable matters. As an example, for fermion fields at two different positions, one have $\psi_{\alpha a}(x)\psi_{\beta b}(y) = -\psi_{\beta b}(y)\psi(x)_{\alpha a}$. For this reason, the field components cannot be treated as usual complex numbers. Instead, they are treated as *Grassmann numbers*. These variables have a peculiar behavior, e.g. an integral and a derivation over them acts in the same fashion.[30,32–33] Also, due to the anti-commutative property, we have that $\psi_i^2 = 0$, meaning that any function of Grassmann variables can be Taylor expanded to first order and the expansion will be exact. Beside the new algebra introduced, the core idea of introducing auxiliary currents conjugate to the fields and computing generating functionals is kept. Since it will require just a bit of algebra, we will not describe the entire procedure, but show the final result, which is called Wick's theorem[30]

$$\begin{aligned} &\langle \psi_{\alpha_1 a_1}(x_1)\bar{\psi}_{\beta_1 b_1}(y_1) \dots \psi_{\alpha_n a_n}(x_n)\bar{\psi}_{\beta_n b_n}(y_n)\rangle_F \\ &\quad = (-1)^n \sum_{P(1,2,\dots,n)} \operatorname{sign}(P) K^{-1}_{\alpha_1 a_1,\, \beta_{P_1} b_{P_1}}(x_1, y_{P_1}) \dots K^{-1}_{\alpha_n a_n,\, \beta_{P_n} b_{P_n}}(x_n, y_{P_n}) \,, \end{aligned} \tag{3.67}$$

where the $\langle\cdot\rangle_F$ means that the average is taken only in terms of the fermions, i.e. only the path integrals with respect to the fermions where performed. Thus, in general, the matrix K^{-1} holds a dependence on the gauge fields, which must be integrated.

A simple case where K^{-1} does not depend on the gauge links is the case of free fermions, i.e. with $U_\mu(x) = \mathbb{1}$. Then one may use the discretization in Eq. (3.66) to compute the two-point correlation function $\langle \psi_{\alpha a}(x)\bar{\psi}_{\beta b}(y)\rangle$. The result in momentum space is

$$\Delta(q) = \frac{m_0 \mathbb{1} - \frac{i}{a}\sum_{\mu=1}^{4} \gamma_\mu \sin(a p_\mu)}{m_0^2 + \frac{1}{a^2}\sum_{\mu=1}^{4} \sin^2(a p_\mu)} \,. \tag{3.68}$$

Consider the case where we take the bare mass to 0. We know that in the continuum this will yield a double pole at $p = 0$. However, in this case, there will be also poles at $p = (\pi/a, 0, 0, 0)$, $p = (\pi/a, \pi/a, 0, 0)$, ... and so on. These poles are nonphysical and are a result of the discretization adopted. The presence of such "doublers" was noticed by K. Wilson, shortly after he proposed the lattice approach to quantum field theories.[34] It was him who also proposed as solution to add a term to the discretized action which behaves as a mass term when one of the momenta $p_\mu = \pi/a$. This term is usually refereed

as the Wilson term and is given by

$$-a\sum_{\mu=1}^{4}\frac{U_\mu(m)\delta(m+\hat{\mu},n)-2\delta(n,m)+U_{-n}(m)\delta(m-\hat{\mu},n)}{2a^2}\,. \tag{3.69}$$

The prefactor a guarantees us that, in the naive continuum limit, it vanishes. At the same time, this term adds to the bare mass a quantity proportional to $1/a$ when $p_\mu = \pi/a$ and nothing when $p_\mu = 0$. Consequently, as we take $a \to 0$, the mass of the doublers becomes infinity and they do not affect the physics of the propagator. The Wilson action is then written as

$$\begin{aligned} S_W \;=\; a^4\sum_f\sum_{m,n}\bar{\psi}^f(m)\Bigg[&\left(m_0^f+\frac{4}{a}\right)\delta(m,n) \\ &-\frac{1}{2a}\sum_{\mu=\pm1}^{\pm4}\left(\mathbb{1}-\gamma_\mu\right)U_\mu(m)\delta(m+\hat{\mu},n)\Bigg]\psi^f(n)\,, \end{aligned} \tag{3.70}$$

where $\gamma_{-\mu} = -\gamma_\mu$.

The Wilson action is not perfect. For instance, since the up and down quarks are very light (a couple of megaelectron volts), it is common to consider QCD at energy scales smaller than the strange mass to posses chiral symmetry, i.e. to neglect quark masses. However, the Wilson action explicitly breaks chiral symmetry. Thus, if one desires to study a phenomenon sensitive to chiral symmetry, as the chiral condensate $\langle\bar{\psi}\psi\rangle$ or the pion mass, the Wilson action is not the ideal tool. In the example, one may desire to use the *staggered fermions* action, which partially restore chiral symmetry, but at the cost of restoring some (but not all) doublers. Another approach is called *domain wall fermions* and consists of considering a fifth dimension for fermions and taking only its 4D boundary values at this extra dimension to compute observables. With this, one may restore chiral symmetry, but it is much more expensive to solve. Yet another example is the *twisted mass fermions*, used for even-flavoured theories. This approach introduces a complex mass term which can be used to introduce a infrared regulator as well as introduce order $\mathcal{O}(a)$ corrections to the action. All these approaches are overvieed in detail at Ref. 30 and references there in.

3.3 Monte Carlo simulation

As stated at the end of Section 3.1.1, it is not possible to evaluate the partition function analytically for the full QCD. We turn to a numerical solution. The most straightforward process would be to discretize the path-integral, assigning an integral to each lattice site and then numerically estimating its value. Although this is a valid procedure, it is not a viable one. Let us suppose that each integral will be evaluated via a method like Simpson's rule.[35] If the integral interval is partitioned in N bins, the precision increases as $N^{-5/D}$, where D is the dimension number of the discretized path integral. In our case, D is the number of sites on the lattice, i.e. $D = N_s^3 N_\tau$. A lattice of modest size

typically has sides sizes of order 10, making $D \sim 10^4$. As a result, to gain one order of magnitude in precision, one would need an effort $10^{N_s^3 N_\tau} \sim 10^{10000}$ times greater. To get an idea of the size of the problem, let us be optimistic and imagine that each integral for a site will require 100k floating operations to evaluate[v]. Therefore, it will be executed around $10^{5\times10^4}$ floating point operations. Let us consider a computer with a processing power of the order 100's of petaflops[vi]. The time it will take to execute such a computation will be $10^{5\times10^4-15}$ s $\approx 10^{5\times10^4}$ s. To better picture this number, the age of the universe is around of 4.4×10^{16} s. It is evident that this straightforward process is hopeless, even for a small lattice. An alternative to evaluating the path-integral is needed.

The Monte Carlo approach is this alternative. The idea is that, due to the exponential e^{-S}, a couple of gauge configurations that yield an action value near zero are the ones that weigh more in the path integrals sums, with the contributions of the remaining configurations being negligible. This is because one could look at e^{-S} as a density probability and thus, if one randomly draws field configurations following this distribution, then it would just be a matter of evaluating the operators at these distributions and take a simple average to get an estimator of the expectation value of the operator. This procedure is called *importance sampling*.

To illustrate, let us apply this procedure to the computation of the expectation value of a function $A(x)$ when x is a stochastic variable following the Gaussian function. We draw N_{MC} points following the Gaussian distribution function. One then writes

$$\int_{-\infty}^{\infty} A(x) \frac{e^{-\frac{x^2}{2\sigma^2}}}{\sqrt{2\pi\sigma^2}} dx \;\cong\; \sum_{i=1}^{N_{MC}} A(x_i)\Delta x\,. \tag{3.71}$$

Since we draw the points following the probability density, then automatically we will have proportionally more terms in the sum near the probability peaks[vii]. Thus we are allowed to omit the probability density in the left-hand side of Eq. (3.71). It remains to determine Δx. Since the Gaussian function is normalized and using $A(x) = 1$, we arrive at $N_{MC}\Delta x = 1$. This yields $\Delta x = 1/N_{MC}$. Therefore, as we said above, if one draws the points x following the probability density, the computation of expected values of an operator is just a matter of averaging over the values of the operator evaluated at these points.

Let us return to the QCD case. Due to the Grassmann number representation of fermions, one is able to evaluate the integrals over them as long as they appear bilinearly

[v] We are estimating that the computation of the exponential of the trace of a plaquette takes around 100 multiplications and sums, and in the process of integrating a site one will repeat the process 1000 times. Notice that, in this estimation, we are being overly optimistic and excluding the computational cost of evaluating the exponentiation.

[vi] At the time of writing this thesis, this is the order of magnitude of computational power of the most powerful computers in the world.

[vii] We stress that a point far away of the peak is not forbidden to be draw, it is just unlikely to be selected because we are following the Gaussian distribution.

in the observable $\hat{A}$. This is shown in Wick's theorem in Eq. (3.67). However, we stress that, there, the gauge fields were frozen, i.e. we did not integrate over the gauge fields. As a result, in the complete computation, Wick's theorem's result should be multiplied by the fermionic partition function $Z_F = \det K_F$, and then one integrates everything in the gauge fields only. As an example, consider the operator $\bar{\psi}(y)U_\nu(y)\psi(y+a\hat{\nu})$, which can be rewritten as $-\operatorname{Tr}[U_\nu(y)\psi(y+a\hat{\nu})\bar{\psi}(y)]$, where the trace is over color and spinor indices. We can write it in terms of path integral as

$$\langle\bar{\psi}(y)U_\nu(y)\psi(y+a\hat{\nu})\rangle = \frac{1}{Z}\int \mathcal{D}[U_\mu(x)]\operatorname{Tr}\left[U_\nu(y)K^{-1}(y+a\hat{\nu},y)\right]e^{-S_G}\det K_F\,, \quad (3.72)$$

$$Z = \int \mathcal{D}[U_\mu(x)]e^{-S_G}\det K_F\,, \quad (3.73)$$

where K_F is a function of $U_\mu(x)$. From Eq. (3.73), it is possible to deduce that we should treat as the distribution function the term $e^{-S_G}\det K_F$. This implies that the gauge action must be real and positive. The same applies to $\det K_F$. However, it is not always true that the determinant obeys these conditions. Depending on the action, some tricks may be employed to ensure these conditions are met. For instance, if the approximation $m_0^{f=u} = m_0^{f=d}$ is made, one may use the property that, for the Wilson action, $\gamma^5 K\gamma^5 = K^\dagger$ and conclude that $\det K_f = \det K_u \det K_f \geq 0$. But not always can such a trick be performed. For instance, if there is a baryon chemical potential present, as was presented in the end of Chapter 2, then $\gamma^5 K\gamma^5 \neq K^\dagger$ and the determinant becomes complex. For such cases, the Monte Carlo approach is not applicable.

For our purposes, let us assume that $e^{-S_G}\det K_F$ can be treated as a probability distribution (at least up to a normalization constant). We must devise a way to select gauge configurations following this distribution. The method used takes inspiration in the evolution of statistical systems in equilibrium. In such cases, the system in an initial state evolves during a time (called thermalization time) to an equilibrium situation. The equilibrium situation is defined as the situation when the set of configurations follows the Boltzmann distribution function. Thus, if one is able to simulate such thermal systems, it is just a matter of replacing the Boltzmann distribution $e^{-\beta E}$ by $e^{-S_G}\det K_F$. In our case, the evolution is not in the real time. We are adding another auxiliary time just to generate many lattice configurations, which can be used to take the average of operators evaluated for each one of these configurations. We will refer to this auxiliary time as Monte Carlo time, denoting it by t_{MC}. One should not mistake the Monte Carlo time for the imaginary one $\tau = it$. These are two unrelated concepts.

In this context, let us denote a particular field configuration by i. The probability to find the system in this configuration is p_i. During a time interval dt_{MC}, the probability of the system changing from configuration i to configuration j is $P(i\to j) = R(i\to j)dt_{MC}$. We assume that the transition rate $R(i\to j)$ is time-independent. Thus, the change of the

probability p_i of finding the system in a state i is given by the *master equation*

$$\frac{dp_i}{dt_{MC}} = \sum_j p_j R(j \to i) - p_i R(i \to j)\,. \tag{3.74}$$

However, at equilibrium, the probability p_i should be time-independent[viii]. Thus, at equilibrium, the master equation can be written, after the Monte Carlo time is integrated, as

$$\sum_j p_j R(j \to i) = \sum_j p_i R(i \to j)\,. \tag{3.75}$$

Eq. (3.75) is a necessary condition for a system to achieve equilibrium. From it, one may get the *detailed balance* condition

$$p_i R(i \to j) = p_j R(j \to i)\,, \tag{3.76}$$

which is a sufficient condition for equilibrium. Eq. (3.76) can be used to impose a constraint in the transition probabilities

$$\frac{R(i \to j)}{R(j \to i)} = \frac{p_j}{p_i}\,. \tag{3.77}$$

Thus, it is enough to draw a number of sample configurations whose probability obeys Eq. (3.77). In practice, it is inefficient to randomly draw two uncorrelated states obeying the detailed balance condition. The procedure usually adopted is to arbitrarily set the fields in a given initial state and then modify it in a way that the probability of a transition from the old state to the modified one follows Eq. (3.77). This chain of configurations is called a *Markov chain*, which is characterized by the fact that a new configuration depends solely on the previous configuration in the chain.

Notice also that, since the starting configuration is chosen in an arbitrary fashion, it typically is not a representative point of the equilibrium state. This means that the probability p_0 of finding the state in this configuration is small and, by the detailed balance condition, it has a high probability of transitioning to a state nearer equilibrium. This also implies that the few initial states are not sampling the system correctly and must be ignored. The number of generated steps that must be discarded are called *thermalization time*.

There is one more detail one must be aware of when devising such an algorithm. The system may not converge to equilibrium, or yet, may generate the wrong sample of equilibrium configurations, if the algorithm used somehow does not allow the transition

[viii] By hypothesis, in equilibrium, the probability of finding the system in a given state depends only on the distribution function (the Boltzmann weight for a classical statistical system or $\det K_F e^{-S_G}$ for QCD).

from the initial states to the equilibrium ones. Since we do not know what the equilibrium configurations are, a way to enforce that the system will eventually converge to it is to impose that the algorithm allows all possible configurations to be visited, given that the simulation runs for a long enough time.

Lastly, we must remark that the sampled configurations will not be completely independent of each other. Since a new configuration is generated from a previous one, it usually is somewhat similar to the previous configuration and it may take a couple of iterations before they look different enough to be treated as an independent sample. The number of iterations between two uncorrelated samples is called *correlation time*.

We will not dwell on a specific algorithm here. Any algorithm satisfying the conditions above is suitable, which gives us a range of possible choices. The choices made will be shown at Chapter 5.

3.3.1 Renormalization procedure on the lattice

By now we have seen the discretization of QCD and explored a way to compute expected values of observables. However, we typically rescale the fields for them to be independent of the lattice spacing. We did this to ensure that in a sum we will be dealing with numbers of the same order of magnitude, thus avoiding numerical errors.

One could argue that, after the simulation is performed, it is time to reintroduce the lattice parameter a, e.g. via the relation between the link $U_\mu(x)$ and the field $A_\mu(x)$ through $U_\mu(x) = \exp\{ig_0 a A_\mu(x + ae_\mu/2)\}$. If we proceed with this idea and naively take the limit $a \to 0$, we would get $U_\mu(x) \to \mathbb{1}$. This cannot work because it corresponds to the trivial solution of the equations of motion $A_\mu(x) = 0$. This issue is related to the divergences that appear in a quantum field theory if one removes its cutoff naively, as we have shown in Section 3.1.1.

The approach to the continuum limit can be better understood by analogy with the numerical solution of differential equations. In these computations, we choose a small integration step. The step size is small enough if it is much smaller than the typical size of the resulting function's features. At the same time, these function features must be much smaller than the integration region. On the lattice simulation, the lattice spacing is similar to the integration step, the correlation function of an operator between two points of the lattice is analogous to the typical size of the differential equation's solution features and the lattice size does the job of the integration region. Therefore, the correlation length should be larger (ideally, much larger) than the lattice spacing. However, this correlation length has to be smaller (ideally, much smaller) than the lattice size. This allows to us to see large distance behaviors and minimizes errors due to the fact that our lattice size is finite.

We stress that, in the above paragraph, the correlation length we are talking about (which we will identify as ξ) is a physical correlation length. It has units of $[E]^{-1}$ and can be related to the mass of a particle, such as a hadron (determined by the choice of the operator). Thus, we cannot compute it directly from the lattice, which knows nothing about scales. But we can compute a correlation function on the lattice $\hat{\xi}$ and relate it to the physical correlation length ξ by $\xi = a\hat{\xi}$.

Since ξ is a physical quantity, it can be used as a reference to introduce the physical scale to the simulation. Also, note that ξ has a fixed finite value. This implies that in the continuum limit $a \to 0$, $\hat{\xi}$ should go to infinity. Therefore, the correct continuum limit procedure in a lattice simulation is to tune the bare lattice parameters as to obtain a lattice correlation length $\hat{\xi}$ that diverges in such a way that one is able to keep constant ξ. Consequently, the lattice spacing a will depend (usually in a non-trivial way) on the bare parameters of the lattice.

An alternative is to use the lattice static potential and compare it with phenomenological potential models for heavy quarks. As explained in Refs. 30 and 32, a lattice static potential can be computed from the expectation value of a Wilson loop (on a plane that contains the spatial direction) by

$$\langle W(I,J)\rangle = C\exp[-I\hat{V}(J)]\,, \tag{3.78}$$

where I is the size of the loop in the temporal direction and J the inter-quark distance. Notice that I and J are given in terms of number of lattice sites and relate to physical quantities by $I = T/a$ and $J = r/a$. The potential is also given in lattice units, being related to the potential model by $\hat{V} = aV$.

To compare with potential models of heavy quarks, we use the Sommer parameter r_0, which is a distance related to the shape of the potential. It is obtained by the observation that in the most successful potential models, such as the Richardson and Cornell, the following holds[36]

$$-r^2\frac{dV}{dr}\bigg|_{r=r_0\approx 0.5\,\mathrm{fm}} = 1.65\,. \tag{3.79}$$

The value of the Sommer parameter can vary slightly according to the potential model considered. For instance, for the Richardson potential, $r_0 = 0.49\,\mathrm{fm}$. With this information, we can obtain the value of the lattice spacing by performing the following procedure

1. Compute the expectation value of the Wilson loop of different sizes in the time direction and fit it to Eq. (3.78) to obtain the lattice potential at a fixed size J.

2. Repeat step 1 for different Wilson loop sizes in the spatial direction to obtain the potential dependence with the inter-quark distance.

3. Use an analytic expression (which may be inspired from a potential model) to fit the lattice potential.

4. Determine the value J_0 for which the following condition is fulfilled

$$-J^2 \frac{d\hat{V}}{dJ}\bigg|_{J=J_0} = 1.65\,. \tag{3.80}$$

5. Since $J = r/a$, we can use J_0 and the Sommer parameter r_0 to the determine that $a = r_0/J_0$.

By performing this operation, one can determine $g_0(a)$ by repeating the procedure above for different values of the bare constant. Notice that although by this method one has a good estimate of the lattice spacing, this does not exempt one from taking care that $a \ll \xi \ll L$, under the penalty of introducing excessive discretization and/or finite size errors.

Once the lattice spacing is determined, regardless of the method, we have that the system's temperature will be given by $1/T = \beta = aN_\tau$. As a result, to keep a constant temperature as the continuum limit is taken, one should increase the temporal lattice side. Since $L = aN_S = \beta N_s/N_\tau$, the increase of temporal lattice side implies the shrinking of the spatial size L, unless the lattice side N_s is increased proportionally. We say that N_s/N_τ defines the *lattice aspect ratio*, which should be kept constant.

In the next chapter, we will look at some phenomenological aspects of QCD at finite temperature, as well as some details of effective models for it.

Chapter 4

Heavy-ion collisions and superfluidity

"*We are rather like children, who must take a watch to pieces to see how it works.*"

Sir Ernest Rutherford

Explaining to a Daily Herald reporter why he wanted to disintegrate nuclei, as quoted in Freeman Dyson, 'Seeing the Unseen', The New York Review of Books (24 Feb 2005), collected in The Scientist as Rebel (2006), 249.

In this chapter, we will review the phenomenology of heavy-ion collisions, with an emphasis on its quark-gluon-plasma stage. We will start by overviewing QCD and why one expects a phase transition from hadronic matter to a deconfined phase. This will enable us to establish the conditions for such a transition to happen and that one is able to reproduce these conditions via a relativistic heavy-ion collision. We outline the basic characteristics of each stage of the collision, giving an emphasis on the relativistic hydrodynamic description of the quark-gluon-plasma stage. Next, motivated by the low viscosity of the plasma, we overview Landau's model of a two-component liquid for superfluids and detail the applicability test of this model to the QGP, as proposed by Chernodub *e*t. al.[14]

4.1 A qualitative description of the QGP

In this section, we will make a qualitative description of the QGP, to provide an understanding of the system we aim to study.

One of the key features of QCD is known as *confinement*, i.e. the force strength between two color charged particles increases at long range. An analytic description of

confinement origin is not available yet. However, it is possible to outline a good motivation for its presence.

Let us consider the perturbative computation of the scattering matrix S for QCD. The fact that the gauge symmetry group of the theory is not Abelian gives rise to terms with third and fourth powers of $A_\mu(x)$ in the Lagrangian. This implies that the fundamental vertices of QCD, when computing Feynman diagrams, will be the ones in Fig. 4.

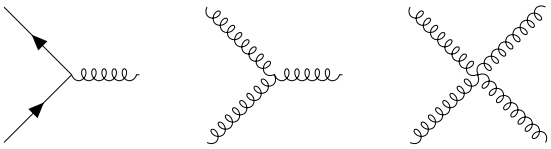

Figure 4 – Fundamental vertices of QCD. Source: Elaborated by the author.

The last two terms have no analogue in QED. This difference impacts the theory's coupling's renormalization. Recall that in QED the coupling (electric charge) renormalization is given by[i]

$$e_R^2(q^2) \;=\; \frac{1}{C\ln\left(\Lambda^2/-q^2\right)}\,, \tag{4.1}$$

where C is a positive constant that depends on the number of fermions. Notice also that, for $-q^2 \to \Lambda^2$, the coupling diverges. Thus, at the energy scale of Λ^2 there is an increase in interaction strength, and perturbation theory fails. Meanwhile, the QCD coupling renormalization is given by

$$\alpha_s(q^2) \;=\; \frac{4\pi}{\left[11-\frac{2}{3}N_f(q^2)\right]\ln(-q^2/\Lambda^2_{QCD})}\,. \tag{4.2}$$

Details of this calculation can be found in Ref. 37 and references therein.

One can see that the difference in coupling renormalization between QCD and QED is essentially in the argument of the logarithm, i.e. in QCD it is the inverse of the one in QED. The implications are better observed by plotting both running couplings, as we do in Fig. 5. We clearly see that, for QED, the divergence of the coupling happens at very large energies. Also, it runs very slowly, being of the order 10^{-2} across several orders of magnitude of energy. Thus, QED is perturbative for all energy ranges accessible currently. QCD has the opposite behavior. It becomes non perturbative at energy scales equal to or below order the hundreds of MeV. Also the change from non-perturbative to perturbative occurs much faster than in QED.

The QCD behavior implies that two color-charged particles that exchange gluons of low momentum interact strongly. This will typically happen for particles that themselves have low momentum. A low-momentum particle has a larger De Broglie wavelength,

[i] The coupling's renormalization assumes a momentum transfer such that $q^2 < 0$.

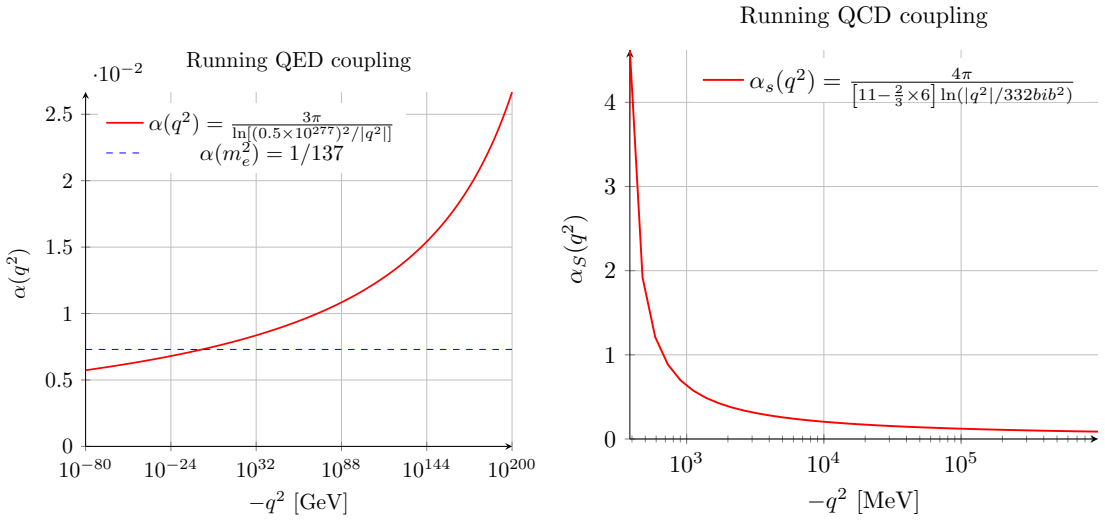

Figure 5 – Comparison between QED (left plot) and QCD (right plot) coupling constants. Besides the divergence occurring at low energy for QCD, we also draw attention for the fact that the QCD coupling changes much faster than the QED coupling. The energy scale $\Lambda_{QED} \simeq 0.5 \times 10^{277}$ GeV and its formula were retrieved from [Ref. 38, Section 5.2], using $m_{e^-} \simeq 0.5$ MeV. The above considers only the electron as part of the theory. According to Ref. 39, when the full standard model is taken into account, $\Lambda_{QED} \simeq 10^{34}$ GeV, which does not change significantly our argument. The value of the energy scale of QCD comes from [Ref. 10, QCD Review] for three quark flavors. Source: Elaborated by the author.

meaning that they are able to probe situations where they are further apart. Thus, it is often said that color-charged particles interact strongly at large distance, and weakly at short distance.

Consequently, it is impossible to have non-color-neutral objects. If you try to take two particles apart, the force binding them increases, confining color charges inside color neutral-objects, thus the name confinement to this phenomenon. On the other hand, as two color charged particles approach each other, their interaction strength gets smaller and, in the limit of infinite energy, they do not interact at all. This is called *asymptotic freedom*.

Confinement and asymptotic freedom are fundamental concepts to understand the reason why the QGP is formed. Imagine we have a set of Hadrons, e.g. nucleons in a star's core. Let us suppose that the density of Hadrons starts to increase. The mean free path between quarks collisions will get shorter and, as consequence, the interaction force that keeps quarks confined inside hadrons starts to decrease. If the mean free path gets small enough, the hadron identity is lost. We only have a "soup" of quarks and gluons. Since they are not in bound states, we say that they are forming a plasma, hence the name quark-gluon plasma. A representation of what happens is shown in Fig. 6.

Another way of obtaining the QGP is by raising the system's temperature, i.e. by

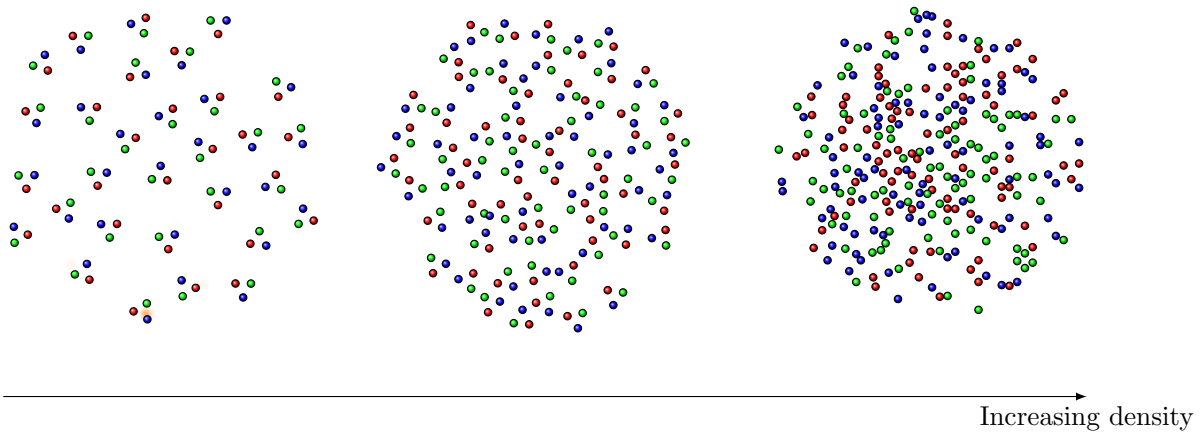

Figure 6 – A representation of QGP formation. As density is increased, quarks and gluons get nearer each other and the interaction force gets weaker, until the point where they deconfine. Source: Elaborated by the author.

increasing the kinetic energy of quarks and gluons (without an increase in the system's total momentum). Since quarks and gluons are now carrying more momentum, they will exchange higher amounts of momentum as well, and thus they interact between each other weakly. Once again, they are free to roam around, unable to form a bound state, forming the QGP.

QGP is a new state of matter, completely different from hadronic matter as found in our daily life. This makes it an interesting system to study on its own right. However, one can find astrophysical and cosmological motivation to its study as well.

The astrophysical interest is related to the equation of state of QGP, since stars do not collapse under their own weight due to the pressure in their cores.[40] In the case of very compact stars, such as neutron stars, many models make use of QGP's equation of state.[9,41–42] A compelling argument to its use starts by looking at the scale of momentum transfer required for QGP formation. From the argumentation above, that would be the scale where the running coupling goes below one, i.e. $\Lambda_{QCD} \approx 200\,\mathrm{MeV}$. Using the De Broglie wave-length, one can them argue that the quarks should be distant from each other by approximately 1 fm. This is the typical nucleon size. A reasonable approach then would be to assign an effective mass to each quark, such that the sum of quark masses yields the nucleon mass. Considering that each quark is inside a sphere of radius of 1 fm, after conversion of units, one obtains a density of about $10^{17}\,\mathrm{kg/m^3}$. This is the same order of magnitude as neutron stars' densities.

The cosmological motivation comes from the early-universe description, where extreme temperature conditions were present. Once again, using Λ_{QCD} as a temperature

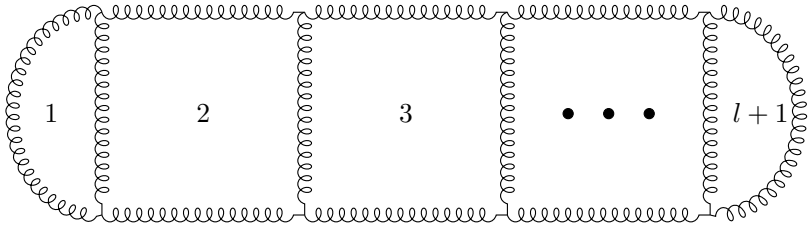

Figure 7 – Linde's diagram: an $l+1$ loop gluon diagram. Source: Elaborated by the author.

scale to the QGP formation, we expect to see its presence at temperatures above 10^{12} K. For comparison, the temperature needed for nuclear fusion is of the order of 10^8 K. Thus, the temperature required for QGP formation is far higher than anything in existence and was only seen in the early stages of the universe. As a consequence, understanding the plasma properties may lead to improvements in our understanding of early universe evolution.

A similar reasoning for the existence of the QGP was performed already in the early days of QCD [e.g. see Ref. 7]. However, it was initially thought that a perturbative approach would suffice, since the plasma forms due to the deconfinement of quarks and gluons caused by the coupling constant getting weaker. Unfortunately, this is wrong and non-perturbative phenomena are still present in the QGP. The issue is usually called Linde's problem.[15] In short, a massless boson in a covariant gauge has a propagator given by (see [Ref. 27, Chap. 6])

$$D_{\mu\nu} = \frac{1}{q^2+G}P^T_{\mu\nu} + \frac{1}{q^2+F}P^L_{\mu\nu} + \frac{\xi}{q^2}\frac{q_\mu q_\nu}{q^2}\,. \tag{4.3}$$

The factors F and G are scalars that will incorporate self-energy corrections, while $P^{L,T}_{\mu\nu}$ are projectors in the directions longitudinal/transversal. It turns out that in the limit of high temperature, both F and G are proportional to a mass dynamically generated by the creation of virtual pairs of charge that screen the real charges.

Now, consider a Feynman diagram of $l+1$ gluon loops, as the one in Fig. 7. This diagram has $2l$ vertices, $3l$ propagators and, as the name suggests, $l+1$ loops. The contribution of this diagram at finite temperature to the partition function will be [Ref. 27, Chap. 10]

$$\left(T\int d^3k\right)^{l+1}\frac{(gk)^{2l}}{(\boldsymbol{k}^2+m^2)^{3l}}\,. \tag{4.4}$$

Notice that we are assuming that the gluons being exchanged have zero frequency, i.e. $k^0=0$. This is because we are interested in investigating if there are infrared divergences in this diagram. If $k^0\neq 0$, then it is guaranteed that there is no infrared divergence in it.

By simply power counting, for 2 and 3 loop computations, there are no infrared divergences. However, for 4 loops we have a result proportional to $g^6T^4\ln(T/m)$ and, for

5 loops or more, it is proportional to $g^6T^4(g^2T/m)^{l-3}$. Now we look into the value of the screening mass m. For QCD, the mass in the longitudinal gluon is different from the one in a transversal gluon. For longitudinal gluons the effective mass is proportional to gT and thus each graph with $l > 4$ will give a contribution proportional to g^{l+3}. Thus, there are no infrared divergences and perturbation theory does not breakdown, since $g = g(T) \ll 1$. However, for transverse gluons, the screening mass is proportional to g^2T. This cancels out completely the numerator, eliminating the dependence in l. Consequently, for all orders greater than 4 loops, the graph contributes with a factor g^6T^4. Perturbation theory break downs in this situation because all terms have the same order of magnitude. So far, there is no a analytic solution for such an issue and a non-perturbative method, such as lattice QCD, should be employed.

4.2 Overview of heavy-ion collisions

Although the QGP formation requires conditions of extreme temperature and density, it is not impossible to achieve experimentally such conditions for short amounts of time. This is typically achieved by the collision of heavy-ions, e.g. Pb + Pb or Au + Au nucleus collisions. The center of mass energy required for QGP formation in such collisions should be of order 10 GeV or larger.[43–44] From the 1980's through the early 2000's, many colliders attempted to study such a system, such as the Bevalac at LBNL, the AGS at BNL and SPS at CERN. In all these, no decisive proof of QGP formation was found, although SPS had signs of a very dense state being formed.[2] The first collider that had robust evidence of QGP being produced experimentally was the Relativistic Heavy-Ion Collider (RHIC) at BNL [see e.g. Ref. 1,45], by means of collisions of gold nuclei at center-of-mass energy up to 200 GeV per nucleon. Later, LHC performed lead-lead collisions at even higher energies, confirming the results from RHIC. For details in the history of the experimental efforts to the QGP discovery, see Refs. 46–47.

We will now proceed to give a brief overview about heavy ion collisions. It is usual to divide the evolution of the system in stages. The durations of these stages are measured in Bjorken proper time (delimited by the hyperbolas in Fig. 8), given by[48–49]

$$\tau \;=\; \sqrt{t^2 - z^2}\,. \tag{4.5}$$

A brief overview of the several stages is

I. Pre-collision: Heavy-ions at relativistic speeds collide at origin. Due to Lorentz contraction, the nucleus seems like a "pancake".

II. Thermalization or pre-equilibrium: The dynamics is dominated by longitudinal expansion, characterized by strong gradients and possibly strong gauge-fields. Lasts for $\tau \simeq 1\,\mathrm{fm}/c$.

III. QGP evolution: System in near-equilibrium for about $\tau \simeq 5 - 10\,\mathrm{fm}/c$. High temperature phase with quarks and gluons deconfined. Description is done via *relativistic hydrodynamics*.

IV. Hadron gas evolution: Matter is cool enough to form hadrons again, but the mean free path between them is comparable to their cross section, resulting in frequent collisions. Possesses large viscosity and is unsuitable to hydrodynamics.

V. Freeze out: Scattering cross-section of hadrons becomes low compared to their mean free path and they fly towards the detector, without interacting with each other.

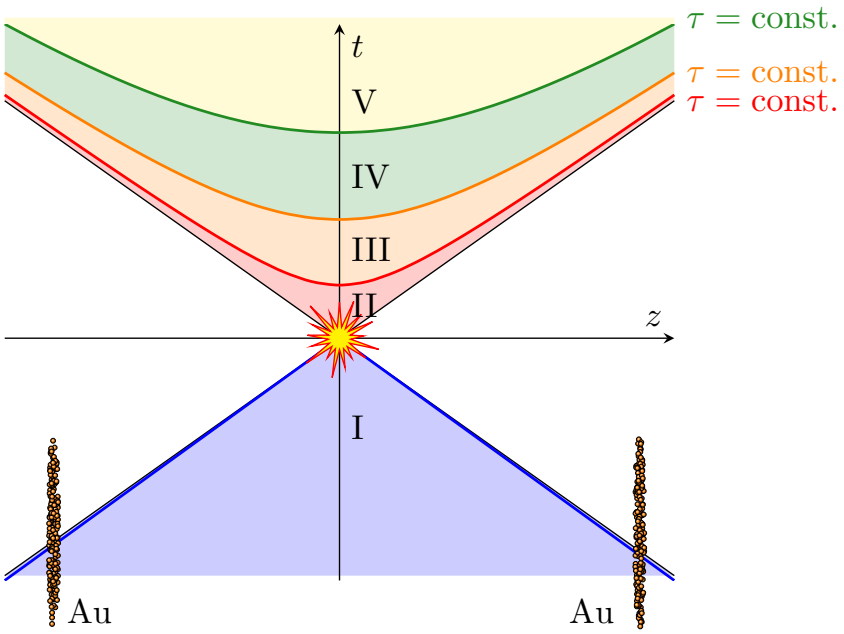

Figure 8 – Stages of evolution of heavy ion collision. Refer to text above for the description of each stage. Source: Elaborated by the author.

In the following sections, we will present in short what are the main characteristics known of each stage shown above.

4.2.1 Stage I: Pre-collision

The way that heavy ions collide will determine the initial conditions of the system and thus its evolution. Using the center of mass frame, one typically models the incoming nuclei as possessing a pancake-like shape (see Fig. 9, left panel), due to the Lorentz contraction. As an example, at RHIC the collision energy is of 200 GeV per nucleon. As a result, each nucleon is carrying 100 GeV on average. By estimating a nucleon rest mass of $\approx 1\,\mathrm{GeV}$, the contraction factor γ is then

$$\gamma = \frac{E_{\mathrm{Total}}}{E_0} = \frac{100\,\mathrm{GeV}}{1\,\mathrm{GeV}} = 100\,. \tag{4.6}$$

As consequence, the collision time is of order $0.15\,\mathrm{fm}/c$, much shorter than the time light would need to cross the nucleus. For this reason, one often considers the collision itself to be instantaneous.

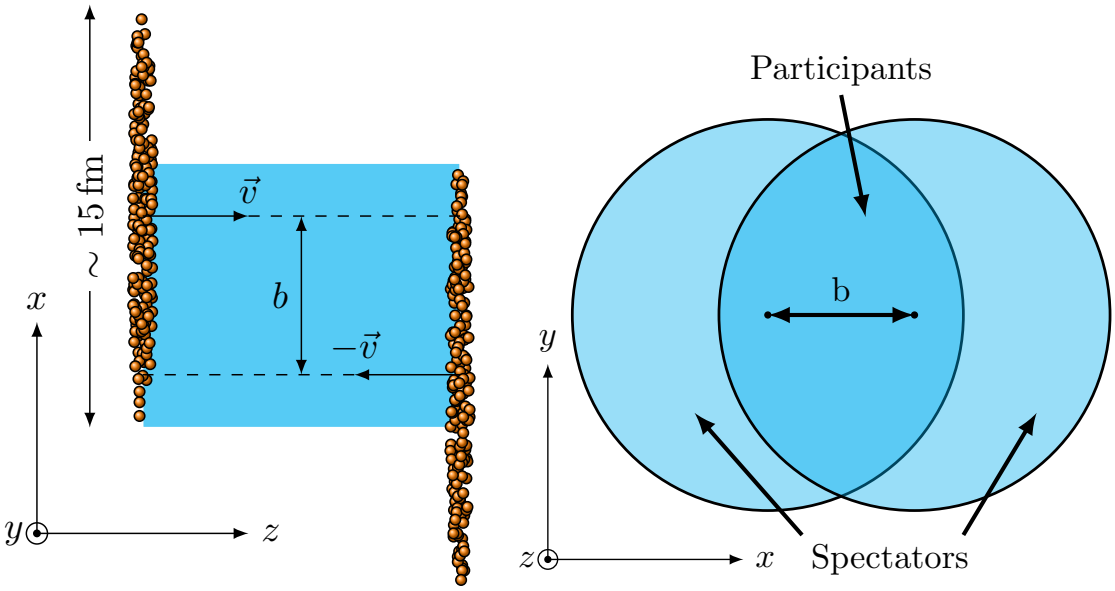

Figure 9 – Left: Sketch of a heavy ion collision with the typical reference frame usually adopted. Right: Geometry of the heavy ion collision. The darker ellipsoid in the center of the figure highlights the nucleons that will take part in the collision. Source: Elaborated by the author.

Another important aspect to take into consideration is the collision geometry. The nuclei will not be with their centers aligned. How far they are apart determines the impact parameter b, as seen in Fig. 9. Since we are considering the collision to be almost instantaneous, not all particles will take part into the collision, with the numbers of nucleons taking part in the interaction decreasing with the increase of the impact parameter. We refer to the nucleons that interact during the collision as the *participants*, with the remaining being named *spectators*.

The impact parameter also helps to define the coordinate system used in the description of the collision. The x axis lies down in its direction while the z axis is defined along the beam direction. One then defines the y axis using a right hand rule, as one can see in Fig. 9.

The collisions are categorized in two types, according to their impact parameters: *central* and *peripheric*. A central collision, is one with a small impact parameter and they happen with less frequency than a peripheric collision. However, more nucleons take part into the collision. These nucleons are called *participants*, while the remaining nucleons are called *spectators* (see above). Since there are more participants nucleons in a central collision, more energy is available and more particles are formed in a central collision.

Another key aspect, which is a direct result of the collision's geometry, is the shape of the interaction region, which takes the form of an ellipsoid (darker cyan in Fig. 9). This is "measured" by the standard eccentricity[50]

$$\varepsilon_{\text{standard}} \;=\; \frac{\{y^2 - x^2\}}{\{y^2 + x^2\}}\,, \tag{4.7}$$

where the curly braces $\{\dots\}$ represent an average over the initial density distribution $\epsilon(x)$

$$\{A(x)\} \;=\; \frac{\int d^3x\,\epsilon(x)A(x)}{\int d^3x\,\epsilon(x)}\,. \tag{4.8}$$

However, there is no way to directly probe the initial density distribution (thus, the quotes in the word measured above). What is seen is rather how the emerging particle momentum is distributed. For the case at hand, one looks at the elliptic flow, defined as[48,50]

$$v_2 \;=\; \langle\cos(2\phi)\rangle_p \;=\; \left\langle \frac{p_y^2 - p_x^2}{p_y^2 + p_x^2} \right\rangle_p\,, \tag{4.9}$$

where ϕ is an angle in the $x-y$ plane. The average $\langle\cdots\rangle_p$ is an average over the final particle distribution. The presence of an elliptic flow is one of the main signatures for the QGP being a liquid of low viscosity. Once one models the collision and determines the viscosity, it is possible to apply near-ideal hydrodynamics and reproduce the elliptic flow observed experimentally. This is typically a concentration of emitted particles along the x axis (defined by the impact parameter). Once one adopts hydrodynamics to describe QGP, such outcome is intuitive. The pressure in the center of the participants region should be zero due to the symmetry of the system, while in the surface it is a constant. Therefore, there is a higher pressure gradient along the x axis and thus more quarks and gluons will be ejected along this direction. As a result, there will be more Hadrons flying along the x axis in stages IV and V.

4.2.2 Stage II: Thermalization or pre-equilibrium

There is not much that is known about this stage. As the name suggests, the system is not at (local) equilibrium and thermodynamics is not applicable. Perturbative approaches will fail to provide a complete picture due to the non-perturbative nature of QCD. Our most reliable tool for a non-perturbative and ab initio approach, lattice QCD, is suitable only for equilibrium situations and thus ill-suited to such case. However, it is crucial to know how the system will be at the end of this stage, since it will fix the initial conditions for the hydrodynamical evolution in the next step.

Given our incapacity so far to calculate QCD out of equilibrium from first principles, the canonical approach is to pick up some selected data and adjust the initial conditions (the red line frontier in Fig. 8). This is not the only possible approach however. For instance, since the system we are dealing with small and at each collision there will be

fluctuations in the initial conditions, a possible approach is to introduce these fluctuations and integrate the system for several of them, taking an average at the end, as done in Refs. 51–53, thus better simulating the experiments.

4.2.3 Stage III: Relativistic hydrodynamics and QGP

In a heavy ion collision, the system is never found at a static equilibrium. It is always expanding and one always needs to perform a dynamical evolution of the system. However, after the pre-equilibrium stage above, one can say that *local equilibrium* is achieved and one can employ relativistic hydrodynamics to evolve the system through these stages. In this subsection, we will do a brief review on the topic of relativistic hydrodynamics, which hopefully will give the reader unfamiliar with the topic a minimum background to be able to follow the coming sections. Refs. 49, 54 have a more detailed introduction to the subject.

First, we delimit the hydrodynamics's regime of applicability. It is a coarse-grained theory, introduced to explain the collective behavior of a many-particle system. As said above, the system is usually not in static equilibrium and its macroscopic thermodynamic variables, such as energy density and pressure, change in both space and time. However, if the change rate is much slower than the microscopic interaction rate, we may divide the system in space-time cells. These cells are much smaller than the system volume but still large enough such that we can consider each one of them to be in static equilibrium. We then say that the system is in local equilibrium. [Ref. 54, Section 4.1] goes deeper into the analysis of the scale separations needed for hydrodynamics to be valid.

In this picture, the system will be described in terms of thermodynamic quantities, which depend on the cell. The typical thermodynamic observables are energy density $\varepsilon(x)$, pressure $P(x)$, temperature $T(x)$, collective four-velocity $u^\mu(x)$, a set of conserved currents densities $j_i^\mu(x)$ and a chemical potential $\mu_i(x)$, associated to the charge densities $j_i^0(x) = \rho_i(x)$. All the microscopic input gets condensed in the form of an *equation of state* $P = P(\varepsilon)$ and the dynamics between the remaining quantities is determined solely by conservation laws.

The ideal fluid us a good initial model and on top of it we may add corrections later. The relevant conservation laws for it are[ii]

$$\partial_\mu T^{\mu\nu} = 0\,, \tag{4.10}$$

$$\partial_\mu j_i^\mu = 0\,. \tag{4.11}$$

Let us explore the features of the energy-momentum tensor. We know that it must transform as a Lorentz tensor and should be symmetric. Therefore, its general form can

[ii] We always use as metric $g_{\mu\nu} = \mathrm{diag}(1, -1, -1, -1)$.

be expressed as

$$T^{\mu\nu} \;=\; c_0 g^{\mu\nu} + c_1 u^\mu u^\nu \,. \tag{4.12}$$

We adopt a local rest-frame, which is defined as a frame where the four-velocity $u^\mu(x)$ for the cell at position x is

$$u^\mu(x) \;=\; \begin{pmatrix} 1 & 0 & 0 & 0 \end{pmatrix} . \tag{4.13}$$

In this reference frame, we know that the four-momentum is given by

$$u_\mu T^{\mu\nu} \;=\; p^\nu \;=\; \begin{pmatrix} \varepsilon & 0 & 0 & 0 \end{pmatrix} . \tag{4.14}$$

This requirement constrains c_0 and c_1 to obey $T^{00} = c_0 + c_1 = \varepsilon$. The cell at point x is also subject to a uniform pressure and thus we expect that $T^{ij} = P\delta^{ij}$. This gives us a second constraint $T^{(i)(i)} = -c_0 = P$. These conditions imply that

$$T^{\mu\nu} \;=\; \varepsilon u^\mu u^\nu - P\Delta^{\mu\nu}, \tag{4.15}$$

where $\Delta^{\mu\nu} = g^{\mu\nu} - u^\mu u^\nu$ is an operator that will decompose whatever vector it contracts with in components orthogonal to the fluid velocity u^μ, e.g. $\Delta^{\mu\nu} u_\mu = 0$.

We draw attention to one point: ε and P in Eq. (4.15) are Lorentz scalars because they are the energy and pressure densities in the local rest-frame of the cell, which all observers will agree to be the same. Notice that this is the same argument made to define the proper time as a Lorentz scalar. In fact, to keep equations covariant, all thermodynamic variables should be computed in this frame and should be called proper-pressure, proper-charge-density, proper-volume and so on. For readability, when we refer to a thermodynamic variable, it should be implicitly understood that we are referring to the proper value of this variable.

So far we have five unknowns: ε, P and three components of the fluid velocity, since $u^\mu u_\mu = 1$. However, Eq. (4.10) defines only four equations. Bringing the conserved current into play does not help, because each conserved current brings together one more variable, its charge density. The missing equation is the equation of state. The methods used in its determination may vary according to the needs. For instance, Ref. 55 uses a parameterized equation which can be used in the later stages of the evolution, i.e. it applies to QGP and Hadron Gas. This parameterization is done using lattice QCD results for the high temperature (QGP) phase and hadron cascades for the low temperature phase.

It is possible to show[49] that once we define the energy-momentum tensor using Eq. (4.15), it is possible to recover the non-relativistic continuity equation and the Euler equation by projecting Eq. (4.10) into components parallel and perpendicular to u^μ and then taking the non-relativistic regime.

As said before, the ideal fluid is a first approximation. However, one must take into account the possibility of dissipative phenomena in the fluid. This is done by adding a term to the ideal energy-momentum tensor

$$T^{\mu\nu} \;=\; T^{\mu\nu}_{\text{ideal}} + \Pi^{\mu\nu} \qquad\qquad \text{and} \qquad\qquad \Pi^{\mu\nu} \;=\; \pi^{\mu\nu} + \Delta^{\mu\nu}\Pi\,. \tag{4.16}$$

We hold the requirement that $u_\mu T^{\mu\nu} = \varepsilon u^\nu$ and thus $u_\mu \Pi^{\mu\nu} = u_\mu \pi^{\mu\nu} = 0$. We then project the continuity equation for $T^{\mu\nu}$ in directions parallel and orthogonal to u^μ. After some algebra, we get

$$\begin{aligned} u_\nu \partial_\mu T^{\mu\nu} \;&=\; u^\mu \partial_\mu \varepsilon + (\varepsilon + P - \Pi)\partial_\mu u^\mu + u_\nu \partial_\mu \pi^{\mu\nu} \;=\; 0\,, \\ \Delta^\alpha_\nu \partial_\mu T^{\mu\nu} \;&=\; (\varepsilon + P - \Pi) u^\mu \partial_\mu u^\alpha - \Delta^{\mu\alpha}\partial_\mu (P - \Pi) + \Delta^\alpha_\nu \partial_\mu \pi^{\mu\nu} \;=\; 0\,. \end{aligned} \tag{4.17}$$

Notice that Π seems to act as creating an effective pressure $P - \Pi$. We can further relate it to the pressure by looking at the trace T^μ_μ

$$T^\mu_\mu \;=\; \varepsilon - 3P + \pi^\mu_\mu + 3\Pi \;=\; \varepsilon - 3(P - \Pi) + \pi^\mu_\mu. \tag{4.18}$$

This equation motivates us to require $\pi^{\mu\nu}$ to be traceless.

The above properties will guide us in specifying the tensor $\pi^{\mu\nu}$ and the scalar Π. These terms being dissipative ones, it is natural to look at the second law of thermodynamics ($\partial_\mu s^\mu \geq 0$, $s^\mu = s u^\mu$) as a possibility to fix them.

The starting point in the procedure is the thermodynamic relations[iii]

$$\varepsilon + P \;=\; sT + \mu_i \rho_i \qquad\qquad T ds \;\geq\; d\varepsilon - \mu_i d\rho_i\,. \tag{4.19}$$

From these, one can establish the derivative $T\partial_\mu s = \partial_\mu \varepsilon - \mu_i \partial_\mu \rho_i$. The second law of thermodynamics becomes

$$\partial_\mu s^\mu \;=\; \frac{u^\nu}{T}\partial_\nu \varepsilon - \frac{\mu_i}{T} u^\nu \partial_\nu \rho_i + \frac{\varepsilon + P - \mu_i \rho_i}{T}\partial_\nu u^\nu \;\geq\; 0\,. \tag{4.20}$$

We use Eq. (4.17) to eliminate $u^\nu \partial_\nu \varepsilon$ in favor of Π and $\pi^{\mu\nu}$. This will result in the term proportional to $(\varepsilon + P)\partial_\nu u^\nu$ canceling. We can also eliminate the terms containing the chemical potential and the densities by using the continuity equation for charges. The result will be

$$\frac{\Pi}{T}\partial_\mu u^\mu + \frac{\pi^{\mu\nu}}{T}\partial_\mu u_\nu \;\geq\; 0\,. \tag{4.21}$$

Since $\pi^{\mu\nu}$ is symmetric, traceless and orthogonal to u^μ, we can write the second term as

$$\pi^{\mu\nu}\partial_\mu u_\nu \;=\; \frac{\pi^{\mu\nu}}{2}\left[\partial_\mu u_\nu + \partial_\nu u_\mu - u_\mu\left(u^\alpha \partial_\alpha u_\nu\right) - u_\nu\left(u^\alpha \partial_\alpha u_\mu\right) - \frac{2}{3}\Delta_{\mu\nu}\partial_\alpha u^\alpha\right]. \tag{4.22}$$

[iii] In the second relation one must take each cell of the fluid to have the same proper-volume.

Using the above mentioned properties, one can notice that the last three terms inside the square brackets are identically zero when contracting with $\pi^{\mu\nu}$. A nice feature of the whole expression inside the square brackets is that it holds all the above properties of $\pi^{\mu\nu}$. Thus, if we define

$$\begin{aligned} \pi^{\mu\nu} &= \eta\left[\partial^\mu u^\nu + \partial^\nu u^\mu - u^\mu\left(u^\alpha\partial_\alpha u^\nu\right) - u^\nu\left(u^\alpha\partial_\alpha u^\mu\right) - \frac{2}{3}\Delta^{\mu\nu}\partial_\alpha u^\alpha\right], \\ \Pi &= \zeta\partial_\mu u^\mu\,, \end{aligned} \tag{4.23}$$

the condition in Eq. (4.21) becomes

$$\frac{\zeta}{T}\left(\partial_\mu u^\mu\right)^2 + \frac{\pi^{\mu\nu}\pi_{\mu\nu}}{2T\eta} \;\geq\; 0\,. \tag{4.24}$$

Thus, if $\eta \geq 0$ (shear viscosity) and $\zeta \geq 0$ (bulk viscosity), then the condition is satisfied identically.

When we use Eq. (4.23) in Eq. (4.17), the resulting equation is called relativistic Navier-Stokes equation. The reason is because they reduce to the Navier-Stokes equation in the non-relativistic regime. It must be pointed out that this equation has its issues. The most severe is that it allows faster-than-light propagation of perturbations. Of course, there are ways to deal with this issue. One popular way is called the "Maxwell-Cattaneo law".[49,56–57] However, this fix is inconvenient since it is introduced in an ad hoc manner. A better solution for this is the Müller-Israel-Stewart theory, which is built by adding to the entropy current s^μ terms proportional to $u^\mu\Pi^2$ and $u^\mu\pi_{\alpha\beta}\pi^{\alpha\beta}$. For our needs, we notice that faster-than-light propagation is related to modes of small wavelengths. However, hydrodynamics is an effective theory for long wavelengths. Thus, when dealing with hydrodynamics, we will be looking at limits of low $\boldsymbol{k}$ and ω.

4.2.4 Stage IV and V: Hadron gas and freeze out

As the system expands, it will cool down, eventually reconfining quarks and gluons into hadrons. Once one has transitioned to hadrons as the new degree of freedom, it is possible to use the knowledge of how hadrons scatter between themselves to evolve the system, using kinetic theory. Notice that this is a microscopic description of the system. The hydrodynamic approach, based in macroscopical variables, such as pressure and temperature, fails in this stage. This is because the system once again is not at local thermal equilibrium. A symptom of the breakdown of hydrodynamics is the increase of viscosity as the system evolves, coming to a point where the viscous terms are not a correction anymore, but dominate the continuity equations.

By the description given above, one can notice that in the initial moments of this stage, it is still possible to describe the hadron gas using hydrodynamics. At the same time, it must be always possible to use kinetic theory to evolve the system. This overlap between hydrodynamics and kinetic theory is the tool used to describe the hadronization

process by setting up the initial conditions for the kinetic theory. The strategy used is, after the hydrodynamical evolution is computed, one finds a hypersurface of hadronization and determines along it the *grand-canonical boosted particle distribution function* $f(x,p)$. The criteria for defining this hypersurface may be various, such as temperature or energy density. Once it is determined, the computation of the distribution function is performed. A common Ansatz for it is[50]

$$\begin{aligned} f(x,p) &= f_{eq}(p^\mu u_\mu) + \delta f(p^\mu)\,, \quad f_{eq}(p^\mu u_\mu) = \frac{1}{\exp\left\{\left[p_\mu u^\mu(x) - \mu(x)\right]/T(x)\right\} \pm 1}\,, \\ \delta f(p^\mu) &= f_{eq}(1 \pm f_{eq})\frac{p_\mu p_\nu \Pi^{\mu\nu}}{T^2\left(\varepsilon + P\right)}\,. \end{aligned} \tag{4.25}$$

The determination of $f(x,p)$ is the main interest in this stage because it is the dynamical variable to evolve. More specifically, assuming that hadrons are on shell, i.e. that the mean free path between them is large enough so Heisenberg's uncertainty principle has little effect on the dispersion relation $p^2 = m^2$, then $f(x,p)$ will follow the Boltzmann equation[54]

$$p^\mu \partial_\mu f(x,p) = C(x,p)\,. \tag{4.26}$$

The term $C(x,p)$ is called collision term. The particles' characteristics, such as interactions' strength will be encoded in it.

As the system evolves, it gets more dilute to the point where particles almost do not collide anymore. When this stage happens, we say that the last stage is achieved and the system freezes out. This is the point where one must connect the particle density function with what the detectors will record, i.e. a flux of particles passing through them. This can be done using the Cooper-Frye formula[58]

$$E\frac{dN}{dp^3} = \int_\sigma f(p,x) p^\mu d\sigma_\mu\,, \tag{4.27}$$

where σ is the freeze out hypersurface. Once the particles flow through the freeze out hypersurface, it is a trivial matter to propagate them towards the detector.

4.3 Superfluids

As stated in Section 4.2.1, data from elliptic flow point out that the QGP behaves as a liquid of extremely low viscosity. The value found was near the lower bound found in AdS/CFT calculations, creating an entire field inside HEP dedicated to development of dual models, connecting QCD with AdS/CFT. However, liquids of near zero viscosity are not something unknown to physicists. We know that liquid helium becomes superfluid since the end of the 1930's and there are several models for such systems available. Thus, it is worth it to give them a look and see if we can learn something useful to the hydrodynamics of QGP.

In this section, we devote ourselves to such a task. After a brief overview of superfluidity, we will focus in the Landau model for superfluid helium and see a test for its applicability to the QGP, as proposed in Ref. 14.

4.3.1 Landau model for superfluids

In 1938, P. Kapitza discovered the phenomenon of superfluidity in liquid helium. At the time, by means of measurements of the specific heat of helium, it was already known that it undergoes a phase transition at $\sim 2.17\,\mathrm{K}$. Kapitza's experiment consisted of connecting two cylinders, one of them filled with liquid helium, with a very thin tube ($\sim 0.5\,\mu\mathrm{m}$ diameter). He noticed that the liquid helium flowed freely from one cylinder to the other only after the phase transition. The interpretation was that, at this phase, helium viscosity was zero.

Shortly after these results, Keesom and Macwood[59] performed yet another experiment, in which they submerged a spinning disc in superfluid helium. They measured that the disc did slow down, indicating the presence of viscosity. This was the motivation for the two-component liquid model. It was proposed by L. Tisza and L. Landau.[12–13] The model supposes that superfluid helium has two indissociable components. Each component has its velocity, density and viscosity. The first component is called the normal component and has this name because it retains the viscosity of liquid Helium. The second component is called superfluid component and has viscosity zero. Thus, in this model, one writes

$$\begin{aligned} T^{\mu\nu} &= T^{\mu\nu}_{\mathrm{n}} + T^{\mu\nu}_{\mathrm{s}} \\ T^{\mu\nu}_{\mathrm{n}} &= \varepsilon_{\mathrm{n}} u^\mu u^\nu + P_{\mathrm{n}} \Delta^{\mu\nu} + \pi^{\mu\nu} + \Delta^{\mu\nu}\Pi \\ T^{\mu\nu}_{\mathrm{s}} &= \varepsilon_{\mathrm{s}} v^\mu v^\nu + P_{\mathrm{s}} \tilde{\Delta}^{\mu\nu}\,, \end{aligned} \tag{4.28}$$

where the "n" subscript represents variables associated to the normal component and "s" subscript to the superfluid component. Exception is made for the velocity of the liquid components, for which we keep using u^μ for the normal component, but use v^μ for the superfluid component. Since the operator $\Delta^{\mu\nu}$ depends on the velocity, we use $\tilde{\Delta}$ to indicate when the operator depends on the superfluid velocity v^μ.

There is also a good theoretical motivation for this model. Helium being a boson, it forms a Bose-Einstein condensate at low temperatures. However, unless absolute zero temperature is reached, there will be room for a portion of the atoms to occupy the excited states. One can show that the condensation appears below a critical temperature.[60] This motivates us to assign to it the superfluid component, while the excitations are the normal component.

One interesting aspect is that it is possible to associate the model's macroscopical observables with field theory observables. This is shown in Ref. 61 and starts by supposing the complex scalar theory with a $|\phi|^4$ potential (the same one which we explored as example

model in the previous chapters)

$$\mathcal{L} \;=\; \partial_\mu\phi\partial^\mu\phi^* - m^2\left|\phi\right|^2 - \lambda\left|\phi\right|^4 . \tag{4.29}$$

Since we are expecting Bose-Einstein condensation, we perform the variable change $\phi \to \phi + \varphi$, where ϕ will be treated as the condensate variable, while φ will be treated as the excitations on top of the condensate. In practice, this implies treating ϕ as a classical field, while φ will be the dummy variable to be integrated by a path integral.

To understand the dynamics of the superfluid component, we neglect the excitations. We perform the change of variable $\phi = \rho\exp(i\psi)/\sqrt{2}$ and rewrite the Lagrangian as

$$\mathcal{L} \;=\; \partial_\mu\rho\partial^\mu\rho - \frac{\rho^2}{2}\left[m^2 - \partial_\mu\psi\partial^\mu\psi\right] . \tag{4.30}$$

As presented in detail in Chapter 2, the Lagrangian possesses also a global phase symmetry, which gives rise to a conserved current via Noether's theorem. In terms of the variables ρ and ψ, the Noether conserved current is

$$j^\mu \;=\; \rho^2\partial^\mu\psi\,. \tag{4.31}$$

Consequently, the macroscopic liquid density may be written as

$$n_\mathrm{s} \;=\; \sqrt{j^\mu j_\mu} \;=\; \rho^2\sqrt{\partial_\mu\psi\partial^\mu\psi}\,. \tag{4.32}$$

Since $j^\mu = nv^\mu$. We can relate the fluid velocity to the derivatives of the field phase as well

$$v^\mu \;=\; \frac{\partial^\mu\psi}{\sigma} \qquad\qquad \text{where} \qquad\qquad \sigma \;\equiv\; \sqrt{\partial_\mu\psi\partial^\mu\psi}\,. \tag{4.33}$$

The result from Eq. (4.33) is important. By using that $v^\mu = \gamma(1,\,\boldsymbol{v})$, one finds that the superfluid is given by $\boldsymbol{v} = -\boldsymbol{\nabla}\psi/\partial_t\psi$. Thus, if $\partial_t\psi$ is constant, the *vorticity* $\nabla\times\boldsymbol{v}$ of the superfluid is zero. This result is crucial for later calculations.

A similar approach can be used to relate the internal energy density of the fluid with the microscopical quantities. We start by computing the energy-momentum tensor of the microscopical theory

$$T^{\mu\nu} \;=\; \partial^\mu\rho\,\partial^\nu\rho + \rho^2\partial^\mu\psi\,\partial^\nu\psi - g^{\mu\nu}\mathcal{L}\,. \tag{4.34}$$

Since $\varepsilon_\mathrm{s} = v_\mu v_\nu T^{\mu\nu}$ and $P_\mathrm{s} = (v_\mu v_\nu - g_{\mu\nu})T^{\mu\nu}$, after some algebra, we get

$$\varepsilon_\mathrm{s} + P_\mathrm{s} \;=\; \mu_\mathrm{s} n_\mathrm{s} + sT \;=\; \rho^2\sigma^2 + \frac{4}{3}\frac{(\partial_\mu\psi\partial^\mu\rho^2)}{\sigma^2} - \frac{1}{3}\partial_\mu\rho\partial^\mu\rho\,. \tag{4.35}$$

However, the condensate is defined as being a coherent state. Therefore, it has minimum entropy and we use it to set entropy's measuring referential. Thus the term sT is zero. If we take a very simple case of constant ρ (which one can see that translates to

a case of constant pressure and energy-density in all points of the liquid), we get a very simple interpretation for σ. Under this condition and using $n_{\mathrm{s}} = \rho^2\sigma$, we get

$$\mu_{\mathrm{s}} n_{\mathrm{s}} \;=\; \mu_{\mathrm{s}}\rho^2\sigma \;=\; \rho^2\sigma^2\,. \tag{4.36}$$

The conclusion is that, in these circumstances, $\mu_{\mathrm{s}} = \sigma$. Notice that we did not supposed the presence of a chemical potential in the microscopic theory. The above shows that, even if we do not consider a chemical potential microscopically, nothing stops the presence of an *effective macroscopic chemical potential*.

As a last remark, we may use that we are setting $s = 0$ and the thermodynamic relation $\varepsilon + P = \mu n + sT$ to rewrite the energy-momentum tensor for the superfluid as

$$T^{\mu\nu}_{\mathrm{s}} \;=\; (\varepsilon_{\mathrm{s}} + P_{\mathrm{s}})v^\mu v^\nu - P_{\mathrm{s}} g^{\mu\nu} \;=\; \mu_{i,\mathrm{s}}\rho_{i,\mathrm{s}} v^\mu v^\nu - P_{\mathrm{s}} g^{\mu\nu}\,, \tag{4.37}$$

and the full tensor for the model as

$$T^{\mu\nu} \;=\; (\varepsilon_{\mathrm{n}} + P_{\mathrm{n}})u^\mu u^\nu + \mu_{i,\mathrm{s}}\rho_{i,\mathrm{s}} v^\mu v^\nu - P_{\mathrm{s}} g^{\mu\nu} + \pi^{\mu\nu} + \Delta^{\mu\nu}\Pi\,. \tag{4.38}$$

The next step is to find a way of verifying the model's applicability to the QGP. To do so, we will use linear response theory. The advantage of such approach is that we are able to connect the dynamics of hydrodynamics with computations in static equilibrium, which can be evaluated via lattice QCD.

4.3.2 Linear response theory

As said above, we will use linear response theory to detail the test proposed by Ref. 14. We will start by exposing how to build linear response theory [as exposed in Ref. 26] and work our way to the test itself.

Consider a system at equilibrium, which is governed by a Hamiltonian H_0. Now, we turn on a small macroscopic perturbation in the form of velocity field $U^i(t, \boldsymbol{x})$ that couples to the momentum density $T^{0i}(t, \boldsymbol{x})$. The Hamiltonian will receive a modification $\delta H(t)$, given by

$$\delta H(t) \;=\; \int d^3x\, U_i(t, \boldsymbol{x}) T^{0i}(t, \boldsymbol{x})\,. \tag{4.39}$$

We suppose also that for $t < t_0$ the perturbation is zero, i.e. we turn on $U^i(t, \boldsymbol{x})$ at $t = t_0$. We expect that the system will answer by changing its momentum density operator $T^{0i}(t, \boldsymbol{x})$. The system evolution will be given by

$$\frac{\partial \langle T^{0i}(t, \boldsymbol{x})\rangle_{\mathrm{Q}}}{\partial t} \;=\; i\left\langle \Big[H_0 + \delta H(t),\, T^{0i}(t, \boldsymbol{x})\Big]\right\rangle_{\mathrm{Q}} \;=\; i\left\langle \Big[\delta H(t),\, T^{0i}(t, \boldsymbol{x})\Big]\right\rangle_{\mathrm{Q}}\,, \tag{4.40}$$

where $\langle\cdot\rangle_{\mathrm{Q}}$ denotes a quantum expectation value, i.e.

$$\langle A\rangle_{\mathrm{Q}} \;=\; \langle\psi|\, A\,|\psi\rangle\ , \tag{4.41}$$

and $|\psi\rangle$ denotes an eigenstate of the unperturbed Hamiltonian H_0.

Integrating Eq. (4.40) from the moment we turn on the perturbation until a time t, we get the integral equation

$$\langle T^{0i}(t,\boldsymbol{x})\rangle_{\mathrm{Q}} \;=\; \langle T^{0i}(t_0,\boldsymbol{x})\rangle_{\mathrm{Q}} + i\int_{t_0}^{t} dt' \int d^3x' \left\langle \left[U_j(t',\boldsymbol{x}')T^{0j}(t',\boldsymbol{x}'),\, T^{0i}(t',\boldsymbol{x})\right]\right\rangle_{\mathrm{Q}} . \tag{4.42}$$

However, as discussed in Section 2.4.1, a thermal system transitions between states very rapidly. Thus, what we observe is a thermal average, which may be written for an operator A as

$$\langle A\rangle_{\mathrm{T}} \;=\; \frac{\sum_\psi e^{-\beta(E_\psi-\mu N_\psi)}\,\langle\psi|\,A\,|\psi\rangle}{\sum_\psi e^{-\beta(E_\psi-\mu N_\psi)}} . \tag{4.43}$$

We then obtain an expression identical to Eq. (4.42), but with $\langle\cdot\rangle_{\mathrm{Q}}$ replaced by $\langle\cdot\rangle_{\mathrm{T}}$. Since the perturbation is small, we expect that the disturbance

$$\delta\langle T^{0i}(t,\boldsymbol{x})\rangle_{\mathrm{T}} \;\equiv\; \langle T^{0i}(t,\boldsymbol{x})\rangle_{\mathrm{T}} - \langle T^{0i}(t_0,\boldsymbol{x})\rangle_{\mathrm{T}} \tag{4.44}$$

to be small and thus, at a first order approximation, we may replace $T^{0i}(t',\boldsymbol{x})$ on the right-hand side of Eq. (4.42) with $T^{0i}(t_0,\boldsymbol{x})$. We also point out that the disturbance field $U_j(t',\boldsymbol{x})$ is classical and thus factors out of the average. We obtain

$$\delta\left\langle T^{0i}(t,\boldsymbol{x})\right\rangle_{\mathrm{T}} \;=\; -i\int_{t_0}^{t} dt' \int d^3x' U_j(t',\boldsymbol{x}') \left\langle \left[T^{0i}(t_0,\boldsymbol{x}),\, T^{0j}(t',\boldsymbol{x}')\right]\right\rangle_{\mathrm{T}} . \tag{4.45}$$

If we introduce a step function $\theta(t-t')$ multiplying the integrand, we may allow the upper integration limit to go to infinity. Under the hypothesis that the perturbation is turned on long enough that we may consider the limit $t_0 \to -\infty$, we obtain

$$\delta\left\langle T^{0i}(t,\boldsymbol{x})\right\rangle_{\mathrm{T}} \;=\; \int_{-\infty}^{\infty} dt' \int d^3\boldsymbol{x}'\, U_i(t',\boldsymbol{x}') G_R^{0i,\,0j}(t-t',|\boldsymbol{x}-\boldsymbol{x}'|) , \tag{4.46}$$

where $\tilde{G}_R^{0i,\,0j}(t-t',|\boldsymbol{x}-\boldsymbol{x}'|)$ is the *retarded Green function*, given by

$$\tilde{G}_R^{0i,\,0j}(t-t',|\boldsymbol{x}-\boldsymbol{x}'|) \;=\; -i\theta(t-t') \left\langle \left[T^{0i}(t,\boldsymbol{x}), T^{0j}(t',\boldsymbol{x}')\right]\right\rangle_{\mathrm{T}} . \tag{4.47}$$

Notice that although the Green function is computed supposing thermal equilibrium, it allows for the computation of a dynamical effect, in our case, $\delta\langle T^{0i}(t,\boldsymbol{x})\rangle$.

For the argument that will be developed, it is useful to work in momentum space. We define the retarded Green function and the classical current in momentum space as

$$G_R^{0i,\,0j}(\omega,\boldsymbol{k}) \;=\; \int dt\, d^3\boldsymbol{x}\;\; e^{i\omega t}e^{-i\boldsymbol{k}\cdot\boldsymbol{x}}\tilde{G}_R^{0i,\,0j}(t,|\boldsymbol{x}|) , \tag{4.48}$$

$$U_i(\omega,\,\boldsymbol{k}) \;=\; \int dt\, d^3\boldsymbol{x}\;\; e^{i\omega t}e^{-i\boldsymbol{k}\cdot\boldsymbol{x}}U_i(t,\boldsymbol{x}) . \tag{4.49}$$

The oscillation of the momentum density is then put in a very simple form $\delta \langle T^{0i}(\omega, \boldsymbol{k})\rangle_{\mathrm{T}}$given by

$$\delta \left\langle T^{0i}(\omega, \boldsymbol{k})\right\rangle_{\mathrm{T}} \;=\; U_j(\omega, \boldsymbol{k}) G_R^{0i,\,0j}(\omega, \boldsymbol{k})\,. \tag{4.50}$$

So far all calculations are performed in Minkowski space. Later, we will be dealing with Euclidean space and will be computing Green functions via Monte Carlo simulations in Euclidean time. To connect the Euclidean Green function to the Minkowski one in Eq. (4.48), one must perform an elaborated procedure of determining spectral functions and performing an analytic continuation[iv]. However, a nice property happens at $\omega = 0$. The Green functions in Euclidean and Minkowski time are equal,[54] i.e. $G_R^{0i,\,0j}(0, \boldsymbol{k}) = G_E^{0i,\,0j}(0, \boldsymbol{k})$.

Now, we follow the argument of Ref. 62. The only anisotropy of the system comes from the perturbation itself. Thus it is natural to separate the Green function in components perpendicular and longitudinal to the perturbation

$$G_R^{0i,\,0j}(0, \boldsymbol{k}) \;=\; \frac{k^i k^j}{\boldsymbol{k}^2} G^{\parallel}(\boldsymbol{k}^2) + \left(\delta^{ij} - \frac{k^i k^j}{\boldsymbol{k}^2}\right) G^{\perp}(\boldsymbol{k}^2)\,. \tag{4.51}$$

Defining $\delta \langle T^{0i}(0, \boldsymbol{k})\rangle_{\mathrm{Thermal}} \equiv \delta p^i(0, \boldsymbol{k})$, we get

$$\delta \boldsymbol{p}(0, \boldsymbol{k}) \;=\; \frac{\boldsymbol{U}\cdot\boldsymbol{k}}{\boldsymbol{k}^2}\boldsymbol{k}\, G^{\parallel}(\boldsymbol{k}^2) + \left(\boldsymbol{U} - \frac{\boldsymbol{U}\cdot\boldsymbol{k}}{\boldsymbol{k}^2}\boldsymbol{k}\right) G^{\perp}(\boldsymbol{k}^2)\,. \tag{4.52}$$

Let us pick a wave-vector $\boldsymbol{k}$ perpendicular to our perturbation. Thus, $\delta\boldsymbol{p} = \boldsymbol{U}(0, \boldsymbol{k}) G^{\perp}(|\boldsymbol{k}|)$. The left panel of Fig. 10 represents the kind of variation in momentum density we expect (in blue). By considering a small loop (in black in the figure), we conclude that the curl of the system's response is not zero. Since the vorticity of the superfluid must be zero, we conclude that, for such mode, the superfluid will not respond to the perturbation. Conversely, if we pick a wave vector parallel to the perturbation, we have $\delta\boldsymbol{p} = \boldsymbol{U}(0, \boldsymbol{k}) G^{\parallel}(|\boldsymbol{k}|)$. The variation of the momentum will look like Fig. 10, right panel. In this case, it is clear that the perturbation will not result in a curl for the velocity and thus both components will respond to the perturbation.

We need to consider a zero-frequency perturbation. This means that this is a static perturbation and will only push the system to a new equilibrium state. By going to the limit $\boldsymbol{k} \to 0$, we will be looking into a uniform perturbation. Since the perturbation is a velocity field, in the uniform and static limit, the only effect should be a shift in velocity, i.e. $\boldsymbol{u}_f = \boldsymbol{u} + \boldsymbol{U}$ and $\boldsymbol{v}_f = \boldsymbol{U} + \boldsymbol{v}$ (only in the case where $\boldsymbol{k}$ is parallel to $\boldsymbol{U}$).

Let us consider the momentum density, given by $p^i \equiv T^{0i}$, and with the energy-momentum tensor given by Eq. (4.38)

$$\boldsymbol{p} \;=\; (\varepsilon_{\mathrm{n}} + P_{\mathrm{n}})\gamma^2\boldsymbol{u} + \boldsymbol{\pi} - \gamma^2\boldsymbol{u}\Pi + \mu_{\mathrm{s}}\rho_s\tilde{\gamma}^2\boldsymbol{v}\,, \tag{4.53}$$

[iv] For details, see [Ref. 26, Section 6.2] about Lehmann representation.

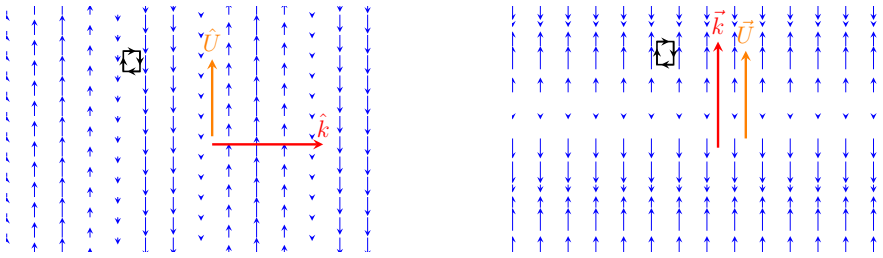

Figure 10 – **Left:** Variation of momentum density for a wave mode perpendicular to the perturbation direction. **Right:** Variation of momentum density for a wave mode parallel to the perturbation direction. Source: Elaborated by the author.

where

$$\boldsymbol{\pi} \;=\; \pi^{0i}\hat{x}^i\,, \quad \gamma \;=\; (1-\boldsymbol{u}^2)^{-1/2} \quad \tilde{\gamma} \;=\; (1-\boldsymbol{v}^2)^{-1/2} \quad \text{and} \quad u^\mu \;=\; \gamma(1,\boldsymbol{u})\,. \tag{4.54}$$

According to what we said above, in the static and uniform limits, there will be no disturbance in the thermodynamic properties, just a change in velocities. Thus, by means of a variational computation, we write

$$\begin{aligned}\delta\boldsymbol{p}(0,\boldsymbol{k}\;\to\;0) \;=\; &(\varepsilon_{\rm n}+P_{\rm n})\left[2\gamma(\delta\gamma)\boldsymbol{u}+\gamma^2\delta\boldsymbol{u}\right]+\mu_{\rm s}\rho_{\rm s}\left[2\tilde{\gamma}(\delta\tilde{\gamma})\boldsymbol{v}+\tilde{\gamma}^2\delta\boldsymbol{v}\right]\\ &+\delta\boldsymbol{\pi}-2\gamma(\delta\gamma)\boldsymbol{u}\Pi-\gamma^2(\delta\boldsymbol{u})\Pi-\gamma^2\boldsymbol{u}\delta\Pi\,.\end{aligned} \tag{4.55}$$

However, we have that $\delta\gamma=\gamma^3\boldsymbol{u}\cdot\delta\boldsymbol{u}$ and an analogous expression for $\delta\tilde{\gamma}$, with $\boldsymbol{u}$ exchanged by $\boldsymbol{v}$. The tensor that Refs. 14 and 62 deal with neglects the contributions given by $\boldsymbol{\pi}$ and Π, so we do the same here

$$\delta\boldsymbol{p}(0,\boldsymbol{k}\;\to\;0) \;=\; (\varepsilon_{\rm n}+P_{\rm n})\left[2\gamma^4\boldsymbol{u}\cdot\delta\boldsymbol{u}+\gamma^2\right]\delta\boldsymbol{u}+\mu_{\rm s}\rho_{\rm s}\left[2\tilde{\gamma}^4\boldsymbol{v}\cdot\delta\boldsymbol{v}+\tilde{\gamma}^2\right]\delta\boldsymbol{v}\,. \tag{4.56}$$

Now, we return to the expressions $\delta\boldsymbol{p}(0,\boldsymbol{k})=\boldsymbol{U}G^{\perp}(0,\boldsymbol{k})$ (valid only if $\boldsymbol{k}\perp\boldsymbol{U}$) and $\delta\boldsymbol{p}(0,\boldsymbol{k})=\boldsymbol{U}G^{\parallel}(0,\boldsymbol{k})$. In both cases we can isolate the form factors $G^{\perp,\parallel}(\boldsymbol{k})$ by computing $\boldsymbol{U}\cdot\delta\boldsymbol{p}(0,\boldsymbol{k})/\boldsymbol{U}^2$. Therefore, we obtain

$$\frac{\boldsymbol{U}\cdot\delta\boldsymbol{p}}{\boldsymbol{U}^2} \;=\; (\varepsilon_{\rm n}+P_{\rm n})\left[2\gamma^4\boldsymbol{u}\cdot\delta\boldsymbol{u}+\gamma^2\right]\frac{\boldsymbol{U}\cdot\delta\boldsymbol{u}}{\boldsymbol{U}^2}+\mu_{\rm s}\rho_{\rm s}\left[2\tilde{\gamma}^4\boldsymbol{v}\cdot\delta\boldsymbol{v}+\tilde{\gamma}^2\right]\frac{\boldsymbol{U}\cdot\delta\boldsymbol{v}}{\boldsymbol{U}^2}\,. \tag{4.57}$$

Let us consider the case where the wave-vector is perpendicular to the perturbation $\boldsymbol{U}$. As exposed above, in this case the superfluid component does not respond and thus $\delta\boldsymbol{v}=0$. Since $\delta\boldsymbol{u}=\boldsymbol{U}$ and denoting by θ the angle between the initial velocity $\boldsymbol{u}$ and the perturbation $\boldsymbol{U}$, we get

$$G^{\perp}(k^2\;\to\;0) \;=\; (\varepsilon_{\rm n}+P_{\rm n})\gamma^2(2\gamma^2\cos^2\theta+1)\,. \tag{4.58}$$

The angular dependence comes from the fact that we picked one particular direction for $\boldsymbol{u}$. We can get rid of this hypothesis by averaging over all directions, i.e.

$$G^{\perp}(k^2\;\to\;0) \;=\; \frac{1}{4\pi}\int d\Omega\, G^{\perp}(k^2\;\to\;0) \;=\; (\varepsilon_{\rm n}+P_{\rm n})\gamma^2\left(\frac{2\gamma^2}{3}+1\right)\,. \tag{4.59}$$

However, for $\boldsymbol{k} \parallel \boldsymbol{U}$, both components respond to the perturbation and $\delta\boldsymbol{v} = \delta\boldsymbol{u} = \boldsymbol{U}$. Notice that the term accompanying $\delta\boldsymbol{v}$ inside the square brackets in Eq. (4.57) is similar to the term accompanying $\delta\boldsymbol{u}$. Therefore, the calculation is similar, and we obtain, after averaging over all possible directions

$$G^{\parallel}(k^2 \to 0) = (\varepsilon_{\rm n} + P_{\rm n})\gamma^2 \left(\frac{2\gamma^2}{3} + 1\right) + \mu_{\rm s}\rho_{\rm s}\tilde{\gamma}^2 \left(\frac{2\tilde{\gamma}^2}{3} + 1\right) . \tag{4.60}$$

When replacing these form factors at the expression for $G_R^{0i,\,0j}(0,\boldsymbol{k})$, we get

$$\lim_{\boldsymbol{k}\to 0} G_R^{0i,\,0j}(0,\boldsymbol{k}) = (\varepsilon_{\rm n} + P_{\rm n} - \Pi)\,\gamma^2 \frac{(2\gamma^2+1)}{3}\delta^{ij} + \mu\rho_{\rm s}\gamma_{\rm s}^2 \frac{(2\gamma_{\rm s}^2+1)}{3}\frac{k^i k^j}{\boldsymbol{k}^2} . \tag{4.61}$$

The test suggested in Ref. 14 consists in computing the off-diagonal components of $G_R^{0i,\,0j}(0,\boldsymbol{k})$ on a lattice-QCD simulation at finite temperature. If the quark-gluon plasma is superfluid at a given temperature, we should expect a non-zero value for it.

Yet another test that is closely related to the one above comes from noting that $G^{\parallel}(|\boldsymbol{k}| \to 0) - G^{\perp}(|\boldsymbol{k}| \to 0) \propto \mu\rho_{\rm s}$. Thus, we must compute the form factors separately and then subtract one from the other. A zero result will tell us that the model does not apply to the theory. We stress that, in general, μ is not a microscopic chemical potential. Thus, even at zero chemical potential, the presence of a condensate may induce an effective chemical potential.

The form factors can be easily extracted from the Green functions by

$$G^{\parallel}(|\boldsymbol{k}|) = \frac{k^i k^j}{\boldsymbol{k}^2} G_R^{0i,\,0j}(0,\boldsymbol{k}) , \tag{4.62}$$

$$G^{\perp}(|\boldsymbol{k}|) = \left(\delta^{ij} - \frac{k^i k^j}{\boldsymbol{k}^2}\right) G_R^{0i,\,0j}(0,\boldsymbol{k}) . \tag{4.63}$$

Thus, as a test of the validity of the model for the gluon-plasma, one can compute $G^{\parallel}(|\boldsymbol{k}| \to 0) - G^{\perp}(|\boldsymbol{k}| \to 0)$. If the result is zero, it is a sign that there is no superfluid component.

In the next chapter, we will detail the simulation performed and the methods used to compute the form factors, as well as the results we obtain from the simulations.

Chapter 5

Methods and Results

> "*I often say that when you can measure what you are speaking about, and express it in numbers, you know something about it.*"
>
> Baron William Thomson Kelvin
> From lecture to the Institution of Civil Engineers, London (3 May 1883), 'Electrical Units of Measurement', Popular Lectures and Addresses (1889), Vol. 1, 80-81.

By now we have overviewed quantum field theory, explored its symmetries in the case of a gauge theory and described a way to compute observables in it. We also presented the phenomenology of Heavy-Ion Collisions and saw that there is the possibility to model the quark-gluon-plasma stage as a superfluid of two components, similar to liquid helium. We also saw that an *ab initio* verification of the viability of such model would be the Green function's computation of the energy-momentum tensor via lattice QCD. In this chapter, we will outline the Monte Carlo algorithm used to generate the lattice configurations as well as the discretization of the tensor on the lattice. Lastly, we present the averaging method used, the lattice parameters adopted and present our results.

5.1 Generation of gauge field configurations via Cabbibo-Marinari pseudo-heat-bath

The first step into any lattice QCD simulation is to generate the samples of field configurations, as explained in Section 3.3. To do so, one must take care of how to store these fields in memory. The wrong parameterization for the group elements $U_\mu(m)$ may result in a slower computation or increase in the memory usage. Typically, a representation which saves memory is computationally more intensive. Thus, one must seek a compromise between these two.

By memory, we refer to both volatile and permanent kinds. During the simulation execution, a single field configuration is stored in RAM and its value is updated as the Monte Carlo algorithm progresses. In a very large lattice (number of sites of order 100^4), a single configuration may get to the size of tens or hundreds of gigabytes. Since the generation of field configurations is computationally intensive, it is a common practice to store them in the hard disk, allowing multiple observables to be computed with a single simulation. Here, one may face storage issues even with smaller lattices (number of sites of order 30^4), since each lattice will have of order of hundreds of megabytes and one tries to store hundreds or even thousands of configurations, depending on the statistical errors.

Notice that, as we have seen in Section 3.2.2, the fermion fields are Grassmann variables. Thus, their path integrals are analytically evaluated and given in terms of the matrix K_F. These depend on the gauge fields $U_\mu(x)$. For this reason, we do not need to store fermion field values. Since the gauge links are SU(3) group elements, we need to study the possible parameterizations of these. We will follow the suggestions in Ref. 30.

Before parameterizing the SU(3) group elements, it is useful to study the SU(2) group. This is because it is easier to deal with, compared to SU(3) but, despite its simplicity, the methods applied to it are portable to SU(3). The second reason is that the method to generate the configurations builds upon the fact that $SU(2)$ is a subgroup of $SU(3)$.

Once could be tempted to use the exponential mapping $U = e^{i\alpha^a T^a}$ as a parameterization of the groups. This has the advantage of being immediately generalizable to any $SU(N)$ group and requiring the minimal amount of memory usage: only $N^2 - 1$ real numbers. Despite this advantage, one must remember that, each time we desire to perform an operation, we will need to determine all the N^2 matrix elements, thus requiring the evaluation of the exponential of a matrix. This is an expensive operation to perform and, typically, the memory economy does not outweigh the increase in computational cost.

We turn to the defining properties of this group, i.e. $UU^\dagger = \mathbb{1}$ and $\det U = 1$. After a small amount of algebra, one gets the following set of equations

$$|U_{11}|^2 + U_{12}U_{21}^* = 1\,, \tag{5.1}$$

$$U_{11}U_{12}^* + U_{12}U_{22}^* = 0\,, \tag{5.2}$$

$$U_{21}U_{11}^* + U_{22}U_{12}^* = 0\,, \tag{5.3}$$

$$U_{21}U_{12}^* + |U_{22}|^2 = 1\,. \tag{5.4}$$

This set of equations can be satisfied by

$$U = \begin{pmatrix} x & y \\ -y^* & x^* \end{pmatrix}, \qquad \text{with} \qquad x,\, y \in \mathbb{C} \quad / \quad |x|^2 + |y|^2 = 1 = \det U\,. \tag{5.5}$$

Thus, one needs only two complex numbers (four real numbers) to parameterize the group. Alternatively, if storage is a crucial problem, it is possible to omit one of the real numbers

and compute it only when needed. Notice that this reduces the number of parameters to be the same as in the exponential mapping, but the additional cost is much smaller than when one needs to exponentiate a matrix.

Another way to write the same condition, which is also very popular and is used in Ref. 32, can be derived by expanding the complex numbers of the above parameterization in its real and imaginary part. The matrix is then written

$$U \;=\; \begin{pmatrix} a_4 + ia_3 & a_2 + ia_1 \\ -a_2 + ia_1 & a_4 - ia_3 \end{pmatrix} \;=\; a_4 \mathbb{1} + i\boldsymbol{a}\cdot\boldsymbol{\sigma}, \quad a_4, \boldsymbol{a} \in \mathbb{R} \quad \text{and} \quad a_4^2 + \boldsymbol{a}^2 \;=\; 1\,. \tag{5.6}$$

Both parameterizations are equally valid. Since we will implement the code in Fortran language, which has native support to complex numbers, we will adopt the former parameterization.

As said above, the SU(2) strategy of using the defining property of the group to determine a reasonable parameterization is portable to SU(3). We start by writing the matrix U as

$$U \;=\; \begin{pmatrix} \boldsymbol{u} \\ \boldsymbol{v} \\ \boldsymbol{w} \end{pmatrix}, \tag{5.7}$$

where $\boldsymbol{u}$, $\boldsymbol{v}$ and $\boldsymbol{w}$ are complex vectors of dimension 3. When we write $V = UU^\dagger$, each element of V will be given by a scalar product of these vectors. By setting $V = \mathbb{1}$ (to impose unitarity in U), we arrive at

$$\boldsymbol{u}\cdot\boldsymbol{v}^* \;=\; 0 \quad \boldsymbol{u}\cdot\boldsymbol{w}^* \;=\; 0 \quad \boldsymbol{v}\cdot\boldsymbol{w}^* \;=\; 0 \quad \text{and} \quad |\boldsymbol{u}|^2 \;=\; |\boldsymbol{v}|^2 \;=\; |\boldsymbol{w}|^2 \;=\; 1\,. \tag{5.8}$$

The above conditions tell us that $\boldsymbol{u}$, $\boldsymbol{v}$ and $\boldsymbol{w}$ must form an orthogonal basis. Therefore, a way to implement this is by setting $\boldsymbol{w}^* = \pm\boldsymbol{u}\times\boldsymbol{v}$. The sign to be used can be determined from the remaining constraint, $\det U = 1$. We have that

$$\det U \;=\; \varepsilon_{ijk} u_i v_j w_k \;=\; \boldsymbol{u}\cdot(\boldsymbol{v}\times\boldsymbol{w}) \;=\; \boldsymbol{w}\cdot(\boldsymbol{u}\times\boldsymbol{v}) \;=\; \boldsymbol{w}\cdot\boldsymbol{w}^* \;=\; 1\,. \tag{5.9}$$

The above can only be satisfied by choosing the positive sign for the vector w. Summarizing, the parameterization for an SU(3) group element can be written as

$$U \;=\; \begin{pmatrix} \boldsymbol{u} \\ \boldsymbol{v} \\ \boldsymbol{u}^*\times\boldsymbol{v}^* \end{pmatrix}, \qquad \text{with} \quad |\boldsymbol{u}| \;=\; |\boldsymbol{v}| \;=\; 1 \qquad \text{and} \quad \boldsymbol{u}\cdot\boldsymbol{v}^* \;=\; 0\,. \tag{5.10}$$

When implementing this parameterization, we may choose between storing only the vectors u and v, or storing all three rows. The former case saves memory, but has as drawback a greater use of computational time due to the need to compute the cross

product every time we need to access the third row. We consider the 33 % saving in memory use does not outweigh the increased computational cost and we use all 9 complex numbers.

Also, notice that variations of this parameterization are valid, e.g. by interpreting the matrix columns as vectors. However, those variations are conceptually equivalent, obeying the same constraints and procedure to check its properties.

Having determined how to parameterize the link variables, we proceed to the generation of field configurations. We will be adopting the (pseudo-)heat-bath method[i], as outlined in the next section. In short, the heat-bath algorithm consists in freezing all variables in the system, except one [in our case, the variables are the gauge links $U_\mu(n)$]. Then, one factors out from the action the unfrozen variable and gets an expression where it is possible to interpret the frozen variables as an external classical field that acts solely on the target variable. Under these conditions, it may be possible to propose a new value for the unfrozen variable that follows its probability distribution exactly. We will show the algorithm in the next section.

The question that follows is how one chooses the link to be updated. There are two possibilities that are usually adopted: to pick a link to update randomly or systematically iterate over all links on the lattice. We use the latter, since it better decorrelates the generated configurations.

There is one additional consideration we must make. From the probability density, as defined in the partition function in Eq. (3.73), and the detailed balance condition in Eq. (3.77), we have that the transition amplitudes must obey

$$\frac{P(i \to j)}{P(j \to i)} = \frac{\det K_F^j}{\det K_F^i} e^{-(S_G^j - S_G^i)} . \tag{5.11}$$

This means that, for each link we update, it will be necessary to take into account $\det K_F$, i.e. we must compute it. There are some strategies that one can adopt, as seen in [Ref. 30, Chap. 8]. However, even with these tricks, such computations are much more expensive than the computation of $S_G^j - S_G^i$ alone. Because of that, a common approximation is to set $\det K_F^j / \det K_F^i = 1$. The simulations where such an approximation is performed are usually called *quenched simulations*, since one interprets it as a suppression of the virtual quark-antiquark sea in the simulation. Contrasting to this, the full simulation, taking into account the computation of the determinant, is called a *dynamical fermion simulation*. In our work, we will be using quenched simulations.

5.1.1 (Pseudo-)heat-bath method for SU(3)

The heat-bath method is the name given to any algorithm that draws a new link variable independently of the previous value.[63] Notice that this does not imply that

[i] The justification for this name follows in the next section.

successive configurations will not be correlated, since the neighboring links affect the probability distribution used in the new value's drawing process.

For SU(3), the most popular method is the one developed by Cabibbo and Marinari,[64] referred to as Cabibbo-Marinari method. This method is powerful because it is built on top of the well-known SU(2) algorithm and is applicable for SU(N). Ref. 30 briefly outlines it. For completeness, I will present here the algorithm in detail.

We start with the local probability distribution

$$dP \;=\; dU \exp\left(\frac{\beta_0}{3}\Re\,\mathrm{Tr}\,[U_\mu(n)A_\mu(n)]\right)\,, \tag{5.12}$$

where $U_\mu \in$ SU(3) is the link which will be updated, the index μ is not summed over and A_μ is the staple, which is defined as the sum of plaquettes which contained $U_\mu(n)$ (or $U_\mu^\dagger$) with $U_\mu(n)$ factored out. One can express A_μ as

$$A_\mu = \sum_{\substack{\nu \\ \nu\neq\mu}} U_\nu(n+\hat{\mu})U_{-\mu}(n+\hat{\mu}+\hat{\nu})U_{-\nu}(n+\hat{\nu}) + U_{-\nu}(n+\hat{\mu})U_{-\mu}(n+\hat{\mu}-\hat{\nu})U_\nu(n-\hat{\nu})\,. \tag{5.13}$$

From now on, all operations will be referent to the update of the link $U_\mu(n)$, thus we omit the argument n and the index μ to simplify our notation.

For the purpose of developing the algorithm, we say that the new link U' is given by$U' = VU$, with $V \in$ SU(3). The link U is fixed and given by the initial configuration. Thus, we may look at this operation as a variable change $U \to U' = VU$ in Eq. (5.12), with V being the variable we are integrating over. Due to the property of the Haar measure[ii] $dU = d(VU)$, this variable change keeps Eq. (5.12) invariant

$$\begin{aligned} dP \;=\; dU' \exp\left(\frac{\beta_0}{3}\Re\,\mathrm{Tr}\,[U'A]\right) \;&=\; d(VU) \exp\left(\frac{\beta_0}{3}\Re\,\mathrm{Tr}\,[VUA]\right) \\ &=\; dV \exp\left(\frac{\beta_0}{3}\Re\,\mathrm{Tr}\,[VW]\right)\,, \end{aligned} \tag{5.14}$$

where $W = UA$.

As said above, SU(2) is a subgroup of SU(3). In fact, we can identify three copies of SU(2) inside SU(3). The elements belonging to these copies can be expressed as

$$R \;=\; \begin{pmatrix} r_1 & r_2 & 0 \\ -r_2^* & r_1^* & 0 \\ 0 & 0 & 1 \end{pmatrix}\,, \quad S \;=\; \begin{pmatrix} s_1 & 0 & s_2 \\ 0 & 1 & 0 \\ -s_2^* & 0 & s_1^* \end{pmatrix} \quad \text{and} \quad T \;=\; \begin{pmatrix} 1 & 0 & 0 \\ 0 & t_1 & t_2 \\ 0 & -t_2^* & t_1^* \end{pmatrix} \tag{5.15}$$

with $r_i, s_i, t_i, \in \mathbb{C}$ and $\sum_{i=1}^{2}|a_i|^2 = 1$ for $a = r, s, t$. One can verify, after some algebra, that any element V of SU(3) can be obtained as $V = TSR$.

[ii] For details in the Haar measure, see Refs. 19 and 32.

The approach adopted in the Cabbibo-Marinari method is to set $T = S = \mathbb{1}$ and thus the trace inside the exponential becomes

$$\begin{aligned} \Re \operatorname{Tr}[VW] &= \Re\left[r_1 w_{11} + r_2 w_{21} - r_2^* w_{12} + r_1^* w_{22} + w_{33}\right] \\ &= \Re(r_1)\Re\left(w_{11} + w_{22}\right) + \Im(r_1)\Im(w_{22} - w_{11}) + \Re(r_2)\Re(w_{21} - w_{12}) \\ &\quad - \Im(r_2)\Im(w_{21} + w_{12}) + \Re(w_{33})\,. \end{aligned} \tag{5.16}$$

Setting aside the term $\Re(w_{33})$, this expression is very similar to what one obtains by the trace of the multiplication of an SU(2) link with its plaquette in an SU(2) gauge theory

$$\Re \operatorname{Tr}[U_{\mathrm{SU}(2)} A_{\mathrm{SU}(2)}] = 2\left[\Re(r_1)\Re(a_1) - \Im(r_1)\Im(a_1) - \Re(r_2)\Re(a_2) - \Im(r_2)\Im(a_2)\right], \tag{5.17}$$

where a_i is the parameterization of the staple A. In fact, if we define

$$\begin{aligned} w_1 &\equiv \frac{\Re\left(w_{11} + w_{22}\right) + i\Im\left(w_{11} - w_{22}\right)}{2} \\ w_2 &\equiv \frac{\Re\left(w_{12} - w_{21}\right) + i\Im\left(w_{12} + w_{21}\right)}{2}, \end{aligned} \tag{5.18}$$

the exponent becomes exactly the same. Due to this result, we reorganize the W matrix's block elements (equivalent to the subgroup R) in a 2×2 matrix W_R, parameterized in the same fashion as an SU(2) matrix [see Eq. (5.5)], except that the parameters w_1 and w_2 will not obey the constraint $|w_1|^2 + |w_2|^2 = 1$. The probability density is then

$$dP = dR \exp\left[\frac{\beta_0}{3} \operatorname{Tr}(R W_R)\right], \tag{5.19}$$

where $R \in SU(2)$. The probability distribution in Eq. (5.19) is very similar to the one in an SU(2) simulation, with R being analogous to a link being updated and W_R analogous to the plaquette. Therefore, the issue now is to find an element R following Eq. (5.15). Then, one promotes R to an SU(3) group element, following Eq. (5.15), and computes $U' = RU$, generating a new link. To guarantee that we can generate any SU(3) element, one must repeat the process using matrices S and T in place of R [see Eq. (5.15)]. The drawback of such an approach is that the new element U' is drawn based on the old element U. This dependence happens at two moments: when one uses $W = UA$ to build the "SU(2) plaquette" W_R and when we set the new link to $U' = TSRU$. Because of this, even if an SU(2) heat-bath algorithm[iii] is used to generate the matrices T, S and R, there is a chance that a high correlation between successive states will persist. Due to the reasons

[iii] We point out that one could use for link generations the more usual Metropolis algorithm, where one proposes a new link that deviates from the previous one by a random small amount, and accept or reject it according to the constraint in Eq. (5.11). However, since the link deviates just a little from the original configuration, it is more correlated than the heat-bath configurations, where a new link value is drawn independently from its previous configuration and following exactly a local probability distribution. Therefore, the Metropolis algorithm is less efficient than the heat-bath one.

just presented, when we use an SU(2) heat-bath in the above procedure, we call this a pseudo-heat-bath algorithm.

We will now dive into the heat-bath algorithm for SU(2). We start by noticing that any matrix which is parameterized as W_R is proportional to an SU(2) group, with the proportionality constant given by the matrix determinant. In other words, we may write

$$W_R \;=\; \alpha V\,, \qquad V \;\in\; \mathrm{SU}(2) \qquad \text{and} \qquad \alpha \;=\; \sqrt{\det W_R}\,. \tag{5.20}$$

In this way, the argument inside the trace is $RV \in \mathrm{SU}(2)$ and the probability density is written as[iv]

$$dP \;=\; dR \exp\left[\frac{\alpha\beta_0}{3}\,\mathrm{Tr}(RV)\right]. \tag{5.21}$$

Next, we perform a change of variable $R = XV^\dagger$ and obtain

$$dP \;=\; dX \exp\left[\frac{\alpha\beta_0}{3}\,\mathrm{Tr}\,X\right] \;=\; dX \exp\left[\frac{2\alpha\beta_0}{3}\Re x_1\right]. \tag{5.22}$$

It remains to express the Haar measure dX in terms of the groups parameters. This will be easier if one decomposes the complex parameters x_1 and x_2 as $x_1 = a_4 + ia_3$ and $x_2 = a_2 + ia_1$, as done in Eq. (5.6). The Haar measure is then expressed as

$$\begin{aligned} dX \;&=\; d^4a \frac{1}{\pi^2}\delta\left(a_4^2 + |\boldsymbol{a}|^2 - 1\right) \\ &=\; d|\boldsymbol{a}|da_4 d\Omega \frac{|\boldsymbol{a}|^2}{2\pi^2} \frac{\delta\left(|\boldsymbol{a}| - \sqrt{1-a_4^2}\right) + \delta\left(|\boldsymbol{a}| + \sqrt{1-a_4^2}\right)}{\sqrt{1-a_4^2}}\,, \end{aligned} \tag{5.23}$$

where we used the property

$$\delta(f(x)) \;=\; \sum_i \frac{\delta\left(x - x_i\right)}{|f'(x_i)|}\,, \tag{5.24}$$

and x_i are the roots of $f(x)$. We integrate out the variable $|\boldsymbol{a}|$, eliminating the Dirac deltas and obtain

$$\begin{aligned} dP \;&=\; d|\boldsymbol{a}|da_4 d\Omega \frac{|\boldsymbol{a}|^2}{2\pi^2} \frac{\delta\left(|\boldsymbol{a}| - \sqrt{1-a_4^2}\right) + \delta\left(|\boldsymbol{a}| + \sqrt{1-a_4^2}\right)}{\sqrt{1-a_4^2}} \exp\left[\frac{2\alpha\beta_0}{3}a_4\right] \\ &=\; d\Omega da_4 \frac{1-a_4^2}{2\pi^2} \frac{\exp\left(\alpha\beta_0 a_4/3\right)}{\sqrt{1-a_4^2}} \;=\; d\Omega da_4 \frac{\sqrt{1-a_4^2}}{2\pi^2} \exp\left(\frac{2\alpha\beta_0}{3}a_4\right). \end{aligned} \tag{5.25}$$

This gives us that a_4 must be picked following the probability density $e^{\frac{2\alpha\beta_0}{3}a_4}\sqrt{1-a_4^2}$, while the vector $\boldsymbol{a}$ should be uniformly distributed on the surface of a sphere of radius $\sqrt{1-a_4^2}$. Notice that, from our parameterization, we must constrain $a_i \in [-1, 1]$.

[iv] In SU(2), the normalization in the denominator is a 2. However, we will use this algorithm in an SU(3) simulation. Thus, we changed the normalization to the one present in Eq. (5.19).

For a_4, a variable change $a_4 = 1 - 2\lambda^2$ yields

$$da_4 \frac{\sqrt{1-a_4^2}}{2\pi^2} \exp\left(\frac{2\alpha\beta_0}{3} a_4\right) = \frac{d\lambda}{\pi^2} \exp\left(\frac{2\alpha\beta_0}{3}\right) \exp\left(-\frac{4\alpha\beta_0}{3}\lambda^2\right) 2\lambda^2\sqrt{1-\lambda^2}\,. \quad (5.26)$$

We absorb the λ-independent factors as a normalization constant. Thus, we must generate numbers λ following the polynomial Gaussian distribution $\lambda^2 \exp\left(-\frac{4\alpha\beta_0}{3}\lambda^2\right)$ and accept them with probability $\sqrt{1-\lambda^2}$. The algorithm to draw the random numbers λ^2 and the points on the surface of the sphere can be chosen at will. For λ^2, the algorithm chosen is the one in Ref. 30, which consists in drawing three random numbers (r_1, r_2 and r_3) uniformly in the range $]0, 1]$. Then λ^2 is given by

$$\lambda^2 = -\frac{3}{4\alpha\beta_0}\left[\ln(r_1) + \cos^2(2\pi r_2)\ln(r_3)\right]. \quad (5.27)$$

As usual, the acceptance step is made by drawing a fourth random number in the range $]0, 1]$ and testing if it is smaller than $\sqrt{1-\lambda^2}$. If this is not the case, we reject the value of λ^2 found and run the algorithm again.

To pick points uniformly on the surface of a sphere of radius $R = \sqrt{1-a_4^2}$, we use the Marsaglia algorithm.[65–66] We draw two random numbers in range $[-1, 1]$ and accept them only if $x_1^2 + x_2^2 \leq 1$. Then the coordinates x_1, x_2 and x_3 are given by

$$\begin{aligned} a_1 &= 2Rx_1\sqrt{1-x_1^2-x_2^2}\,, \\ a_2 &= 2Rx_2\sqrt{1-x_1^2-x_2^2}\,, \\ a_3 &= R - 2R(x_1^2+x_2^2)\,. \end{aligned} \quad (5.28)$$

Once we finish this process, we have an SU(2) element X drawn following Eq. (5.22). We then can compute $R \in \mathrm{SU}(2)$ as $R = XV^\dagger = XW_R^\dagger/\alpha$. Then it is just a matter of promoting R to be an SU(3) group element belonging to the appropriate subgroup and update the link with $U' = RU$. Of course, we must repeat the entire procedure for the other two subgroups.

Thus, the pseudo-heat-bath algorithm for an SU(3) gauge theory can be summarized by the following steps

1. Compute the staple A using Eq. (5.13).
2. For each $SU(2)$ subgroup of SU(3):
   a) Close the staple with the link U to form the matrix W.
   b) Write W as a 2×2 matrix W_R proportional to a SU(2) element using Eq. (5.18).
   c) Compute the determinant of $\alpha = \det W_R$.
   d) Obtain an SU(2) group element $V = W_R/\alpha$.

e) Draw four random numbers r_1, r_2, r_3 and r_4 to find λ^2 following Eq. (5.27).

f) If $r_4^2 > 1 - \lambda^2$, repeat the previous step.

g) Set $a_4 = 1 - 2\lambda^2$.

h) Draw two random numbers x_1 and x_2.

i) If $x_1^2 + x_2^2 > 1$, then repeat the previous step.

j) Set a_1, a_2 and a_3 according to Eq. (5.28), with $R = \sqrt{1 - a_4^2}$.

k) Interpret a_1, a_2, a_3 and a_4 as an SU(2) matrix X, parameterized as in Eq. (5.6) and use it to generate another SU(2) group element $R = XV^\dagger = XW_R^\dagger/\alpha$.

l) Promote R to an element of SU(3) belonging to the SU(2) subgroup of the current step.

m) Update the link U with $U \to U' = RU$.

n) Use the updated link in the next subgroup.

There is a subtlety that we must be aware of. Computers use floating-point numbers and thus have a limited precision when storing them. Once the above algorithm is executed many times for the same lattice, it is natural the accumulation of numerical errors. These errors lead the matrix U' generated to be slightly outside of the SU(3) group. One can easily verify such an effect by computing their determinants and multiplying them by their transpose conjugate, or yet by checking if the parameters are following the imposed parameterization constraints. For a short run, the deviations will be small and this should not be an issue. However, for longer runs, we frequently check these parameters looking if they deviate more than a tolerated amount. In case this happens, we project them back onto SU(3).

The projection procedure is based on the observation that the three rows of the group elements form an orthonormal base. We use the Gram-Schmidt approach to fix this[30]

$$\boldsymbol{u'} = \frac{\boldsymbol{u}}{|\boldsymbol{u}|}, \qquad \boldsymbol{v'} = \frac{\tilde{\boldsymbol{v}}}{|\tilde{\boldsymbol{v}}|} \qquad \text{with} \quad \tilde{\boldsymbol{v}} = \boldsymbol{v} - \boldsymbol{u'}(\boldsymbol{v} \cdot \boldsymbol{u'}^*)\,. \tag{5.29}$$

A last issue remains. As mentioned above, this is a pseudo-heat-bath. Thus, the gauge configurations being generated may be highly correlated. If this happens, we will need to discard a large amount of configurations because they are correlated. It would be beneficial if one could devise a way for the new configurations to be as far as possible, in the configuration space, from the previous one, which would minimize the computational effort. This is the aim of the *overrelaxation* procedure and will be the subject of the next section.

5.1.2 Overrelaxation

As we just stated, the overrelaxation method is a way to mitigate correlations between two successive gauge configurations. The idea is to modify the link proposed by the heat-bath, as a way to get "as far as possible" from the previous configurations. There are several tactics that are used, especially by proposing to choose another link which does not change the value of S. If the value of S does not change, neither does the probability of selecting the proposed configuration instead of the previous one. Thus, one does not change the sampling performed by the Monte Carlo algorithm. The approach we used is based in the one proposed by Creutz[67] and we present it bellow.

The overrelaxation procedure is applied after the heat-bath algorithm explained above is finished and a new link $U' = TSRU$ is available. We use the staple that is already computed and project it onto the SU(3) group, using the Gram-Schmidt procedure of Eq. (5.29). Then we compute the transpose conjugate of it. The result of this operation we call V_0. We then propose a new U' by $U' = V_0 U^\dagger V_0$.

The above procedure, for SU(2), draws a new link that has the same probability to be drawn as the one from the heat-bath algorithm. This can be easily verified by remembering the property in Eq. (5.20), which states that the sum of SU(2) group elements is proportional to an SU(2) matrix as well. Thus our transformation takes $\mathrm{Tr}[UA] \to \mathrm{Tr}[A^\dagger U^\dagger]$. Now, in SU(2) the trace is real and thus our transformation does not change the value of the action of the new configuration.

The above reasoning does not hold for $SU(3)$, however. The property in Eq. (5.20) holds only for the SU(2) group and thus the transformation $\mathrm{Tr}[UA] \to \mathrm{Tr}[A^\dagger U^\dagger]$ does not hold true. This means that once the above procedure is applied, we will not be drawing U' with the Boltzmann weight $\exp[\beta_0 \Re\,\mathrm{Tr}(UA)/3]$. The result is that if we always accept U', we will thermalize to the wrong states.

The solution found was to apply a Metropolis acceptance test once the link is modified by the overrelaxation procedure. More precisely, when a modification of the link is proposed, one must accept or reject it, in such a way that the detailed balance equation in Eq. (5.11) is respected (in our case, in the quenched approximation). This is done by computing $\Delta S = S_G^j - S_G^i$. If $\Delta S < 0$, the proposed link is always accepted. Else, one draws a random number $r \in [0, 1[$ and accepts it only if $r \leq e^{-\Delta S}$.

The Metropolis algorithm can be used as the main engine in generation of new links. In these cases, one typically proposes the new link by introducing a small modification in the previous one. This is not the case here. The proposed link comes from the overrelaxation procedure. In case the link is rejected by the Metropolis algorithm, we simply keep it as it was, i.e. with the value coming from the heat-bath algorithm.

5.1.3 Implementation details

To generate the lattice configurations, the program needs to know some parameters. The application developed reads these parameters from an XML file, using the FoX Fortran library.[68] The parameters read are the lattice sides N_x, N_y, N_z, N_τ and the coupling parameter β_0. Furthermore, we also read how the lattice will be initialized. We allow three options for this. The first one is called *cold start* and consists in setting all link values to $U_\mu(x) = \mathbb{1}$. The name is due to the fact that such a configuration resembles the equilibrium state of an Ising model at zero temperature. The second possibility of start is called a *hot start*, which consists of randomly picking SU(2) group elements R, S and T, promoting them to SU(3) matrices, as in Eq. (5.15), and multiplying them to get a random SU(3) group element[v]. This is analogous to what one would observe in an Ising model at infinite temperature, thus the name hot start. The last option given is to use a lattice configuration previously generated. This enables one to skip the thermalization steps, since we start from an already thermalized lattice. It can be also used to simulate[vi] the continuation of a previously stopped simulation.

We recall that, due to the renormalization procedure one must perform, the parameter $g_0 = \sqrt{6/\beta_0}$ depends on the lattice spacing. Or conversely, fixing the parameter β_0 will fix the lattice spacing. We recall yet that the temperature of the simulation will be given by $N_\tau a(\beta_0) = 1/T$. Thus, the value of β_0 and lattice dimensions must be chosen with care. Fortunately, there are works performed tabling these values. We use Ref. 69, which gives us directly the ratio between the temperature and the temperature of the phase transition, T_C

$$\begin{aligned} \frac{T}{T_C} &= \frac{1}{34.38 N_\tau R(\beta_0)\lambda(\beta_0)}\,, & R(\beta_0) &= \left(\frac{\beta_0}{6b_0}\right)^{\frac{b_1}{2b_0^2}} e^{-\frac{\beta_0}{12b_0}}\,, \\ b_0 &= \frac{11}{16\pi^2}\,, & b_1 &= \frac{34}{3}\left(\frac{3}{16\pi^2}\right)^2 \end{aligned} \tag{5.30}$$

and $\lambda(\beta_0)$ is tabled in Ref. 69.

There is yet other two parameters which are read from the XML file: The number of Monte Carlo steps which will be computed and the interval, in Monte Carlo steps, between configurations that are saved to disk. A Monte Carlo step is defined as a sweep across the entire lattice of the heat-bath plus overrelaxation algorithm.

In a first run, we do fewer Monte Carlo steps, but saving every configuration generated. This allows one to determine the correlation and thermalization times. After

[v] For the generation of random SU(2) group elements, one must pick a random point on the surface of a hyper-sphere. This is done by drawing four random numbers following a normal distribution and normalizing them. See Appendix A for details.

[vi] To really be a continuation of the simulation, we should supply the state of the random number generator at the time that the configuration was saved. This is something which we plan to implement some time in the future.

this, we perform a long run, saving to disk only the uncorrelated configurations. In addition to saving space, this saves time as well, since the operation of writing a configuration to disk is a slow one.

The above determinations (correlation and thermalization times) may depend on the choice of operator. Thus, we should use the operator which we are interested in measuring, i.e. the energy-momentum tensor. However, its calculation is expensive and the thermalization and correlation times should not be significantly different if a simpler operator is chosen. Thus, we use the average plaquette to perform these calculations, defined by

$$P \;=\; \frac{1}{6N_xN_yN_zN_\tau}\sum_n\sum_{C(\mu,\,\nu)}\frac{1}{3}\Re\,\mathrm{Tr}\,[U_{\mu\nu}(n)]\;. \tag{5.31}$$

Once we obtain the sequence of values of the average plaquette, we use the methods presented in Appendix B. It is also possible to plot P vs. the Monte Carlo time, allowing an estimation of the thermalization time. Once this procedure is finished, one proceeds to the production run, generating the field configurations that will be used in the subsequent steps.

5.2 Energy-momentum-tensor discretization

Once the gauge configurations are generated, one must work on the computation of the energy-momentum tensor. As usual, we break the problem into the gauge term and the fermion term. We recover from Eq. (2.61)

$$T^G_{\mu\nu} \;=\; 2\,\mathrm{Tr}\left[F_{\mu\rho}F_{\nu\rho} - \frac{\delta_{\mu\nu}}{4}F_{\rho\sigma}F_{\rho\sigma}\right]\;. \tag{5.32}$$

The strategy is to find a discrete version of the tensor $F_{\mu\nu}(n)$ and then employ Eq. (5.32) to compute $T^G_{\mu\nu}$. Fortunately, a good discretization of $F_{\mu\nu}$ is easy to come by. We start by recovering from Eq. (3.60)

$$U_{\mu\nu}(x) \;=\; \mathbb{1} \;-\; ig_0a^2F_{\mu\nu} \;-\; \frac{g_0^2a^4}{2}F^2_{\mu\nu} \;+\; \mathcal{O}(a^6)\,. \tag{5.33}$$

We then define a clover as

$$Q_{\mu\nu}(n) \;=\; U_{\mu\nu}(n) + U_{\nu,\,-\mu}(n) + U_{-\mu,\,-\nu}(n) + U_{-\nu,\,\mu}(n)\,. \tag{5.34}$$

The name clover comes from the resemblance to a clover when the graphic representation of it is drawn, as seen in Fig. 11. We stress that the clover-leafs(i.e., plaquettes) must always start from the point n, and follow the counter-clock wise orientation.

Under the assumption that $F_{\mu,\,-\nu}(x) = -F_{\mu\nu}$, the clover term can be approximated as

$$Q_{\mu\nu} \;=\; 4\left[\mathbb{1} - ig_0a^2F_{\mu\nu}(x) - \frac{g_0^2a^4}{2}F^2_{\mu\nu}(x)\right] + \mathcal{O}(a^6)\,. \tag{5.35}$$

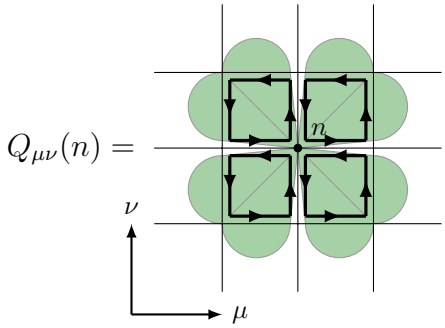

Figure 11 – Representation of the clover operator. Source: Elaborated by the author.

Notice also that $Q^{\dagger}_{\mu\nu} = Q_{\nu\mu}$. Thus, we get

$$Q_{\mu\nu} - Q_{\nu\mu} \;=\; -8ig_0a^2F_{\mu\nu} + \mathcal{O}(a^6)\,. \tag{5.36}$$

The above discretization for $F_{\mu\nu}$ is called *clover-leaf discretization* and is suggested for the calculation of the gauge part of the energy-momentum tensor by Ref. 21. It is also present in Ref. 30 as a discretization of the field strength tensor, but in the context of improvement of the Wilson action.

We proceed to compute the Fermionic part of the tensor. Recovering Eq. (2.73) we get

$$T^F_{\mu\nu} \;=\; \bar{\psi}\left[\gamma_\mu \overset{\leftrightarrow}{D}_\nu + \gamma_\nu \overset{\leftrightarrow}{D}_\mu\right]\psi - \delta_{\mu\nu}\bar{\psi}\left(\overset{\leftrightarrow}{\not{D}} - m\right)\psi. \tag{5.37}$$

The term accompanying $\delta_{\mu\nu}$ is just the fermion Lagrangian and one may use the Wilson fermion discretization in Eq. (3.70), with the modification of excluding the sum in m and the global factor a^4. We now worry about the discretization of the first factor. To this end, let us recall the definition of $\overset{\leftrightarrow}{D}_\mu$

$$\overset{\leftrightarrow}{D}_\mu \;=\; \frac{1}{2}(\overset{\leftarrow}{D}_\nu + D_\mu)\,, \qquad D_\mu\psi \;=\; \partial_\mu\bar{\psi} - ig\bar{\psi}A_\mu\,, \qquad \bar{\psi}\overset{\leftarrow}{D}_\mu \;=\; -\partial_\mu\bar{\psi} - ig\bar{\psi}A_\mu\,. \tag{5.38}$$

We have already discretized the covariant derivative D_μ in Section 3.2.2. We use it as an inspiration to propose the following discretization for $\bar{\psi}\overset{\leftarrow}{D}_\mu$

$$\bar{\psi}\overset{\leftarrow}{D}_\mu \;\to\; \frac{\bar{\psi}(n-\hat{\mu})U_\mu(n-\hat{\mu} - \bar{\psi}(n+\hat{\mu})U_{-\mu}(n+\hat{\mu})}{2a}\,. \tag{5.39}$$

Thus, a term like $\bar{\psi}(n)\gamma_\nu\overset{\leftrightarrow}{D}_\mu\psi(n)$ is written as

$$\begin{aligned}\bar{\psi}(n)\gamma_\nu\overset{\leftrightarrow}{D}_\mu\psi(n) \;=\; \frac{1}{4a}\Big[&\bar{\psi}(n)\gamma_\nu U_\mu(n)\psi(n+\hat{\mu}) - \bar{\psi}(n)\gamma_\nu U_{-\mu}(n)\psi(n-\hat{\mu}) \\ &+\bar{\psi}(n-\hat{\mu})\gamma_\nu U_\mu(n-\hat{\mu})\psi(n) - \bar{\psi}(n+\hat{\mu})\gamma_\nu\psi(n)U_{-\mu}(n+\hat{\mu})\Big]\,.\end{aligned} \tag{5.40}$$

The above relation may be put into a more palatable way by noticing that $\bar{\psi}(n)\psi(m) \;=\; -\,\mathrm{Tr}[\psi(m)\bar{\psi}(n)] \;=\; -a^{-3}\,\mathrm{Tr}[\mathcal{S}(m|n)]$, where $\mathcal{S}$ is the fermion propagator,

i.e. the inverse of the Dirac operator $K(m|n)$, given by the term inside square brackets in Eq. (3.70). The factor a^{-3} comes from the scaling of the propagator, performed to obtain a dimensionless observable, better suited for numerical evaluation. After these operations, the fermionic energy-momentum tensor can be written as

$$\begin{aligned} T^F_{\mu\nu}(n) \;=\; -\frac{1}{4a^4}\,\mathrm{Tr}\,[&\mathcal{S}(n+\hat{\nu}|n)\gamma_\mu U_\nu(n) - \mathcal{S}(n-\hat{\nu}|n)\gamma_\mu U_{-\nu}(n) \\ &+\mathcal{S}(n+\hat{\mu}|n)\gamma_\nu U_\mu(n) - \mathcal{S}(n-\hat{\mu}|n)\gamma_\nu U_{-\mu}(n) \\ &+\mathcal{S}(n|n-\hat{\nu})\gamma_\mu U_\nu(n-\hat{\nu}) - \mathcal{S}(n|n+\hat{\nu})\gamma_\mu U_{-\nu}(n+\hat{\nu}) \\ &+\mathcal{S}(n|n-\hat{\mu})\gamma_\nu U_\mu(n-\hat{\mu}) - \mathcal{S}(n|n+\hat{\mu})\gamma_\nu U_{-\mu}(n+\hat{\mu})]\ . \end{aligned} \tag{5.41}$$

The above discretization matches the one proposed in Ref. 21. However, we may simplify the calculation further. Notice that the first and second lines in the above equation are the same tensor, with its indices μ and ν swapped. The same happens between the third and fourth line. However, it is possible to reduce it in terms of a single object. To this end, we use the γ^5-hermiticity property, which states[30] $\mathcal{S}(m|n) = \gamma^5\mathcal{S}^\dagger(n|m)\gamma^5$. We also write $U_\nu(n-\hat{\mu}) = U^\dagger_{-\mu}(n)$ and use $\gamma_\mu = \gamma^\dagger_\mu$. Since $\mathrm{Tr}\,A^\dagger = (\mathrm{Tr}\,A)^*$, and picking the third line of Eq. (5.41), we rewrite it as

$$\mathrm{Tr}\left[U_{-\nu}(n)\gamma_\mu\gamma^5\mathcal{S}(n-\hat{\nu}|n)\gamma^5 - U_\nu(n)\gamma_\mu\gamma^5\mathcal{S}(n+\hat{\nu}|n)\gamma^5\right]^*\ . \tag{5.42}$$

However, we may use the cyclic property of the trace to bring the γ^5 at the end of the expression to the beginning. We also know that the gamma matrices commute with the links and thus in both terms we have a factor $\gamma^5\gamma_\mu\gamma^5 = -\gamma_\mu$. If we use again the cyclic property of the trace to bring the propagator to the expression's beginning, we find that the third line is just the complex conjugate of the first line. Thus, if we define

$$C_{\mu\nu} \;=\; \frac{1}{4}\,\mathrm{Tr}\,[\mathcal{S}(n-\hat{\mu}|n)U_{-\mu}(n)\gamma_\nu - \mathcal{S}(n+\hat{\mu}|n)U_\mu(n)\gamma_\nu]\ , \tag{5.43}$$

we have that the energy-momentum tensor may be written as

$$T^F_{\mu\nu}(n) \;=\; \frac{2}{a^4}\Re\,[C_{\mu\nu}(n) + C_{\nu\mu}(n)]\ ,\ \text{for}\ \mu \;\neq\; \nu\,. \tag{5.44}$$

Notice yet that the Green function which we wish to calculate depends solely on off-diagonal components of the tensor. For this reason, we will not dwell on the diagonal components' calculation.

The implementation of the bosonic tensor's computation is straightforward. The program receives as input the lattice dimension, the value of β_0 and the file name where the field states are stored, which is then loaded to memory. A shell script is used to run the application several times, each one for a different field configuration previously generated. Once a configuration is loaded, $F_{\mu\nu}(n)$ is computed for $\nu > \mu$. The remaining components are then computed using the symmetry property $F_{\mu\nu}(n) = -F_{\nu\mu}(n)$. Then it

is just a matter of employing Eq. (5.32) for $\mu \geq \nu$. Once again, we use the tensor symmetry $T_{\mu\nu}(n) = T_{\nu\mu}(n)$ to fill the remaining of the tensor. Once the computation is done, the result is saved to disk for later use.

For fermions, the procedure is more involved, due to the need to compute the propagator $\mathcal{S}(n \pm \hat{\mu}|n)$. The algorithms most widely known, such as the Bi-CGStab,[30,70] compute only one column of $\mathcal{S}$, i.e., for fixed α_0, a_0 and m_0, one computes $\mathcal{S}^{aa_0}_{\alpha\alpha_0}(n|m_0)$ for every α, a and n. However, since we will take the Fourier transform later, we need $\mathcal{S}^{aa_0}_{\alpha\alpha_0}(n + \hat{\mu}|n)$ for all sites n. As one can see, we are not interested in a single column, but rather in the elements neighboring the diagonal $\mathcal{S}(n|n)$. At the time of the writing of this thesis, it is not clear to us how best to proceed. One possibility is that, if one manages to compute the propagator already in momentum space, as in Ref. 71, then the issue might not matter. For the time being, the result presented does not include contributions coming from the fermionic term and should be seen as a simulation of a "gluon plasma", without any contributions from fermions.

5.3 Green-function computation

We are finally in a position where we can compute our observable, the Euclidean Green function for the energy-momentum tensor, which can be written from Eq. (4.47) and Eq. (4.48), after Wick rotation, as

$$G^E_{4i,\,4j}(k) \;=\; \int d^4x \;\; e^{-ik_\mu x_\mu} \left\langle T_{4i}(x) T_{4j}(0) \right\rangle \,. \tag{5.45}$$

To compute the correlation function, one uses the procedures outlined in Appendix B. Since we are interested in the Green function in momentum space, we have

$$\begin{aligned} G^E_{4i,\,4j}(k) \;&=\; \langle \mathcal{F}\left[T_{4i}(x) T_{4j}(0), k\right] \rangle \;=\; \frac{1}{N_x N_y N_z N_\tau} \left\langle \mathcal{F}\left[\mathcal{F}^{-1}\left[\tilde{T}_{4i}(p)\tilde{T}^*_{4j}(p), x\right], k\right] \right\rangle \\ &=\; \left\langle \tilde{T}_{4i}(k)\tilde{T}^*_{4j}(k) \right\rangle \,, \end{aligned} \tag{5.46}$$

where $\tilde{T}_{4i}(k)$ is the Fourier transform of $T_{4i}(n)$.

The above computations are not particularly intensive, thus it is worth it to load all values of the $T_{\mu\nu}(n)$ for all field configurations. Then, for each configuration, we compute $\tilde{T}_{4i}(k)\tilde{T}_{4j}(k)$. To perform the transformation, we use the discrete Fourier transforms provided in the Intel Math Kernel Library (MKL). It has the advantage that it can be easily configured to run on a cluster, if necessary in the future.

The operation performed by the library is given by [Ref. 72, Chap. 9]

$$\tilde{f}(k_1, \ldots, k_d) \;=\; \sigma \sum_{j_d=0}^{n_d-1} \cdots \sum_{j_1=0}^{n_1-1} f(j_1, \ldots, j_d) \exp\left[\delta i 2\pi \sum_{l=1}^{d} \frac{j_l k_l}{n_l}\right] \,. \tag{5.47}$$

In our case, $d = 4$ and we choose $\sigma = 1$ and $\delta = -1$. The output will be a complex array of the same size as the input. Since our input data are real, $k_i \in [N_i/2 + 1, N_i - 1]$ is

the complex conjugate of the data in $[1, N_i/2]$. Thus, we only save to file the data in the range $[0, N_i/2]$.

After the computation of $T_{4i}(k)T_{4j}(k)$, for each i, j and k, it is employed the procedure of statistical treatment in Appendix B. Contrary to what was done for the generation of configurations and for the computation of the energy-momentum tensor, the results are stored as a text file, instead of in a binary format.

5.4 Orbit average

The last step consists of reading the text file and treating it to generate plots. The low computational cost made us switch from Fortran to Python, which is easier to program.

We start by assuming that the lattice has an H(3) symmetry, i.e. we should be able to rotate on space planes by 90 degrees and not see difference in results. Notice that time direction does not take part in this symmetry. This is because in finite temperature simulations we need a lattice in which the time direction is smaller than the spatial ones, breaking the H(4) symmetry into H(3).

The consequence of the H(3) symmetry is that an observable $\mathcal{O}$ can be written as $\mathcal{O}(p^{[2]}, p^{[4]}, p^{[6]}, \omega)$, where

$$p^{[n]} \;=\; p_x^n + p_y^n + p_z^n \,. \tag{5.48}$$

This allow us to define an "orbit", which consists of all points with the same set of $p^{[2]}$, $p^{[4]}$, $p^{[6]}$, ω. These points should have the same values of the observable and thus we can average over them, which is the job of this application.

In the continuum, is expected that we recover the O(4) symmetry and we should see a very strong dependence on p^2 (if the observable depends on it) and a weak dependency on $p^{[4]}$, $p^{[6]}$, ω, which can be regarded as lattice artifacts. Details of all these issues can be found in Ref. 73. Notice that although we are using the momentum notation, this will hold in the coordinate space as well.

After the average over orbits is performed, we may employ Eq. (4.62) and Eq. (4.63) to compute $G^{\parallel}(|\boldsymbol{k}|)$ and $G^{\perp}(|\boldsymbol{k}|)$. We them perform the plot of $G^{\parallel}(|\boldsymbol{k}|) - G^{\perp}(|\boldsymbol{k}|)$ to perform the test, as suggested at the end of Section 4.3.2.

5.5 Results

We start by performing some test runs using small lattices. The idea is to be able to compare the average plaquette with data from Ref. 74. These tests were made on a computer equipped with an Intel(R) Core(TM) i5-4460 CPU @ 3.20GHz, with 8 GB of RAM available, running Arch Linux. The compiler used was the PGI Fortran Compiler,

available in the PGI Community compiler suit. We choose this compiler because it is the only one which supports GPU parallelization natively in Fortran. Although we did not use this feature in the present work, we plan to incorporate it later. All code developed is publicly available at `https://github.com/willian-m/SU3SimSuit/tree/v0.2`.

We start by generating 1000 configurations on an 8^4 lattice with $\beta = 5.7$. We choose to perform a "hot" lattice initialization. For this run, we record every configuration generated. The entire execution takes around two minutes to complete. We also measure the acceptance rate of the Metropolis test in the overrelaxation method and obtain that it was 52.50% . This number is important because it asserts the efficacy of the overrelaxation step. If we had a low acceptance rate it would mean that we just wasted computational time trying to guess an uncorrelated field configuration but ended up using mostly the ones from the pseudo-heat-bath.

Next, we proceed to run the program to compute the average plaquette. It outputs just the average plaquette for each configuration in a text file, which later is read by a Python script, which does the statistic work. We estimate the exponential correlation time to be around 7 and thus set the thermalization time to be 70. This is in line with the estimate of the integrated correlation time of 8. We obtain an average plaquette of $\langle P \rangle = 0.54924(42)$, thus in agreement with Ref. 74. We performed a couple more runs, at different lattice spacings and coupling values, to guarantee that our field configuration generator is working. A summary of the results is presented in Table 1. We also present in Fig. 12 the thermalization evolution for all our test cases. The acceptance rate of the overrelaxation step did not change much, staying in the 52-55% range.

Table 1 – Results for the average plaquette in several test scenarios and their comparison with the values present in Ref. 74.

Lattice size	β_0	Therm. time	Int. correlation time	$\langle P \rangle$	Ref. 74
8^4	5.70	70	8	0.54924(42)	0.549123(56)
10^4	5.80	80	9	0.56742(22)	0.567633(12)
10^4	5.90	30	5	0.58197(16)	0.58187(3)
12^4	5.90	30	10	0.58188(19)	0.58185(2)
12^4	5.90	20	6	0.58570(19)	0.585600(15)

Source: Elaborated by the author.

The above results give us confidence that using as thermalization time 100 Monte Carlo steps and saving to disk in steps of 10 Monte Carlo steps will yield good results. But, as a precaution, we executed the same procedure for our finite temperature lattice. For these, we use $N_s = 32$ and $N_\tau = 6$. To generate 1000 configurations (saving every one of them to disk) takes about 110 minutes. No significant change of the acceptance rate of the overrelaxation step was noticed. In Table 2 we summarize what we obtain at all temperatures used. We see that our criteria of discarding the first 100 steps and recording at each 10 steps are good enough.

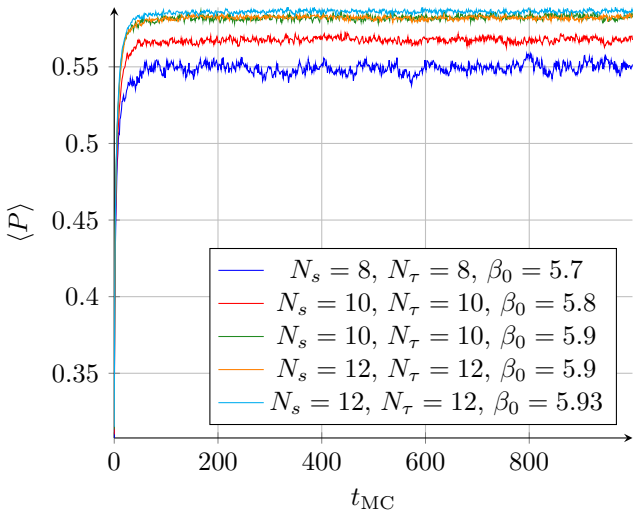

Figure 12 – Average plaquette values as a function of Monte Carlo time for several lattice sizes and coupling values. Source: Elaborated by the author.

Table 2 – Results for the average plaquette at finite temperature. We always used $N_s = 32$ and $N_\tau = 6$.

β_0	T/T_c	Therm. time	Int. correlation time	$\langle P \rangle$
5.70	0.67	50	7	0.549659(68)
5.90	1.01	40	11	0.582096(94)
6.00	1.20	80	26	0.5941(10)
6.10	1.42	40	28	0.60427(17)

Source: Elaborated by the author.

Since the data from Table 2 show that 1000 samples seems to yield a good statistic, we will perform 10 000 Monte Carlo steps to get the thousand samples above mentioned.

We present our results as a plot of $G^{\parallel}(0, \boldsymbol{k}^2)$ and $G^{\perp}(0, \boldsymbol{k}^2)$, computed as defined in Eqs. (4.62) and (4.63). We also average points in the same orbit, as described in Section 5.4. These results are presented in Fig. 13. Notice the "fish bone" structure towards higher momentum. This is a direct consequence of the orbit averaging procedure and thus caused by the breaking of rotational symmetry by the lattice discretization. However, we are interested in the limit $k^2 \to 0$ and thus we do not worry about the removal of these lattice artifacts.

As noted at the end of 4, if there is a superfluid, we should see $G^{\parallel}(0, \boldsymbol{k}^2 \to 0) \neq G^{\perp}(0, \boldsymbol{k}^2 \to 0)$. However, the data obtained suggest that $G^{\parallel}(0, \boldsymbol{k}^2) = G^{\perp}(0, \boldsymbol{k}^2)$. If we neglect for a moment the lattice artifact by averaging over all points with the same k^2 and then compute $G^{\parallel}(0, \boldsymbol{k}^2) - G^{\perp}(0, \boldsymbol{k}^2)$, this becomes more evident, as Fig. 14 shows.

Therefore, the simulations performed indicate that Landau's two-component model is not applicable to a pure-gluon theory at finite temperature. However, one must be careful not to generalize this result to the QGP. We must remember that we did not

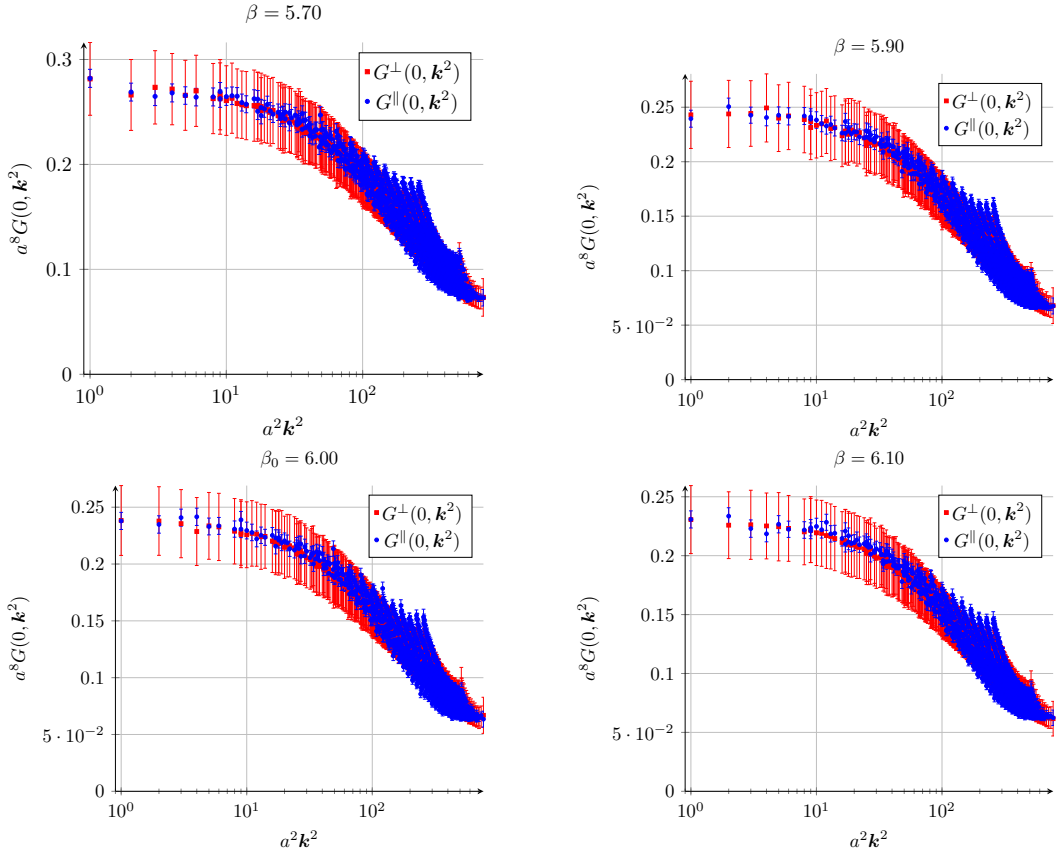

Figure 13 – Computation of the decomposition of the Green function in its longitudinal and transverse component, as a function of the wave mode $\boldsymbol{k}^2$, for several temperatures. Source: Elaborated by the author.

take into account the fermionic term of the energy-momentum tensor. To be certain, one must compute it as well. In fact, Kalaydzhyan proposes[75] that the superfluid component consists of fermionic states moving freely. Chernodub *et. al.* also propose[76] a mechanism that would allow these fermionic states «««< HEAD to move freely. Therefore, we plan to corry out a simulation including the fermionic term as soon as possible. ======= to move freely. Therefore, we plan to execute a simulation of the fermionic term as soon as possible. »»»> ebed36c4cbe0fe329566eb59dffbd52f0bfad281

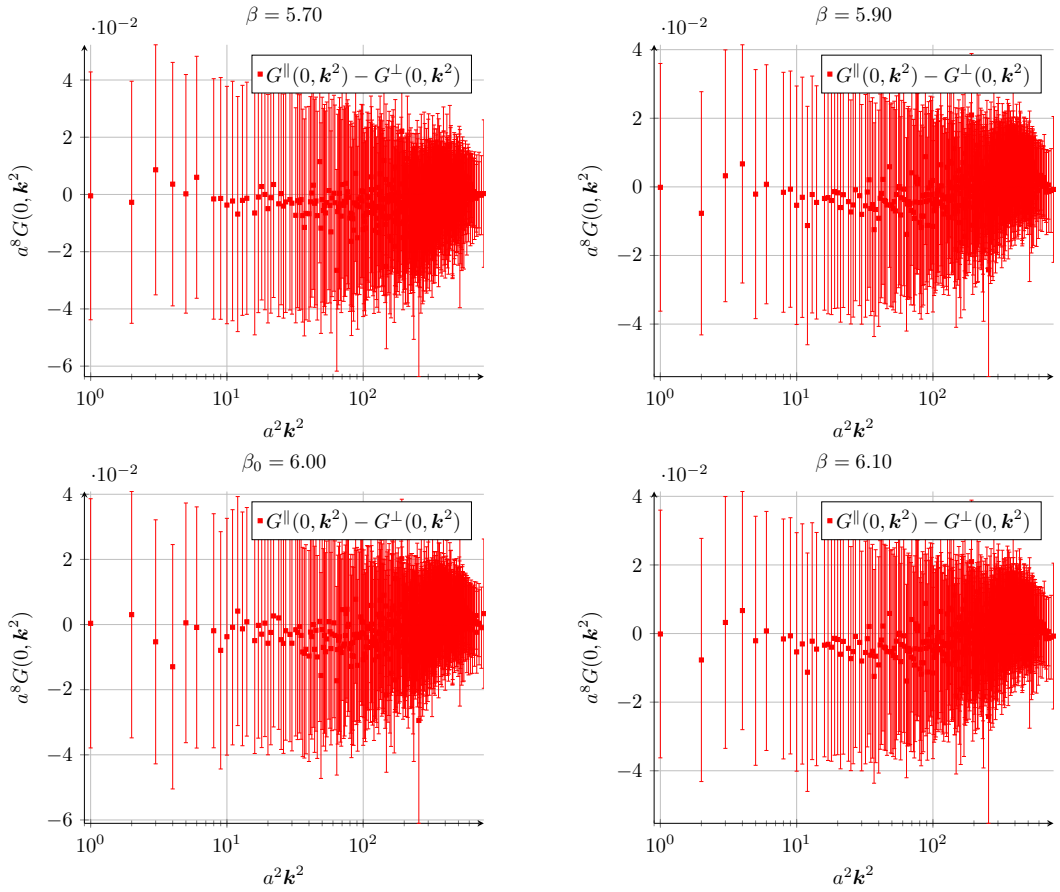

Figure 14 – The difference between the Green's function longitudinal and transverse components, computed after an average over all points of the same $\boldsymbol{k}^2$ is computed. Source: Elaborated by the author.

Chapter 6

Conclusions

"*Look at me still talking when there's science to do*"

Jonathan Coulton
Song "Still Alive"

In this thesis we initially reviewed the motivation for building a field theory with gauge symmetry and explored Noether's theorem to build conserved quantities, giving special attention to the energy-momentum tensor. We also noticed that such a procedure gives us a problematic tensor since it is not symmetrical and breaks gauge symmetry. Nevertheless, we showed that it is possible to patch it and obtain a result which matches an alternative approach, which uses General Relativity.[21] Next, we used the quantum formulation of statistical mechanics to quantize the field theory and arrived at the path integral formulation of quantum field theory in imaginary time, taking as a toy model a complex scalar theory. We used it to show the need of a regulator in quantum field theories, especially in interacting ones. Our choice was to use the lattice as a regulator since it allows non-perturbative calculations, even if they are numerical ones.

We then turned to study our system of interest, the quark-gluon plasma. We saw that it may occur naturally at the early moments of the universe as well as in the interior of neutron stars, which makes the determination of its properties of cosmological and astrophysical interest as well. We outlined the phenomenological aspects of relativistic heavy-ion collisions, used for experimental study of the QGP. We took this opportunity to make a brief introduction to relativistic hydrodynamics, used to model the plasma. Since the QGP hydrodynamic model points at a low viscosity liquid, the idea to treat it as a superfluid is natural. Hence, we presented Landau's two-component model for superfluids. As the name suggests, this model says that the plasma should have two components: one of near-zero viscosity and a second one with higher viscosity. We then explained in detail

the test suggested by Chernodub[14] *et. al.* to validate its applicability to the QGP, i.e. the computation of the correlation function of the energy-momentum tensor.

After this lengthy theoretical overview, we showed the implementation details of our Monte Carlo simulation, as well as the discretization used for the energy-momentum tensor, necessary for the execution of tests. Our simulation has the shortcoming of not taking into account any form of fermions, due to the complexity of its implementation. Therefore, our results are applicable to a "gluon plasma" rather than QGP itself. With this in mind, we computed the correlation function of the energy-momentum tensor to execute the test for several temperature ranges. Our results did not indicate the presence of the superfluid component. However, there are arguments[75–76] for the fermions being responsible for the superfluid component. Thus, we are working towards the computation of the fermionic term of the tensor to get a better idea of the feasibility of the model.

References

1 ADCOX, K. et al. Formation of dense partonic matter in relativistic nucleus-nucleus collisions at RHIC: Experimental evaluation by the PHENIX collaboration. **Nuclear Physics A**, v. 757, n. 1, p. 184–283, 2005.

2 ARSENE, I. et al. Quark gluon plasma and color glass condensate at RHIC? The Perspective from the BRAHMS experiment. **Nuclear Physics A**, v. 757, n. 1, p. 1–27, 2005.

3 AAD, G. et al. Observation of a new particle in the search for the Standard Model Higgs boson with the ATLAS detector at the LHC. **Physics Letters B**, v. 716, n. 1, p. 1–29, 2012.

4 CHATRCHYAN, S. et al. Observation of a new boson at a mass of 125 GeV with the CMS experiment at the LHC. **Physics Letters B**, v. 716, n. 1, p. 30–61, 2012.

5 ABBOTT, B. P. et al. GW170817: Observation of gravitational waves from a binary neutron star inspiral. **Physical Review Letters**, v. 119, n. 16, p. 161101, 2017.

6 CABIBBO, N.; PARISI, G. Exponential hadronic spectrum and quark liberation. **Physics Letters B**, v. 59, n. 1, p. 67–69, 1975.

7 COLLINS, J. C.; PERRY, M. J. Superdense matter: neutrons or asymptotically free quarks? **Physical Review Letters**, v. 34, n. 21, p. 1353–1356, 1975.

8 BLÜMLEIN, J. The theory of deeply inelastic scattering. **Progress in Particle and Nuclear Physics**, v. 69, p. 28–84, 2013.

9 BAYM, G. et al. From hadrons to quarks in neutron stars: a review. **Reports on Progress in Physics**, v. 81, n. 5, p. 056902, 2018.

10 TANABASHI, M. et al. Review of particle physics. **Physical Review D**, v. 98, n. 3, p. 030001, 2018.

11 NATSUUME, M. **AdS/CFT duality user guide**. Tokyo: Springer Japan, 2015. v. 903. (Lectures Notes in Physics, v. 903).

12 TISZA, L. Transport phenomena in helium II. **Nature**, v. 141, n. 3577, p. 913, 1938.

13 LANDAU, L. Theory of the superfluidity of helium II. **Physical Review**, v. 60, n. 4, p. 356–358, 1941.

14 CHERNODUB, M. N.; VERSCHELDE, H.; ZAKHAROV, V. I. Two-component liquid model for the quark-gluon plasma. **Theoretical and Mathematical Physics**, v. 170, n. 2, p. 211–216, 2012.

15 LINDE, A. D. Infrared problem in thermodynamics of the Yang-Mills gas. **Physics Letters B**, v. 96, n. 3, p. 289–292, 1980.

16 DIRAC, P. A. M. The quantum theory of the electron. **Proceedings of Royal Society A**, v. 117, n. 778, p. 610–624, 1928.

17 PESKIN, M. E.; SCHROEDER, D. V. **Introduction to quantum field theory**. Boca Raton: Westview Press, 1995.

18 MORIYASU, K. **An elementary primer for gauge theory**. Singapore: World Scientific, 1983.

19 SERENONE, W. M. **Heavy-quarkonium potential with input from lattice gauge theory**. 2014. 151 p. Dissertation (Master of Science) — Instituto de Física de São Carlos, Universidade de São Paulo, São Carlos, 2014.

20 GROSS, F. **Relativistic quantum mechanics and field theory**. New York: Wiley, 1993.

21 CARACCIOLO, S.; CURCI, G.; MENOTTI, P.; PELISSETTO, A. The energy momentum tensor for lattice gauge theories. **Annals of Physics**, v. 197, n. 1, p. 119–153, 1990.

22 BLASCHKE, D. N. et al. The energy–momentum tensor(s) in classical gauge theories. **Nuclear Physics B**, v. 912, p. 192–223, 2016.

23 BELINFANTE, F. J. On the spin angular momentum of mesons. **Physica**, v. 6, n. 7, p. 887–898, 1939.

24 ERIKSEN, E.; LEINAAS, J. M. Gauge invariance and the transformation properties of the electromagnetic four potential. **Physica Scripta**, v. 22, n. 3, p. 199, 1980.

25 TAKAHASHI, Y. Energy momentum tensors in relativistic and nonrelativistic classical field theory. **Fortschritte der Physik**, v. 34, n. 5, p. 323–344, 1986.

26 KAPUSTA, J. I.; GALE, C. **Finite-temperature field theory**: principles and applications. Cambridge: Cambridge University Press, 2006. (Cambridge Monographs on Mathematical Physics).

27 BELLAC, M. L. **Thermal field theory**. Cambridge: Cambridge University Press, 1996. (Cambridge Monographs on Mathematical Physics).

28 CASAS, F.; MURUA, A.; NADINIC, M. Efficient computation of the Zassenhaus formula. **Computer Physics Communications**, v. 183, n. 11, p. 2386–2391, 2012.

29 AARTS, G. Introductory lectures on lattice QCD at nonzero baryon number. **Journal of Physics:** conference series, v. 706, n. 2, p. 022004, 2016.

30 GATTRINGER, C.; LANG, C. **Quantum chromodynamics on the lattice**: an introductory presentation. Berlin Heidelberg: Springer, 2009. v. 788. (Lecture Notes in Physics, v. 788).

31 WILSON, K. G. Confinement of quarks. **Physical Review D**, v. 10, n. 8, p. 2445–2459, 1974.

32 CREUTZ, M. **Quarks, gluons and lattices**. Cambridge: Cambridge University Press, 1985. (Cambridge Monographs on Mathematical Physics).

33 ROTHE, H. J. **Lattice gauge theories**. Singapore: World Scientific, 2012.

34 WILSON, K. G. Quarks and strings on a lattice. In: ZICHICHI, A. (Ed.). **New phenomena in subnuclear physics**. Boston: Springer, 1977, p. 69–142. (The Subnuclear Series).

35 KOONIN, S.; MERIDITH, D. **Computational physics**: Fortran version. Boca Raton: Westview Press, 1990.

36 SOMMER, R. A New way to set the energy scale in lattice gauge theories and its applications to the static force and alpha-s in SU(2) Yang-Mills theory. **Nuclear Physics B**, v. 411, n. 2, p. 839–854, 1994.

37 GREINER, W.; SCHRAMM, S.; STEIN, E. **Quantum chromodynamics**. Berlin, Heidelberg: Springer, 2004.

38 GREINER, W.; REINHARDT, J. **Quantum electrodynamics**. Berlin, Heidelberg: Springer, 2003.

39 GÖCKELER, M.; HORSLEY, R.; LINKE, V.; RAKOW, P.; SCHIERHOLZ, G.; STÜBEN, H. Is there a Landau pole problem in QED? **Physical Review Letters**, v. 80, n. 19, p. 4119–4122, 1998.

40 FRAGA, E. S.; KURKELA, A.; VUORINEN, A. Interacting quark matter equation of state for compact stars. **The Astrophysical Journal**, v. 781, n. 2, p. L25, 2014.

41 FRANZON, B. C. de S. **Gluons em estrelas de nêutrons**. 2012. Thesis (Doctor of Science) — Instituto de Física, Universidade de São Paulo, São Paulo, 2012.

42 PASECHNIK, R.; ŠUMBERA, M. Phenomenological review on quark–gluon plasma: concepts vs. observations. **Universe**, v. 3, n. 1, p. 7, 2017.

43 KARSCH, F. The phase transition to the quark gluon plasma: recent results from lattice calculations. **Nuclear Physics A**, A90, n. 1, p. 367–381, 1995.

44 STOCK, R. Relativistic nucleus-nucleus collisions and the QCD matter phase diagram. In: SCHOPPER, H. (Ed.). **Theory and experiments**. Berlin Heidelberg: Springer, 2008, (Landolt-Börnstein - Group I Elementary Particles, Nuclei and Atoms, 21).

45 GYULASSY, M. The QGP discovered at RHIC. In: GREINER, W. et al. (Ed.). **Structure and dynamics of elementary matter**. Dordrecht: Springer Science Business Media, 2004. p. 159–182. (NATO Science Series, v. 166)

46 RAFELSKI, J. (Ed.). **Melting hadrons, boiling quarks - from Hagedorn temperature to ultra-relativistic heavy-ion collisions at CERN**: With a tribute to Rolf Hagedorn. Berlin Heidelberg: Springer, 2015.

47 TANNENBAUM, M. J. How hadron collider experiments contributed to the development of QCD: from hard-scattering to the perfect liquid. **The European Physical Journal H**, v. 43, n. 2, p. 119–183, 2018.

48 TEANEY, D.; LAURET, J.; SHURYAK, E. V. A hydrodynamic description of heavy ion collisions at the SPS and RHIC. **Physical Review Letters**, v. 86, n. 21, p. 4783–4786, 2001.

49 ROMATSCHKE, P. New developments in relativistic viscous hydrodynamics. **International Journal of Modern Physics E**, v. 19, n. 1, p. 1–53, 2010.

50 LUZUM, M.; PETERSEN, H. Initial state fluctuations and final state correlations in relativistic heavy-ion collisions. **Journal of Physics G**, v. 41, p. 063102, 2014.

51 AGUIAR, C. E.; HAMA, Y.; KODAMA, T.; OSADA, T. Event-by-event fluctuations in hydrodynamical description of heavy ion collisions. **Nuclear Physics A**, v. 698, n. 1, p. 639–642, 2002.

52 ANDRADE, R.; GRASSI, F.; HAMA, Y.; KODAMA, T.; SOCOLOWSKI JR., O. On the necessity to include event-by-event fluctuations in experimental evaluation of elliptical flow. **Physical Review Letters**, v. 97, n. 20, p. 202302, 2006.

53 ANDRADE, R. P. G.; GRASSI, F.; HAMA, Y.; KODAMA, T.; QIAN, W. L. Importance of granular structure in the initial conditions for the elliptic flow. **Physical Review Letters**, v. 101, p. 112301, 2008.

54 JEON, S.; HEINZ, U. Introduction to hydrodynamics. **International Journal of Modern Physics E**, v. 24, n. 10, p. 1530010, 2015.

55 HIRANO, T.; HUOVINEN, P.; MURASE, K.; NARA, Y. Integrated dynamical approach to relativistic heavy ion collisions. **Progress in Particle and Nuclear Physics**, v. 70, p. 108–158, 2013.

56 MAXWELL, J. C. IV. On the dynamical theory of gases. **Philosophical Transactions of the Royal Society of London**, v. 157, p. 49–88, 1867.

57 CATTANEO, C. "Sulla conduzione del calore" (On the conduction of heat). In: PIGNEDOLI, A. (Ed.). **Some aspects of diffusion theory**. Berlin, Heidelberg: Springer, 1948. p. 485. (C.I.M.E. Summer Schools, v. 42).

58 COOPER, F.; FRYE, G.; SCHONBERG, E. Electron positron annihilation into hadrons and Landau's hydrodynamic model. **Physical Review Letters**, v. 32, n. 15, p. 862–865, 1974.

59 KEESOM, W.; MACWOOD, G. The viscosity of liquid helium. **Physica**, v. 5, n. 8, p. 737–744, 1938.

60 REICHL, L. E. **A modern course in statistical physics**. Weinheim: Wiley, 2016.

61 SCHMITT, A. **Introduction to superfluidity**. Berlin, Heidelberg: Springer, 2014.

62 HERZOG, C. P.; YAROM, A. Sound modes in holographic superfluids. **Physical Review D**, v. 80, p. 106002, 2009.

63 KENNEDY, A.; PENDLETON, B. J. Improved heatbath method for Monte Carlo calculations in lattice gauge theories. **Physics Letters B**, v. 156, n. 5-6, p. 393–399, 1985.

64 CABIBBO, N.; MARINARI, E. A new method for updating SU(N) matrices in computer simulations of gauge theories. **Physics Letters B**, v. 119, n. 4, p. 387–390, 1982.

65 MARSAGLIA, G. Choosing a point from the surface of a sphere. **Annals of Mathematical Statistics**, v. 43, n. 2, p. 645–646, 1972.

66 WEISSTEIN, E. W. **Sphere point picking**. 2018. From MathWorld— a Wolfram web resource. Available from: <http://mathworld.wolfram.com/SpherePointPicking.html>. Acessed at: August 11th, 2016.

67 CREUTZ, M. Overrelaxation and Monte Carlo simulation. **Physical Review D**, v. 36, n. 2, p. 515–519, 1987.

68 WHITE, T.; WALKER, A. **A Fortran library for XML**. 2018. Available from: <https://homepages.see.leeds.ac.uk/~earawa/FoX/>. Acessed at: July 12th, 2018.

69 BOYD, G. et al. Thermodynamics of SU(3) lattice gauge theory. **Nuclear Physics B**, v. 469, n. 3, p. 419–444, 1996.

70 GUTKNECHT, M. H. Variants of BICGSTAB for matrices with complex spectrum. **SIAM Journal on Scientific Computing**, v. 14, n. 5, p. 1020–1033, 1993.

71 CUCCHIERI, A. Gribov copies in the minimal Landau gauge: the influence on gluon and ghost propagators. **Nuclear Physics B**, v. 508, n. 1, p. 353–370, 1997.

72 INTEL CORPORATION. **Intel® Math Kernel Library - reference manual. revision 072. MKL 11.2**. [S.l.], 2018. Available from: <https://software.intel.com/en-us/articles/mkl-reference-manual>. Acessed at: October 23rd, 2018.

73 SOTO, F. de; ROIESNEL, C. On the reduction of hypercubic lattice artifacts. **Journal of High Energy Physics**, v. 09, p. 007, 2007.

74 LUCINI, B.; TEPER, M. SU(N) gauge theories in four-dimensions: exploring the approach to N = infinity. **Journal of High Energy Physics**, v. 06, p. 050, 2001.

75 KALAYDZHYAN, T. Chiral superfluidity of the quark-gluon plasma. **Nuclear Physics A**, v. 913, p. 243–263, 2013.

76 CHERNODUB, M. N. et al. On chromoelectric (super)conductivity of the Yang-Mills vacuum. **Physics Letters B**, v. 730, p. 63–66, 2014.

77 SOKAL, A. Monte Carlo methods in statistical mechanics: foundations and new algorithms. In: DEWITT-MORETTE, C.; CARTIER, P.; FOLACCI, A. (Ed.). **Functional integration**: basics and applications. Boston, MA: Springer, 1997. cap. 6, p. 131–192.

78 BERG, B. A. **Markov chain Monte Carlo simulations and their statistical analysis**. Singapore: World Scientific, 2004.

Appendix

APPENDIX A

Uniform hypersphere point-picking

When performing a lattice simulation, we need to randomly generate SU(N) group elements, usually for $N = 3$, to perform the "hot" initialization of the lattice. As we have seen in the main body of the thesis, a SU(3) element may be generated by getting three SU(2) elements, properly embedding them in SU(3) matrices and multiplying them. This reduces the problem to the random generation of SU(2) group elements. A SU(2) group element U may be parameterized by $U = a_0\mathbb{1} + ia_j\sigma_j$, where σ_j are the Pauli matrices. The variables a_μ are real numbers that must obey the constraint $a_\mu a_\mu = 1$. This is the equation of an hypersphere[i]. Thus, we need to uniformly pick random points in the surface of this hypersphere. This appendix will focus on demonstrating that this is possible by picking 4 random numbers following a Gaussian distribution and normalizing them.

Our aim is to demonstrate an algorithm which can be used to pick a point in the surface of a hypersphere following an uniform distribution, i.e. avoiding to generating spots where points concentrate.

The method consists in picking four numbers x_μ that will be chosen randomly following a Gaussian distribution $P(x_\mu) = e^{-x_\mu^2/2}/\sqrt{2\pi}$. Then we obtain the coordinates a_μ of our point through the following operation

$$a_\mu = \frac{x_\mu}{\sqrt{x_\nu x_\nu}}\,. \tag{A.1}$$

The coordinates a_μ are the object of interest in our application, since we can readily use them to build the SU(2) group elements. But they are not practical to show that the points will be uniformly distributed in the surface of the hypersphere. It will be useful to

[i] We stress that this is an object immersed in a 4D euclidean space.

jump to hyperspherical coordinates

$$\begin{aligned} r &= \sqrt{a_\mu a_\mu} &&= 1 \\ \theta &= \arccos a_0 &&= \arccos \frac{x_0}{\sqrt{x_\mu x_\mu}} \\ \varphi &= \arctan \frac{\sqrt{a_2^2 + a_3^2}}{a_1} &&= \arctan \frac{\sqrt{x_2^2 + x_3^2}}{x_1} \\ \psi &= \arctan \frac{a_3}{a_2} &&= \arctan \frac{x_3}{x_2} \end{aligned} \tag{A.2}$$

One easy way to check that the distribution is uniform is to check if the following condition holds

$$\frac{dP}{d\Omega} = \frac{1}{2\pi^2}\,, \tag{A.3}$$

where $d\Omega = \sin^2\theta \sin\varphi \, d\theta \, d\phi \, d\psi$ is the four-dimensional analogue of the solid angle.

We know the probability density function for the variables x_μ

$$dP = \frac{1}{4\pi^4} e^{-\frac{x_0^2+x_1^2+x_2^2+x_3^2}{2}} \, dx_0 \, dx_1 \, dx_2 \, dx_3\,. \tag{A.4}$$

However, we desire it as a function of the hyperspherical coordinates, i.e. the $p(r, \theta, \varphi, \psi)$ in $dP = p(r, \theta, \varphi, \psi) \, dr \, d\theta \, d\phi \, d\psi$. If we show that it is a constant, then we prove our algorithm. Fortunately, it is easy to calculate it[60]

$$\begin{aligned} p(r, \theta, \varphi, \psi) \;=\; & \left(\prod_{\mu=0}^{3} \int_{-\infty}^{\infty} dx_\mu \right) \delta(r-1)\, \delta\!\left(\theta - \arccos \frac{x_0}{\sqrt{x_\nu x_\nu}} \right) \times \\ & \delta\!\left(\varphi - \arctan \frac{\sqrt{x_2^2 + x_3^2}}{x_1} \right) \delta\!\left(\psi - \arctan \frac{x_3}{x_2} \right) \frac{e^{-\frac{x_\mu x_\mu}{2}}}{4\pi^2} \end{aligned} \tag{A.5}$$

This integral can be solved in a much easier way if we perform the following change of variables

$$\begin{aligned} x_0 &= \rho \cos q \\ x_1 &= \rho \sin q \cos f \\ x_2 &= \rho \sin q \sin f \cos y \\ x_3 &= \rho \sin q \sin f \sin y\,, \end{aligned} \tag{A.6}$$

which have the Jacobian

$$J(\rho, q, f, y) = \rho^3 \sin^2 q \sin f\,. \tag{A.7}$$

The integral becomes

$$\begin{aligned} p(r, \theta, \varphi, \psi) \;=\; & \int_0^\infty \int_0^\pi \int_0^\pi \int_0^{2\pi} \frac{\delta(r-1)\, e^{-\rho^2/2}}{4\pi^2} \times \\ & \delta(\theta - q)\, \delta(\varphi - f)\, \delta(\psi - y)\, \rho^3 \sin^2 q \sin f \, dy \, df \, dq \, d\rho\,. \end{aligned} \tag{A.8}$$

Thanks to the Dirac deltas, the integral trivially reduces to

$$p(r,\theta,\varphi,\psi) = \frac{\delta(r-1)}{4\pi^2}\sin^2\theta\sin\varphi\int_0^\infty \rho^3 e^{-\rho^2/2}\,d\rho\,. \tag{A.9}$$

The remaining integral can be easily by noticing that

$$\rho^3 e^{-\rho^2/2} = \frac{d}{d\beta}\left[\frac{1}{2\beta}\frac{d}{d\rho}e^{-\beta\rho^2}\right]\Bigg|_{\beta=1/2}\,. \tag{A.10}$$

Thus

$$\int_0^\infty \rho^3 e^{-\rho^2/2}d\rho = \frac{d}{d\beta}\left[\frac{1}{2\beta}\int_0^\infty \frac{d}{d\rho}e^{-\beta\rho^2}d\rho\right]\Bigg|_{\beta=1/2} = 2\,. \tag{A.11}$$

We finally obtain that

$$\begin{aligned} dP \;=\; p(r,\theta,\varphi,\psi)dr\,d\theta\,d\phi\,d\psi \;&=\; \frac{\delta(r-1)}{2\pi^2}\sin^2\theta\sin\varphi dr\,d\theta\,d\phi\,d\psi \\ &=\; \frac{\delta(r-1)}{2\pi^2}\,dr\,d\Omega \end{aligned} \tag{A.12}$$

The remaining Dirac delta is there just to remember us that our results is constrained to $r = 1$, as desired. Thus, we can integrate in r to get rid of it. After this, we obtain Eq. (A.3) as we desired.

APPENDIX B

Statistical Error and Correlation Functions

The Monte Carlo method generates field states following a specified distribution. However, since a finite number of configurations is drawn, we are able to only approximate the distribution. Of course, the law of large numbers guarantees that the more configurations are drawn, more accurately we will represent the probability distribution. As a complication, the above holds only for independently drawn samples. Thus we must deal with the correlation between samples. This appendix is a summary on how we deal with such issues. It is based in Refs. 77 and 78 with some tricks learned informally along the way.

The two main components in our analysis are the estimator $\bar{f}$ of the expectation value $\hat{f}$, given by

$$\bar{f} \;=\; \frac{1}{N_{MC}} \sum_{i=1}^{N_{MC}} f_i \tag{B.1}$$

and the autocorrelation function of the operator $\hat{f}$, defined as

$$C_{ij} \;=\; \langle (f_i - \langle f_i \rangle)(f_j - \langle f_j \rangle) \rangle \;=\; \langle f_i f_j \rangle - \hat{f}^2 \,, \tag{B.2}$$

where we are assuming that, since we are in a equilibrium situation, we have Monte Carlo time invariance and thus a periodic boundary condition.

Our main concern is with the correct assessment of the standard deviation $\sigma^2(\bar{f})$, which will tell us the statistical error present in the estimation $\bar{f}$, defined as

$$\sigma^2(\bar{f}) \;=\; \langle (\bar{f} - \hat{f})^2 \rangle \;=\; \frac{1}{N_{MC}^2} \sum_{i=1}^{N_{MC}} \sum_{j=1}^{N_{MC}} \langle (f_i - \hat{f})(f_j - \hat{f}) \rangle \;=\; \frac{1}{N_{MC}^2} \sum_{i=1}^{N_{MC}} \sum_{j=1}^{N_{MC}} C_{ij} \,. \tag{B.3}$$

Notice that, due to the Monte Carlo invariance, the only thing that matters is the distance $t = |i - j|$. We have N terms for which $i = j$. The remaining terms appears

$2(N-t)$ times. Defining $C(t) = C_{ij}$, we also have that $C(0) = \sigma^2(f)$. Thus, we may write

$$\begin{aligned} \sigma^2(\bar{f}) &= \frac{1}{N_{MC}^2}\left[\sigma^2(f)N_{MC} + 2\sum_{t=1}^{N_{MC}-1}(N_{MC}-t)C(t)\right] \\ &= \frac{\sigma^2(f)}{N_{MC}}\left[1 + 2\sum_{t=1}^{N_{MC}-1}\left(1-\frac{t}{N_{MC}}\right)\frac{C(t)}{C(0)}\right]. \end{aligned} \tag{B.4}$$

The prefactor $\sigma^2(f)/N_{MC}$ is what one would expect if the samples drawn were completely uncorrelated. This can be seen by setting $C(t) = 0$ for $t \neq 0$. The term inside the square bracket defines the integrated autocorrelation time τ_{int}. The motivation for such nomenclature come from the supposition that

$$C(t) = C(0)e^{-t/\tau_{\text{exp}}}. \tag{B.5}$$

if $N_{MC} \to \infty$. Then a way to compute the correlation time would be

$$\tau_{\text{exp}} = \int_0^\infty \frac{C(t)}{C(0)}\,dt. \tag{B.6}$$

In Eq. (B.6), we are approximating the discrete time by a continuous one. However, if consider the discrete version of the integral, we have

$$\tau_{\text{exp}} = \sum_{t=1}^{\infty}\frac{C(t)}{C(0)}. \tag{B.7}$$

Thus, in the limit of large N_{MC}, we have

$$\tau_{\text{int}} = 1 + 2\tau_{\text{exp}}. \tag{B.8}$$

The above give us two ways one may use the integrated autocorrelation time. The first one is as a factor that will increase the statistical error as naively calculated, i.e. as the data were uncorrelated. The second one is as the number of Monte Carlo steps one must take before one may consider the two points of data to be uncorrelated.

For the time being, let us suppose that we computed the autocorrelation function. Since it is numerically calculated over a finite number of samples, $C(t)$ does not dies off exponentially, as in Eq. (B.5), but rather fluctuates around zero. Thus, when one tries to compute

$$\tau_{\text{int}} = 1 + 2\sum_{t=1}^{\infty}\frac{C(t)}{C(0)}, \tag{B.9}$$

we will sum a lot of noise for $t \gg \tau_{\text{exp}}$. Two solutions may be adopted. The first one is to define

$$\tau_{\text{int}}(t) = 1 + 2\sum_{t'=1}^{t}\frac{C(t')}{C(0)}, \tag{B.10}$$

and look for a value of t where $\tau_{\text{int}}(t)$ is approximately constant. Ref. 77 proposes as an algorithm that one must set t as the minimum value for which $t \geq c\tau_{\text{int}}(t)$, where c is a fixed integer. The suggestion in the aforementioned reference is for c to be at least 6, but according the needs, values as large as 10 may be used.

The other method is known as binning method, and is explored in Ref. 78. The idea behind it is that one can estimate correctly the error if the data is binned in bins large enough to hold at least one set of correlated data, i.e. if the bin is larger than the autocorrelation time. To this end, one averages the data inside each bin and uses this set of averages to compute the standard deviation. The ratio between this standard deviation and the one calculated with the full data set then yields the integrated autocorrelation time.

It remains to compute the autocorrelation function. We will derive a way to perform such computation using discrete Fourier transform. From the computational point of view, this allows one to use libraries which are readily available, turning the implementation of this calculation easier.

Correlation functions computed via Fourier transform

To employ this method, it is necessary that the data obeys a periodic boundary conditions, e.g. $f_{i+N_{MC}} = f_i$. We will go further and consider the case of a correlation function instead of a autocorrelation function, i.e. we will consider two distinct observables A and B and compute

$$C_{AB}(t) \;=\; \langle A(t)B(0)\rangle \;\equiv\; \frac{1}{N}\sum_{j=1}^{N} A(j+t)B(j)\,. \tag{B.11}$$

The result derived here holds for any correlation function, even if we are not in the context of a Markov chain. For instance, we may be interested in the correlation between two observables evaluated at points which are distant of each other by an amount $d = |n - m|$ in a fixed field configuration. In such a example, the correlation $C_{AB}(d)$, for every d, would be the observable f which we are interested in estimating its expected value. In this case, one would employ the method in two moments. First for computing $C_{AB}(d)$ in each field state. Then later for computing the autocorrelation of $C_{AB}(d)$ between the different field configurations. Then one could obtain the integrated autocorrelation time and estimate the statistical errors associated to it.

Since by hypothesis there is periodicity in the time t, we may decompose the operators $A(t)$ and $B(t)$ in their Fourier components $a(\omega)$ and $b(\omega)$

$$A(t) \;=\; \frac{1}{N}\sum_{\omega=1}^{N} a(\omega)e^{-2\pi i\frac{\omega}{N}t} \qquad \text{and} \qquad B(t) \;=\; \frac{1}{N}\sum_{\omega=1}^{N} a(\omega)e^{-2\pi i\frac{\omega}{N}t}\,. \tag{B.12}$$

The correlation function in Eq. (B.11) will then be written as

$$C_{AB}(t) \;=\; \frac{1}{N^3}\sum_{j=1}^{N}\sum_{\omega=1}^{N}\sum_{\rho=1}^{N} e^{-\frac{2\pi i}{N}(\omega+\rho)j} e^{-\frac{2\pi i}{N}\omega t} a(\omega)b(\rho)\,. \tag{B.13}$$

The sum in j will yield $N\delta(\omega,-\rho)$. This allow us to perform the sum in ρ, to obtain

$$\mathcal{C}_{AB}(t) \;=\; \frac{1}{N^2}\sum_{\omega=1}^{N} a(\omega)b(-\omega)e^{-\frac{2\pi i}{N}\omega t} \;\equiv\; \frac{1}{N}\mathcal{F}^{-1}\left[a(\omega)b(-\omega),\, t\right]\,, \tag{B.14}$$

where $\mathcal{F}^{-1}\left[f(\omega),\, t\right]$ denotes the inverse of the Fourier transform of the function $f(\omega)$. The autocorrelation function is a particular case of correlation when $B = A$ and thus, we may write

$$C(t) \;=\; C_{AA}(t) \;=\; \frac{1}{N}\mathcal{F}^{-1}\left[a(\omega)a(-\omega)\right]\,. \tag{B.15}$$

Another interesting case happens when $B(t) \in \mathbb{R}$. Then its Fourier components obeys $b(-\omega) = b^*(\omega)$. Then the correlation and auto-correlation functions becomes

$$C_{AB}(t) \;=\; \frac{1}{N}\mathcal{F}^{-1}\left[a(\omega)b^*(\omega), t\right] \tag{B.16}$$

$$C_{AA}(t) \;=\; \frac{1}{N}\mathcal{F}^{-1}\left[|a(\omega)|^2\right]\,. \tag{B.17}$$

As a bonus of computing the Fourier transform, one has that

$$a(\omega = 0) \;=\; \sum_{t=1}^{N} A(t) \;=\; N\langle A\rangle\,, \tag{B.18}$$

i.e. we get for free the computation of the expected value of A.

The reader may notice that the correlation function definition in Eq. (B.11) does not match the autocorrelation function in Eq. (B.2). The formula that matches it will be given by the *connected* (auto)correlation function

$$C^c_{AB}(t) \;=\; C_{AB}(t) - \langle A\rangle\langle B\rangle\,. \tag{B.19}$$

We stress that, albeit we consider the one dimensional case, all the results are readily generalizable for more dimensions, by simply using the Fourier transform appropriate for the problem dimension.